Ruthenium (II) polypyridyl complexes as two-photon absorbers and sensitizers: Design, structure-properties relationships and applications

Jean-Luc Fillaut

Coordination Chemistry Reviews 518 (2024) 216050

Contents lists available at ScienceDirect

Coordination Chemistry Reviews

journal homepage: www.elsevier.com/locate/ccr

Review

Ruthenium (II) polypyridyl complexes as two-photon absorbers and sensitizers: Design, structure-properties relationships and applications

Jean-Luc Fillaut

Université de Rennes, Institut des Sciences Chimiques de Rennes CNRS UMR 6226, 263 Av. Général Leclerc, 35700 Rennes, France

ARTICLE INFO

Keywords:
Ruthenium polypyridyl complexes for two-photon applications
Design and synthesis of Ru(II) two-photon photosensitizers
Biological Imaging and Anti-Cancer Therapies
Near-infrared activated photocatalysis
Three-dimensional fabrication of optical devices and advanced micromaterials

ABSTRACT

This review addresses recent advancements in understanding multiphoton excitation of ruthenium polypyridyl complexes, highlighting their relevance in the fields of molecular materials and bio-medical applications. Emphasis is placed on two-photon absorption and two-photon excited photoluminescence for which these complexes meet several requirements as two-photon sensitizers. Alongside their appealing one-photon properties, these complexes are photostable under two-photon excitation and can exhibit noticeable two-photon absorption cross-sections in the near-infrared (NIR) region. Moreover, the presence of the ruthenium atom favors spin–orbit coupling, facilitating rapid and efficient population of triplet excited states, thereby extending emission lifetimes, or uncaging reactions, according to their structural characteristics. Indeed, ruthenium polypyridyl complexes offer great versatility in terms of functionalization, enabling property fine-tuning. This review also outlines forthcoming challenges and prospects in the field through representative examples in the area of materials, bio-imaging and phototherapies.

Abbreviations: 3D, Three dimensions or three dimensional; 3DMCS, 3D multicellular spheroid; ^{3}MC, Triplet metal-centered state; 4AP, 4-aminopyridine; 5-E-Phen, 5-ethynyl-1,10-phenanthroline; 5-Fluo-Phen, 5-dihexylfluorene-1,10-phenanthroline; 5-HT, 5-hydrotryptamine (serotonin); A549, Lung human carcinoma cells; A549R, Cis-platin resistant human lung carcinoma cells; ACN, acetonitrile; aPDT, Antibacterial Photodynamic Therapy; APTSi, 3-aminopropyltriethoxysilane; BP, 1,3-phenylenebis(pyren-1-ylmethanone); bpy, 2,2′-bipyridine; BR, Biotin Receptor; C8161, Invasive and spontaneously metastatic human melanoma cell line; CD, Carbon Nanodot; dcbpy, 2,2′-bipyridine-4,4′-dicarboxylic acid; DCM, dichloromethane; dip, 4,7-diphenyl-1,10-phenanthroline; DMF, dimethyl formamide ; DMSO, dimethylsulfoxide; DNA, DeoxyriboNucleic Acid; Dopa, Dopamine; dpp, 4,7-diphenyl-1,10-phenanthroline; EDOT, 3,4-ethylenedioxythiophene; ER, Estrogen Receptor; FLIM, Fluorescence Lifetime Imaging; FRET, Förster Resonance Energy Transfer; FWHM, Full Width at Half Maximum; g-C_3N_4, Graphitic Carbon Nitride Nanosheets; GelMA, Gelatin methacryloyl; GM, Goeppert–Mayer, 1 GM = 10^{-50} cm^4·s·photon^{-1}·molecule^{-1}; GLUT, Glucose Transporter; Gluta, L-glutamate; GSH, Glutathione (γ-glutatamylcysteinylglycine); GST, Glutathione S-transferase; H_2TPP, tetraphenylporphyrin; HaCaT, Human epidermal keratinocyte cells; HeLa, Human cervical epithelioid carcinoma; HK-1, Human nasopharyngeal carcinoma cell; HSA, Human serum albumin; IC_{50}, Inhibitory potency, concentration at which a 50% of cells are dead; ICP-MS, Inductively Coupled Plasma Mass Spectrometry; ILCT, Intra-Ligand Charge Transfer; ISC, Inter-System Crossing; LLCT, Ligand-to-Ligand Charge Transfer; LMCT, Ligand-to-Metal Charge Transfer; Man, mannose; MCF-7, Non-invasive human breast cancer; MCTSs, 3D multicellular tumor spheroids; MLCT, Metal-to-Ligand Charge Transfer; MOF, Metal–Organic Framework; NIR, Near Infared; NLA, Non Linear Absorption; NLO, Non Linear Optics or Non Linear Optical; NLR, Non Linear Refraction; N^{NC}, 6-phenyl-2,2′-bipyridine (quasi tpy); N^{NN}, 2,2′, 6′,2″-terpyridine (tpy); OPA, One-Photon Absorption; OPEF, One-Photon Excited Fluorescence; OPM, One-Photon Microscopy; PACT, PhotoActivated ChemoTherapy; PDT, PhotoDynamic Therapy; PEDOT, Poly-(3,4-ethylenedioxythiophene); PEG, Poly(ethylene glycol); PeT, Photo-induced Electron Transfer; phen, phenanthroline; PI, Phototoxicity Index; PLIM, Phosphorescence Lifetime Imaging; pO_2, Partial pressure of oxygen; PS, Photosensitizer; pSiNP, porous Silicon NanoParticles; ptrpy, 4′-phenyl-2,2′:6′,2″-terpyridine; PTT, Photo-Thermal Therapy; quasi tpy, 6-phenyl-2, 2′-bipyridine; RGD, Arginylglycylaspartic acid; ROS, Reactive Oxygen Species; TAP, 1,4,5,8-tetraazaphenanthrene; TLD-1433, [Ru(II)(4,4′-dimethyl-2,2′-bipyridine(dmb))2-(2-(2′,2″:5″,2‴-terthiophene) imidazo[4,5f][1,10]phenanthroline)]$^{2+}$; TP, Two-Photon; TPA, Two-Photon Absorption; TPE, Two-Photon Excitation; TPEF, Two-Photon Excited Fluorescence; TPEL, Two-Photon Excited Photoluminescence; TPIP, Two-Photon Induced Photopolymerization; TPM, Two-Photon Microscopy; TP-PACT, Two-Photon PhotoActivated Chemotherapy; TP-PDT, Two-Photon PhotoDynamic Therapy; tpphz, tetrapyrido[3,2-*a*:2′,3′-*c*:3″,2″-*h*:2‴,3‴-*j*]phenazine; TREM, Time-Resolved Emission Microscopy; αvβ3 Integrin, a glycoprotein membrane receptor, upregulated in many types of tumors; η2, Two-Photon Luminescence Quantum Yield; σ_{EN}, electron-normalized cross-section (σ_{TPA} divided by the number of π electrons); σ_{TPA}, Two-Photon Absorption Cross-Section.

E-mail address: jean-luc.fillaut@univ-rennes.fr.

https://doi.org/10.1016/j.ccr.2024.216050
Received 13 May 2024; Accepted 22 June 2024
Available online 7 July 2024

1. Introduction

Two-photon absorption (TPA) [1,2] is a nonlinear optical process wherein a molecule absorbs two photons of low energy simultaneously, regardless of whether their frequencies are identical or different. Indeed, unlike conventional single-photon absorption, TPA occurs when the combined energy of two photons meets the energy required for the transition. This process has received considerable attention, experimentally as well as theoretically, owing to recognized advantages that encompass the capacity for precise spatiotemporal excitation control and three-dimensional resolution, coupled with enhanced penetration depth into tissues or materials, all while minimizing damages to samples, whether biological or material. These advantages fulfill the criteria for applications ranging from materials science to healthcare, such as microfabrication [3–8], 3D optical data processing and storage [9–16], bio-imaging [14,17,18], and photodynamic therapy [19–23].

After setting out the fundamental principles of two-photon absorption and the engineering of molecules and materials with two-photon absorption abilities, this review presents how these principles apply to the design of two-photon-active polypyridyl ruthenium complexes. The more substantial parts of this review describe current advances on the design of functionalized materials with precise specifications for developments in advanced materials, bio-imaging and in-cell phototherapies.

2. Theory of two-photon absorption

2.1. Fundamental principles

Two-photon absorption involves the simultaneous absorption of two low-energy photons by a molecule, irrespective of whether their frequencies are the same (υ) or different (υ1 and υ2). It results in the activation of a resonant excited state with an energy equivalent to 2hυ or $h\upsilon_1 + h\upsilon_2$ (Fig. 1) [1]. The combined energy of these photons matches that typically required for exciting the fluorophore through conventional one-photon absorption (OPA) processes at high energies. However, the probability of two-photon excitation is notably lower compared to one-photon excitation, and substantial two-photon excitation only occurs within regions of high temporal and spatial photon concentration (as depicted in Fig. 1a) [24–26].

The spatial distribution of photons can be precisely densified in a specific area, a diffraction-limited spot, by using a high numerical aperture objective to focus the laser light. Similarly, achieving high temporal photon density involves the utilization of ultrashort pulsed lasers instead of continuous-wave illumination. By concentrating in both space and time, the occurrences of multi-photon absorption are significantly heightened. So, two-photon absorption plays a pivotal role in super-resolution imaging and spectroscopy due to this enhanced probability. Moreover, as two-photon excitation employs longer wavelength light, it exerts less damage on materials or living cells, thereby minimizing issues associated with fluorophore photodamage or photobleaching.

Powerful two-photon absorbers are requested in the applications mentioned above [25,26]. Such absorbers are characterized by a large two-photon absorption cross-section, denoted as σ_{TPA}, which is directly related to the imaginary part of the second-order hyperpolarizability 3D tensor γ [27]. This parameter, expressed in Goeppert-Mayer units (GM, 1 GM = 10^{-50} cm^4.s.photon^{-1}.molecule^{-1}) [1] reflects the probability of the excited state to be reached upon two-photon absorption, as the molecular absorption coefficient ε does in one-photon absorption.

The determination of TPA cross-section σ_{TPA} is thus key for assessing the excitation capabilities of the two-photon absorbers. The most commonly employed techniques for this determination are the open aperture Z-scan method [28] and two-photon excited fluorescence (TPEF) method [29,30] using ultra-short laser pulses. However, it's noteworthy that comparing σ_{TPA} acquired through these methods

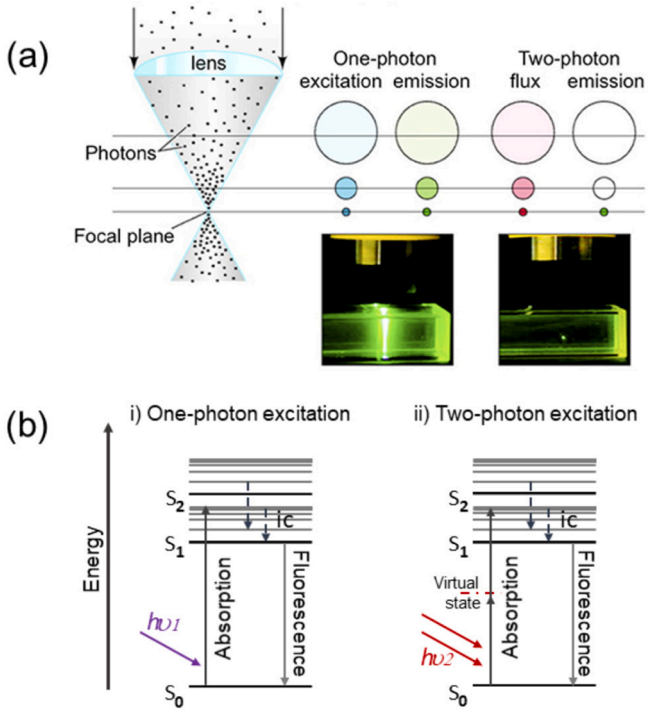

Fig. 1. Comparison of one- and two-photon processes. (a) As one-photon absorption occurs at low intensities of light, fluorescein molecules become excited uniformly across each z-section, following the Beer-Lambert attenuation law for light propagation along the z-axis. Most of the incident light is absorbed as it enters the sample and fluorescence can be seen everywhere along the path of the light. By contrast, excitation occurs only at the focus for a two-photon irradiation in the near infrared: as light is focused by a lens, the closer the molecules to the focal point, the more photons they are exposed to. Consequently, emission is localized: owing to the nonlinear interaction between light and matter, the excited region is confined to the focal volume of the laser light, known as the voxel. Adapted with permission from Ref. [24]. Copyright 2011 American Chemical Society. (b) Simplified Jablonski diagram: in one-photon absorption, light transitions directly from the ground state (S0) to the excited state (S1) through the absorption of a single photon (hυ1). However, in the case of two-photon excitation, this transition proceeds through a "virtual state" before reaching the excited state (S1), involving the absorption of two photons (hυ2).

requires careful consideration, as they may exhibit discrepancies of up to one order of magnitude [31–33]. Additionally, the data obtained from different laboratories can be difficult to compare because of variations in measurement techniques, pulsed lasers, and experimental conditions. External factors such as the duration of the pulsed laser source, spatial and temporal fluctuations of the laser beam, and the excitation wavelength can significantly influence the two-photon absorption characteristics of a system.

The Z-scan method (Fig. 2a) consists in scanning a sample along the focal axis of a laser beam and recording the transmittance relative to the sample localization, connected to the focal point changes [34]. This technique yields two measurable indexes: the nonlinear absorption (NLA) and the nonlinear refraction (NLR). These values, correlated to the imaginary and real parts of the 3rd nonlinear susceptibility $\chi^{(3)}$, give valuable insights into the two-photon properties of the sample. The Z-scan method, which is applicable to both fluorescent and non-fluorescent samples, is widely employed in material characterization due to its simplicity, high sensitivity, and well-developed theory. However, this transmission method should be used with caution, as it can be influenced by orientational, electronic and thermal effects [28,32,35,36]. A precise understanding of the laser beam features (such as average power, peak power, repetition rate, pulse duration, and

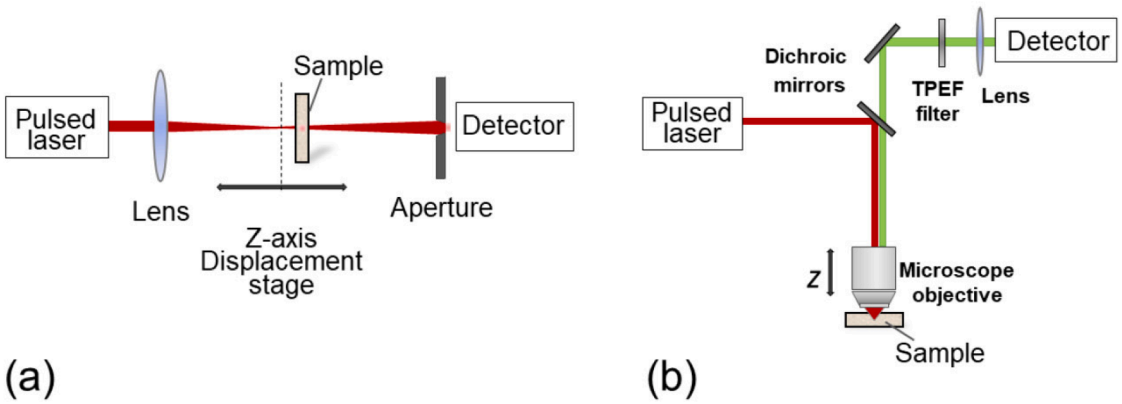

Fig. 2. (a) The Z-scan experiment entails moving a sample along the trajectory of a concentrated laser beam (the *z*-axis) and recording the light brightness at the detector as a function of its position along this *z*-axis [34]. (b) The measurement of two-photon excited fluorescence requires a pulsed laser to produce high energy fs pulses; the laser beam is directed onto the sample cell via a microscope objective; the resulting two-photon emission fluorescence is collected at 90° and directed onto a detection unit using a lens [29].

shape) is essential, in this context.

An alternative approach for determining two-photon cross-sections, albeit limited to luminescent molecules, is two-photon excited fluorescence, as illustrated in Fig. 2b. In TPEF, a high-intensity pulsed laser is used to excite the sample via two-photon absorption. The efficiency of two-photon excitation greatly relies on the space and time coherence of laser pulses, which typically fluctuate across the laser's tuning range. Hence, precise corrections are applied to derive the pure molecular two-photon absorption spectral shape and absolute cross-section values. These corrections can be achieved through either absolute or relative measurement methods [37–39]. In the absolute method, laser features such as power, pulse duration, shape, and spatial profile of the beam (*i.e.*, intensity distribution within the sample solution's x, y, and z coordinates) must be specified at each wavelength. Conversely, the relative method involves comparing the sample's emission with that of previously characterized reference standards (e.g., fluorescein, rhodamine) with known TPA cross-sections across a range of wavelengths, under identical excitation and fluorescence registration conditions [30].

There are no discernible differences in the emission spectra between one-photon excited fluorescence (OPEF) and two-photon excited fluorescence (TPEF), as both one-photon and two-photon excitation processes lead to similar excited states within the fluorophore molecule. As a result, the subsequent relaxation pathways and emitted photons may not exhibit distinctive differences between OPEF and TPEF. Typically, TPEF necessitates low molar concentrations of the probe (in the range of 10^{-4}–10^{-5} M) and a low-power femtosecond pulsed laser (up to 100 GW.cm^{-2}). For an accurate σ_{TPA} determination, it is crucial to ascertain the quadratic power dependence, to avoid overestimating σ_{TPA} due to fluorescence contributions induced by OPA. Indeed, when the excitation energy approaches the lower energy absorption band, one-photon absorption predominates, leading to a notable enhancement of fluorescence intensity and consequently to an overestimation of σ_{TPA} [40].

2.2. Molecular design

A primary challenge in the field of two-photon absorption lies in discovering novel molecular configurations that exhibit efficient TPA capabilities. Typically, two-photon cross-sections are very small, often around 1 GM or even less. Consequently, intense efforts have been directed towards identifying molecules and materials with substantially larger TPA cross-sections at the wavelengths of available laser sources. Higher TPA cross-sections make it possible to avoid using extremely high-power laser excitation, which can potentially induce damages on materials or biological tissues. Both experimental investigations and theoretical simulations provided valuable insights into designing π-conjugated molecules with high TP cross-sections [40–47]. The main strategies include: i) extending the π-conjugated system between the donor (D) and acceptor (A) units; ii) strengthening the donor–acceptor interactions while maintaining the flatness and rigidity of the π-conjugated assembly to favor charge transfer; iii) integrating multi-dipolar, quadrupolar or even octupolar arrangements into the chromophore. It was observed that TPA is notably influenced by the photoinduced intramolecular charge redistribution occurring within multipolar conjugated systems [43,46,48], while symmetrical quadrupolar and octupolar compounds tend to demonstrate improved TPA compared to their dipolar counterparts [49]. In particular, there has been increasing interest for octupolar systems, that either result of the projection of a cubic structure on a C_3 axis, resulting in D_{3h} or D_3 symmetries, or from fusing one of the charges into the barycenter, leading to D_3, T_d or D_{2h} symmetries (Fig. 3).

2.3. Metal complexes as NLO chromophores

Coordination chemistry is a valuable approach to design molecules with interesting nonlinear optical (NLO) activities [51–54]. Organometallic and coordination complexes present a wide variety of molecular structures in which the central metal ions not only contribute to high environmental stability but also act as electronic bridges and afford a broad spectrum of photophysical properties crucial for nonlinear optical activity. In particular, complexes possess a large panel of charge transfer transitions such as: *i)* Metal-to-ligand charge transfer (MLCT) at relatively low energy. *ii)* Ligand-to-metal charge transfer (LMCT) [mainly for complexes with metals in high oxidation numbers]. *iii)* Intra-ligand charge transfer (ILCT) transitions. All these distinctive charge transfer processes participate to improve the efficiency of electronic delocalization which is seen as a key to improving NLO performance. In addition, the prospect of multi-functional materials incorporating metal complexes is promising, enabling us to envisage combinations of optical non-linearity with magnetic, optical or electrical properties [55,56].

Among the wide choice of metal complexes investigated, coordination complexes featuring nitrogen-heterocyclic ligands, like bipyridines, terpyridines, phenanthrolines… have received increasing attention as chromophores to form nonlinear optical materials. This interest predominantly stems from their photophysical and photochemical characteristics, which are generally associated with intense MLCT or ILCT excitations. In addition, these properties can be adjusted by modifying the nature and the number of pyridyl or polypyridyl ligands surrounding the central metal atom. Finally, bipyridyl ligands excel as fundamental elements for the design of push–pull and octupolar metal complexes [57–59] of D_3 symmetry like $[M(bpy)_3]^{n+}$ or tetrahedral D_{2d} symmetry

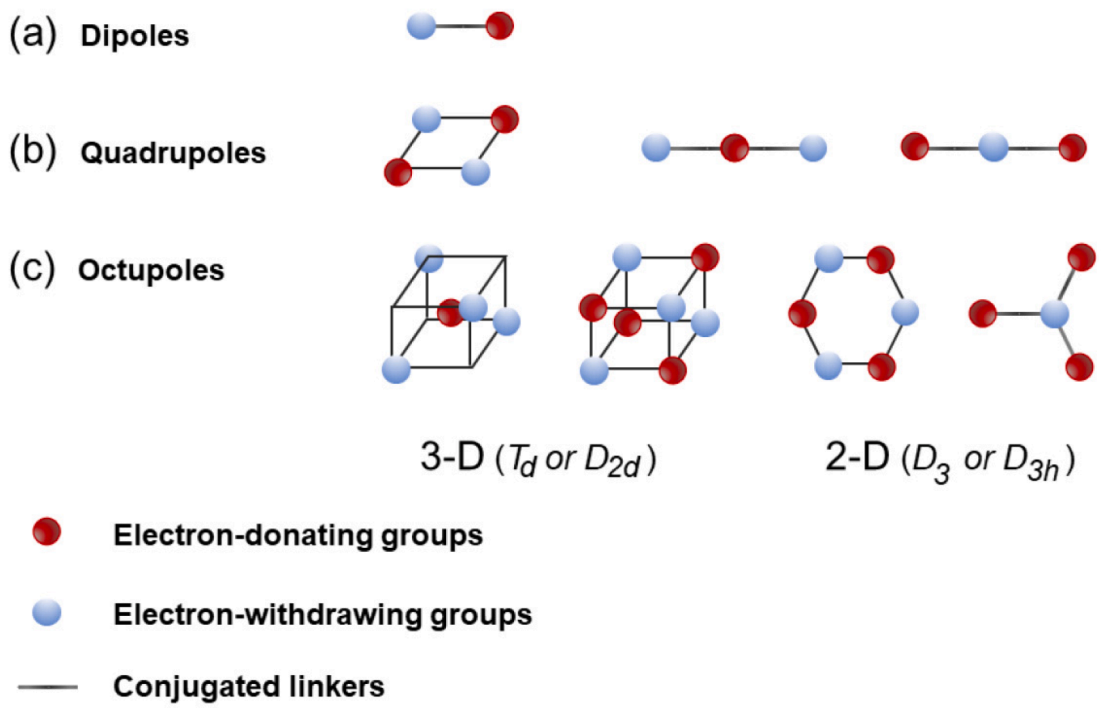

Fig. 3. Representation of the main classes of NLO chromophores. An octupolar arrangement is characterized by a cubic structure where donor and acceptor groups alternate along its edges. The projection of this cubic structure gives rise to configurations exhibiting D_{3h}, D_3, T_d, or D_{2d} symmetries [50].

like $[M(bpy)_2]^{n+}$ [51,60–63]. On the other side, introducing electron donor and acceptor substituents onto the bipyridine ligands induces an asymmetric molecular arrangement, potentially amplifying NLO responses. The pivotal influence of the metal ion lies in its ability to increase the charge transfer nature at the excited state [63]. Finally, the NLO responses are enhanced in the case of multipolar systems thanks to the proliferation of multidirectional ILCT excitations and MLCT transitions [54,63–67].

2.4. Design of d^6 Ru (II) polypyridyl complexes for two-photon absorption

The interest in Ru (II) polypyridyl complexes lies in the diversity of their photochemical, photophysical and redox properties, as well as photobiological properties, which can be easily regulated via well-established synthetic routes. $[Ru(bpy)_3]^{2+}$ and its derivatives have been extensively investigated in the fields of photocatalysis [68], photovoltaics [69], phosphorescent sensing [70], imaging [71,72] or phototherapy [70,73,74]. Whatever the field, the properties of these systems are closely related to the generation of various classes of excited states, upon absorption of photons of appropriate energy [75].

The octahedral configuration of ruthenium polypyridyl complexes, coupled with the significant overlap between the metal *d*-orbitals and the ligand orbitals, has stimulated interest in studying the nonlinear optical properties of these compounds. F. Castellano, J. R. Lakowicz et al. were the first to demonstrate that MLCT excited states of Ru (II) bipyridyl compounds can be generated through multi-photon processes (Fig. 4 right) [76]. Investigation on steady-state and time-resolved photoemission induced by two-photon excitation (TPE) of both $[Ru(bpy)_3]^{2+}$ **1** and $[Ru(bpy)_2(dcbpy)]^{2+}$ **2**, where dcbpy represents 2,2′-bipyridine-4,4′-dicarboxylic acid (Fig. 4, left), were conducted. For each complex, two-photon excitation produced identical emission spectra and single-exponential decays compared to one-photon excitation across various temperatures and solvents. Linear dependence was observed at 440 nm, while within the wavelength range of 820–900 nm, both complexes exhibited TPE, evidenced by a quadratic dependence of emission intensity on incident power. The TPE cross-section, defined as the product of the two-photon luminescence quantum yield ($\eta 2$) and two-photon absorption cross-section σ_{TPA}, was determined as 4.3 GM for $[Ru(bpy)_3]^{2+}$ in water at 880 nm, using Rhodamine B as the reference. Efforts to measure the two-photon excitation cross-section of $[Ru(bpy)_2(dcbpy)]^{2+}$ were unsuccessful due to its extremely low photoluminescence response.

Few years later, Yamagishi evaluated the two-photon excited emission properties of tris(4,7-diphenyl-1,10-phenanthroline)-ruthenium (II) perchlorate $[Ru(dpp)_3]^{2+}$, upon 830 nm excitation [77]. Noteworthy, the maximum of the two-photon absorption cross-section was slightly blue-shifted in comparison to the one-photon absorption maximum occurring at double the wavelength. This blue shift was attributed to parity selection rules,[1] favoring excitation to energy levels higher than those induced by one-photon transitions [78].

The relationships between the TPA properties and molecular structures in diimine ruthenium complexes remain largely unestablished. In a much recent paper, A. Rebane et al. explored the two-photon absorption of Ruthenium(II) tris(2,2′-bipyridine) ($[Ru(bpy)_3]^{2+}$) **1** and Ruthenium (II) tris(1,10-phenanthroline) ($[Ru(phen)_3]^{2+}$) **3** (Fig. 5) [79]. The TPA spectrum of $[Ru(bpy)_3]^{2+}$ exhibits a prominent band with a λ_{max} of of ~885 nm, almost double the wavelength of the ^{1}MLCT OPA maximum (450 nm), along with two much weaker bands at around 800 nm and 740 nm. The TPA cross-section was estimated at 56 GM in water. A clear decrease of the cross-section was observed in aprotic or less polar solvents ($\sigma_{TPA} = 32$ GM in DMSO; $\sigma_{TPA} = 27$ GM in ACN; $\sigma_{TPA} = 26$ GM in DCM).

Studies on tris(bipyridine)ruthenium(II) complexes have shown that changing the counter anion can lead to detectable changes in their absorption and emission spectra. These changes were attributed to different degrees of ion pairing and solvation effects, which ultimately

[1] Two-photon processes can be viewed as sequential one-photon transitions. Whereas Laporte's selection rules dictate that one-photon dipolar transitions should only occur between states of different parity (gerade-ungerade transition), two-photon transitions are only allowed between states of the same parity (gerade-ungerade transition).

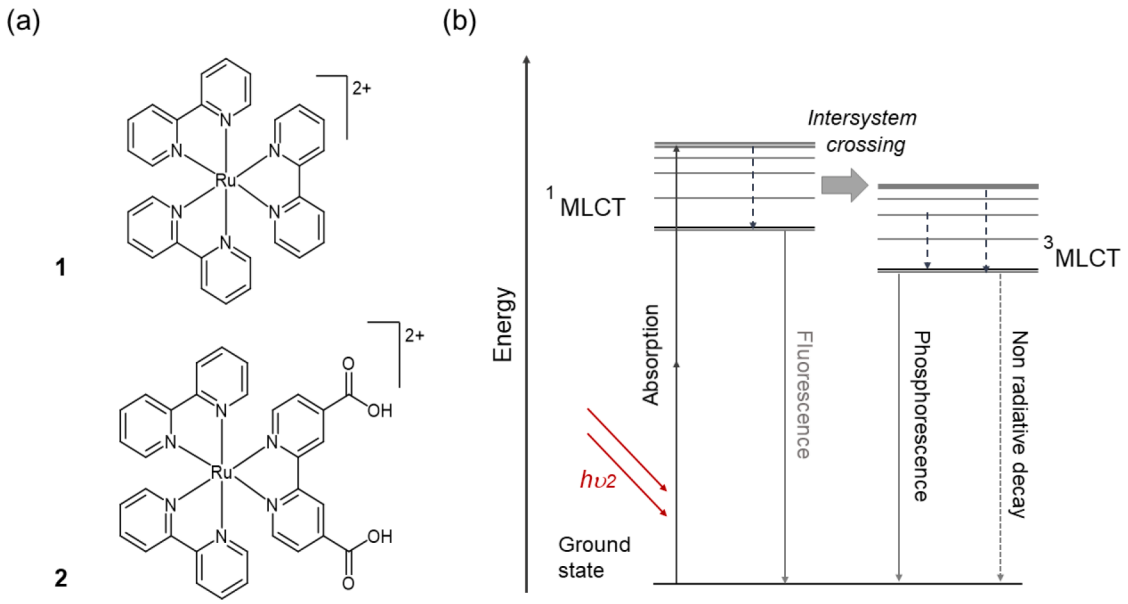

Fig. 4. (a) Chemical structures of $[Ru(bpy)_3]^{2+}$ **1** and $[Ru(bpy)_2(dcbpy)]^{2+}$ **2**, dcbpy represents 2,2′-bipyridine-4,4′-dicarboxylic acid [76]. (b) A simplified Jablonski diagram illustrating two-photon excitations of $[Ru(bpy)_3]^{2+}$-like complexes. Two-photon excitation involves transitions between the ground state and vibrational levels of the first electronic excited state. The fluorophore relaxes to the lowest energy level ^{1}MLCT via vibrational processes, then undergoes intersystem crossing to the lowest triplet state ^{3}MLCT, from which emission occurs. The following steps are thus the same for both one- and two-photon excitations.

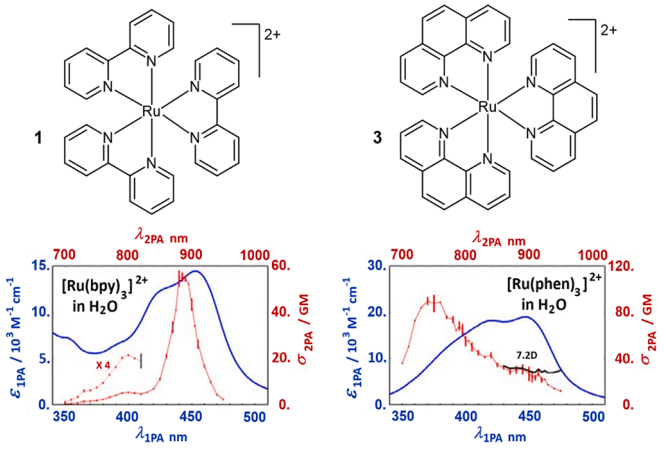

Fig. 5. (a) Structures of $[Ru(bpy)_3]^{2+}$ (left) and $[Ru(phen)_3]^{2+}$ (right). (b) OPA (blue) and TPA (red) spectra of the $[Ru(bpy)_3]^{2+}$ (left) and $[Ru(phen)_3]^{2+}$ (right) complexes in water. The black line (right) indicates the dipole moment calculated for the phenanthroline complex. Adapted with permission from Ref. [79]. © (2018) The Authors. Published by Society of Photo-Optical Instrumentation Engineers (SPIE).

affect the electronic structure of the complex. As far as we know, no mention has been made of such considerations with regard to the two-photon properties of Ru(II) based TPPs.

The TPA spectrum of $[Ru(phen)_3]^{2+}$ appears very different. It features a broad profile with a λ_{max} around ~750 nm, this peak is notably shifted towards the blue end of the spectrum compared to the corresponding OPA ^{1}MLCT maximum (450 nm). The cross-section of this band is 83 GM, in water, that is larger compared with $[Ru(bpy)_3]^{2+}$ (σ_{TPA} = 56 GM). Finally, the cross-section values indicate a much slighter decrease than was the case for $[Ru(bpy)_3]^{2+}$ when aprotic or less polar solvents are used ($[Ru(phen)_3]^{2+}$: σ_{TPA} = 93 GM in DMSO; σ_{TPA} = 73 GM in ACN; σ_{TPA} = 54 GM in DCM). Taking these results together, the authors suggested that the larger differences between the TPA spectra of $[Ru(bpy)_3]^{2+}$ and $[Ru(phen)_3]^{2+}$, in view of their almost similar OPA spectra, would result from alternative parity selection rules for the two complexes, depending on structural differences in the ground state.

The ground state of $[Ru(phen)_3]^{2+}$ complex would appear close to the expected D_3 symmetry. Consequently, one-photon absorption would occur between orbitals of opposite parity, while two-photon absorption would be allowed between orbitals of similar parity, making them mutually exclusive. However, for $[Ru(bpy)_3]^{2+}$, the presence of an intense band at approximately 885 nm, nearly twice the wavelength of the OPA ^{1}MLCT maximum, suggests no such selection limitation. These results are in agreement with the assumption that $[Ru(bpy)_3]^{2+}$ adopts a distorted D_3 geometry in the ground state, even in relatively nonpolar solvents, which may result from the greater flexibility of bipyridyne ligands compared to phenanthroline ligands [80].

Enhancing the two-photon absorption properties of diimine ruthenium complexes involves optimizing the ligands, a crucial step in the process. Various studies have rationalized the impact of introducing electron-donor and electron-acceptor substituents on the bipyridine ligands to modulate the TPA responses of d^6 Ru (II) polypyridyl complexes. For instance, B. J. Coe et al. studied the two-photon absorption behavior of a series of Ru (II) complexes featuring N-methyl/aryl-2,2′:4,4″:4′,4‴-quarter-pyridinium ligands (Fig. 6) [81]. They carried out Z-scan measurements at 750 nm, in DMF solutions. This wavelength was chosen to avoid excessive one-photon absorption.

The Z-scan measurements for these Ru (II) complexes resulted in TPA cross-sections σ_{TPA} of ca. 62–180 GM. The cross-section values for compounds **5**–**8** compared with compound **4** (Fig. 6) highlighted the importance of charge redistribution involving the peripheral groups and the central metal core in this series of complexes. Specifically, when peripheral electron-donor groups are absent, these ruthenium complexes do not exhibit ILCT transition but MLCT.

All pyridinium compounds **5**–**8** showed TPA cross-sections at least ten times higher than those of complex **4** (σ_{TPA} = 5 GM) at 750 nm. Then, B. J. Coe et al. reported the two-photon absorption cross-sections of trinuclear $RuPt_2$ and heptanuclear $RuPt_6$ complexes, which were synthesized by appending Pt(II) 2,2′:6′,2″-terpyridine (tpy) units to Ru (II) 4,4′:2′,2″:4″,4‴-quaterpyridine (qpy) complexes (Fig. 7) [82]. These TPA cross-section values were obtained by the Z-scan technique spanning from 650 to 900 nm, enabling the extraction of both the real and imaginary components of the second hyperpolarizability γ. The absolute σ_{TPA} values measured for **11** (301 ± 23 GM) and **9** (523 ± 35 GM)

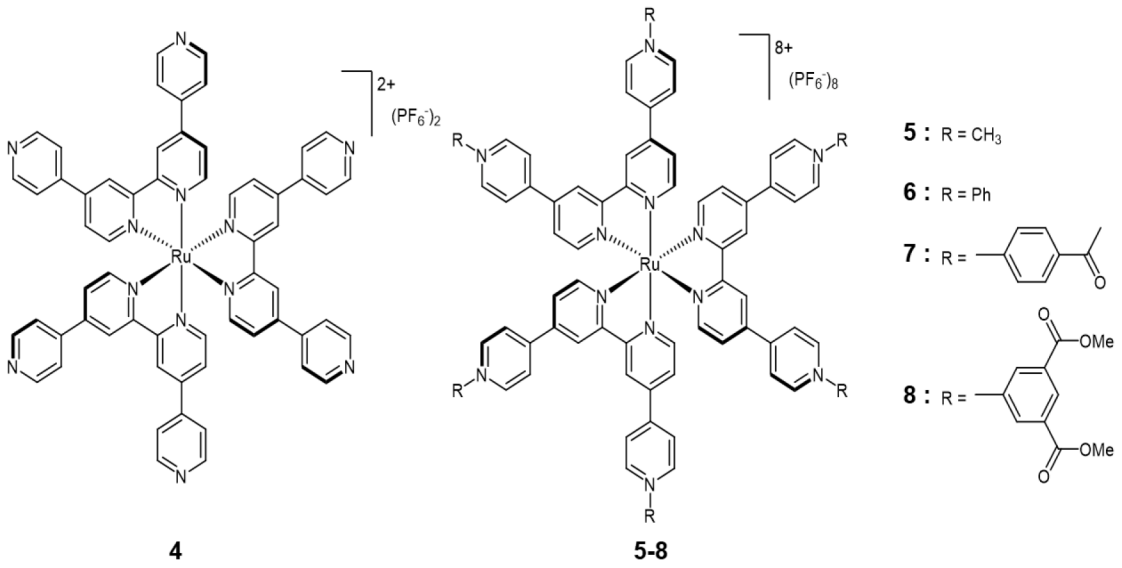

Fig. 6. Structures of Ru (II) complexes of quarter-pyridinium ligands studied by B. J. Coe et al. [81].

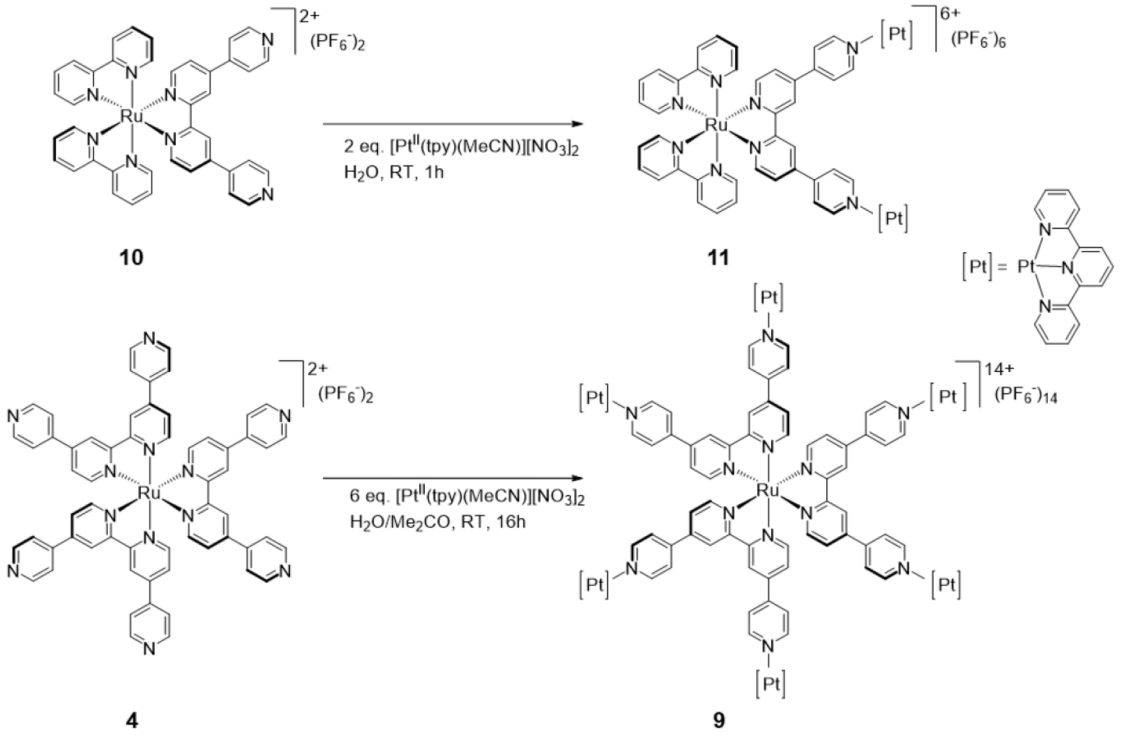

Fig. 7. Syntheses of $RuPt_2$ and $RuPt_6$ complexes obtained by linking Pt(II) 2,2′:6′,2″-terpyridine (tpy) moieties to Ru (II) complexes **4** and **10** [82].

substantially exceed those of their precursors **10** and **4** (83 ± 5 GM and 159 ± 17 GM respectively). The relatively large values for these trinuclear $RuPt_2$ and heptanuclear $RuPt_6$ complexes revealed the incidence of the complexation by Pt units and of the increased number of branches on these TPA properties.[2]

[2] Optimizing the TPA cross-section is not the only concern when conceiving a two-photon dye. Introducing the ratio σ_{TPA}/Ne (where Ne represents the number of π-electrons) [83] becomes invaluable, particularly when it comes to packing the maximum two-photon effect into the smallest possible chromophore. It may be more relevant to divide the σ_{TPA} value by factors such as the molecular weight, molecular volume, solubility limit or maximum number density (N) of the dye, depending on the specific application concerned.

The reported differences in σ_{TPA} values assessed by Z-scan for **4**, 5 ± 3 GM at 750 nm [81]; 159 ± 17 GM at 818 nm [82] respectively, are significant of the dispersion of these values over the range 650–900 nm, as illustrated in Fig. 8.

The same research team explored how the length of the polyene chain influences the two-photon characteristics of complexes incorporating ruthenium(II) pyridinium electron acceptor groups (Fig. 9) [84]. As the π-systems extended in the Ru series, from **12** to **14**, a total σ_{TPA} increase by over 24-fold was observed (**12**: σ_{TPA} = 62 ± 8 GM; **13**: σ_{TPA} = 720 ± 90 GM, **14**: σ_{TPA} = 1500 ± 170 GM assessed by Z-scan), while the σ_{TPA} for **15** is substantially larger σ_{TPA} = 2500 ± 250 GM at 750 nm.

At the same time, Le Bozec et al. showed that both the optical and nonlinear optical (NLO) properties of Ru (II) polypyridyl complexes are

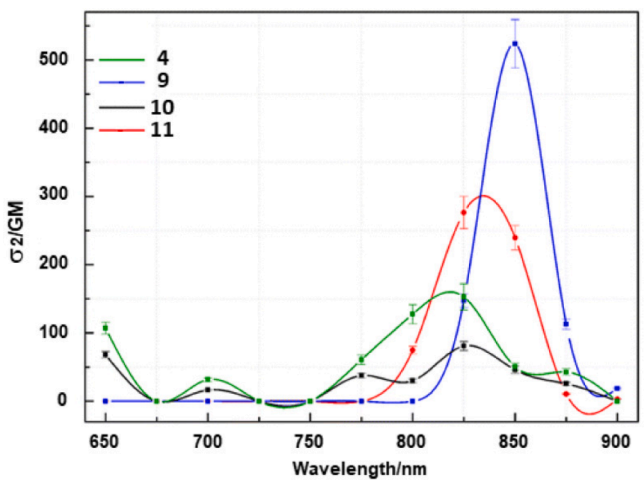

Fig. 8. TPA spectra for complexes **4**, **9**, **10** and **11**, assessed by Z-scan. Reproduced with permission from Ref. [82]. Copyright © 2015, American Chemical Society.

significantly affected not only by the length of the conjugated π linkers but also by the features of the end groups [64]. They reported a σ_{TPA} value of ca. 2200 GM for the complex **16** (Fig. 10), in which the Ru (II) center is connected to *N*-dialkylamine groups through stilbenyl bridges. This value, which was obtained by Z-scan measurements at 750 nm, is thus at least ten times higher than the maximum values reported for the pyridinium derivatives by Coe et al. [81]. Hence, substituting an electron-accepting N-methylpyridinium group with a di-*n*-butylamino donor significantly amplifies the two-photon absorption activity of corresponding Ru (II) polypyridyl complexes.

Finally, G. Lemercier et al. determined σ_{TPA} cross-sections of 90 GM at 750 nm and 120 GM at 830 nm, respectively for the 1,10-phenanthroline based Ru (II) derivatives **17** and **18** (Fig. 11) featuring six fluorenyl substituents, by using two-photon excited luminescence measurements [85]. **18** differs from **17** because of the presence of a triple bond between the 1,10-phenanthroline and the bi-fluorene moiety. These rather moderate values are likely due to constrained π-conjugation, together with inter-annular torsion in the extended ligands.

Altogether, these works illustrated the significance of intramolecular charge redistribution occurring between the metal core and the peripheral groups of the molecules. Additionally, studies conducted by H. Le Bozec [64] or B. J. Coe et al. [81] to name just a few, emphasized the critical role of the metallic core not only as a structural scaffold but also for its direct involvement in the nonlinear optical activity of the d^6 M^{II} polypyridyl complexes. Of course, the coordination provokes a substantial enhancement in the charge transfer character, at the excited state, thereby amplifying the two-photon absorption features of the complexes relative to those of the pare ligands. The role of the metal core, however, is still not fully elucidated. In particular, the conflicting contributions of both intervalence charge transfer and metal-to-ligand charge transfer, as depicted in Fig. 12, pose challenges in fully rationalizing all experimental findings when comparing the cross-sections of various metal polypyridyl complexes. Even minor distortions from the D_3 octupolar symmetry as well as an extended delocalization through the metal center should perhaps be envisaged to account for these differences.

Several methods were developed for the synthesis of heteroleptic polypyridyl ruthenium complexes [87]. Meanwhile, the TPA properties of heteroleptic complexes were far less investigated as a basic level. In the seminal paper by Coe et al. [82] (*vide supra*) maximal σ_{TPA} values of 83 ± 5 GM for the heteroleptic complex $Ru(L)(bpy)_2^{2+}$ **10** and 159 ± 17 GM for the "corresponding" homoleptic complex $Ru(L)_3^{2+}$ **4** (Fig. 7) were observed. Thus, the shift from the heteroleptic complex **10** to its homoleptic analog **4** resulted in a significant enhancement of the TPA cross-section. Meanwhile, this observation must be moderated by taking in account the electron-normalized cross-section σ_{EN} values of these complexes. These intrinsic cross-section values are obtained by dividing σ_{TPA} by the overall number of π electrons in the conjugated system, according to M. G. Kuzyk [83]. This leads to the normalization of the TPA cross-sections for the complexes **10** and **4**. Although they contain undoubtedly different numbers of extended ligands, these complexes display similar intrinsic cross-sections (σ_{EN} = 0.036 GM for **10** and 0.031 for **4**), within the limits of experimental uncertainty.

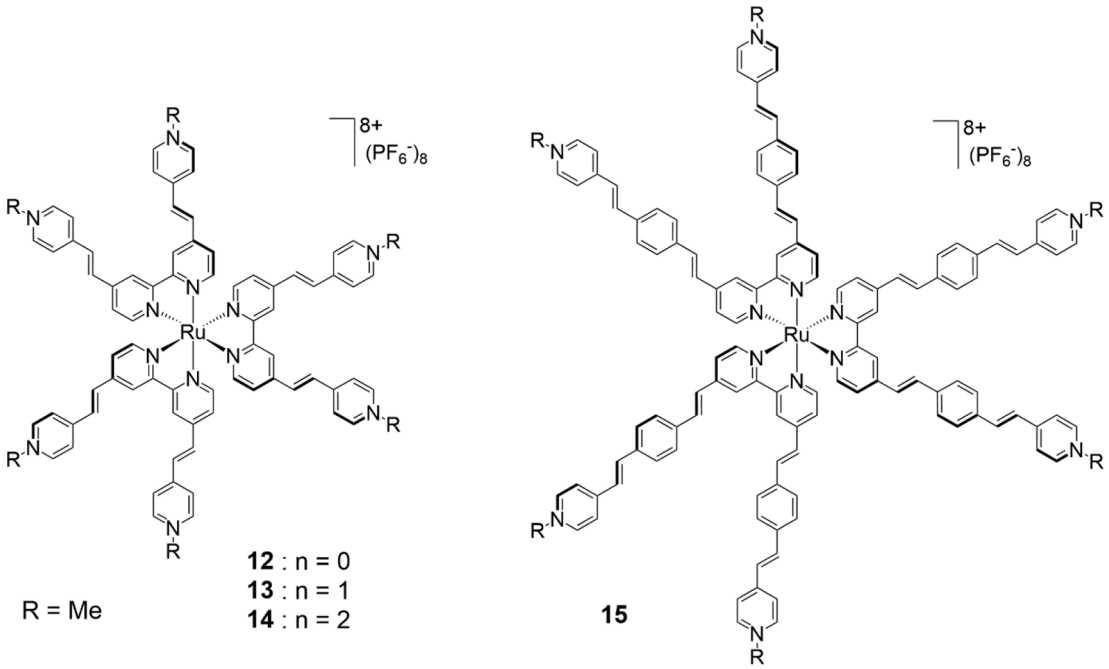

Fig. 9. Structures of complexes featuring $[Ru(bpy)_3]^{2+}$-like centers connected to six electron-accepting *N*-methyl-/*N*-arylpyridinium groups through π-extended bridges [84].

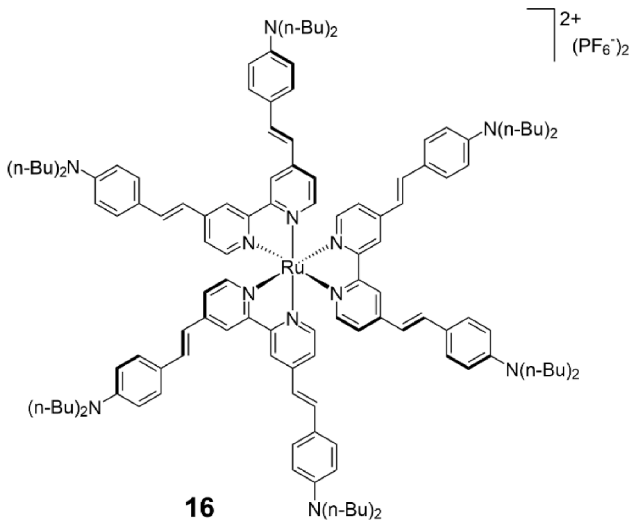

Fig. 10. Structure of complex **16** in which 6 dialkylamino units are linked to a $[Ru(bpy)_3]^{2+}$-like core via extended π-conjugated bridges [64].

Less studies focused on the TPA properties of Ru (II) complexes of 2,2′: 6′,2″-terpyridine (N^N^N), 6-phenyl-2, 2′-bipyridine (N^N^C) or their derivatives, abbreviated as tpy (N^N^N), or quasi-tpy (N^N^C). Xiao et al. reported on mixed (N^N^N) and (N^N^C) Ru (II) complexes (Fig. 13) [88], in which the tpy or quasi-tpy ligands act as acceptor units linked to carbazole appended moieties acting as peripheral electron-donating entities.

Their cross-section values were assessed through Z-scan technique in DMSO, utilizing femtosecond laser pulses (680–1080 nm, 80 MHz, 140 fs). The reported σ_{TPA} values of the cyclometalated Ru (II) complexes with X = C (3888 and 4747 GM) exceed those of their non-cyclometalated counterparts when X = N (from 1427 to 3766 GM). These findings could indicate that substituting the nitrogen donor with a formal carbanion donor significantly enhances the electron density around the metal ion, thereby reinforcing the overall intramolecular charge transfer and consequently the nonlinear optical capability of the complexes [89].

The two-photon absorption characteristics of a series of dinuclear complexes, where two $[Ru(bpy)_3]^{2+}$-like units are interconnected via oligothiophene bridges with varying numbers of rings (1, 3, and 6), were thoroughly examined by the Z-scan method using a tunable femtosecond laser (Fig. 14) [90]. The number of thiophene units was crucial for determining both the linear and nonlinear behaviors of these systems. Compounds featuring longer oligothiophene bridges with 3 and 6 thiophene rings exhibited no emission, whereas the compound featuring the shortest bridge (one thiophene unit) displayed remarkable photophysical characteristics. The ^{3}MLCT character of the lowest-energy triplet state was preserved while the luminescent features of the end-capping complexes were maintained in this compound with the shortest bridge. Conversely, for the compounds with a larger number of thiophene rings, the lowest triplet excited state assimilated to a non-emissive $^3\pi$-π^* state located on the conjugated oligothiophene part.

The TPA spectra of compounds **19**–**21** display closely matching peaks positioned at approximately 625 nm [90]. These peaks show a slight red shift compared to the reference compound $[Ru(bpy)_3]^{2+}$ **1**. This finding indicates that the TPA characteristics are primarily governed by the polypyridyl ruthenium moiety; at the same time, the observed shift suggests that the bridges also play a role in adjusting the two-photon absorption process. Moreover, there is a substantial increase in the σ_{TPA} values on going from reference compound **1** (85 ± 10 % GM) to compound **19** (870 ± 10 % GM). This notable increase of the TPA cross-sections was attributed by the authors to charge-transfer excitations involving both the π orbitals of the thienylene-based bridge and the Ru-dπ orbitals. Extending the conjugated system between the end-capping tris(bipyridine)ruthenium units leads to particularly large σ_{TPA} values (**20**: 1600 ± 10 % GM; **21**: 5200 ± 10 % GM), with compound **21** exhibiting the highest TPA activity for this series. This design strategy, wherein photoinduced charge transfer processes engage the π orbitals of the bridge and dπ orbitals of the metal center, suggests promising potential for boosting the TPA characteristics of materials with substantial optical non-linearity.

Another factor to take in account is the possibility of cooperative

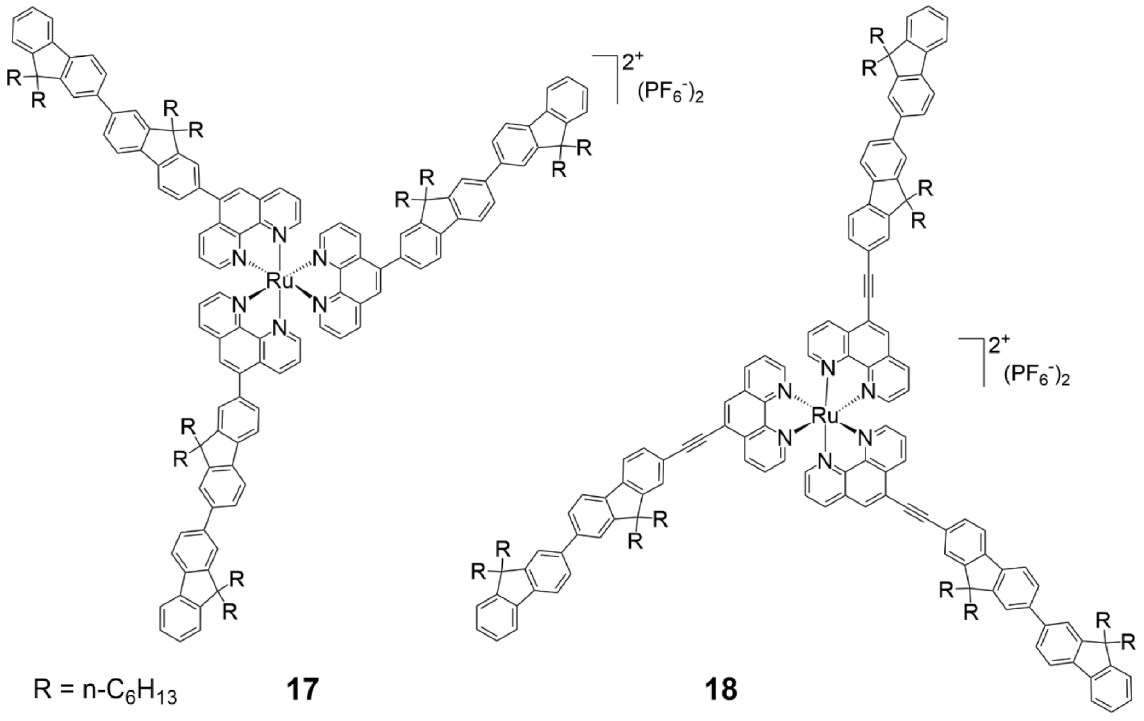

Fig. 11. Chemical structure of ruthenium (II) phenanthroline complexes linked to fluorene-substituted 1,10- ligands [85].

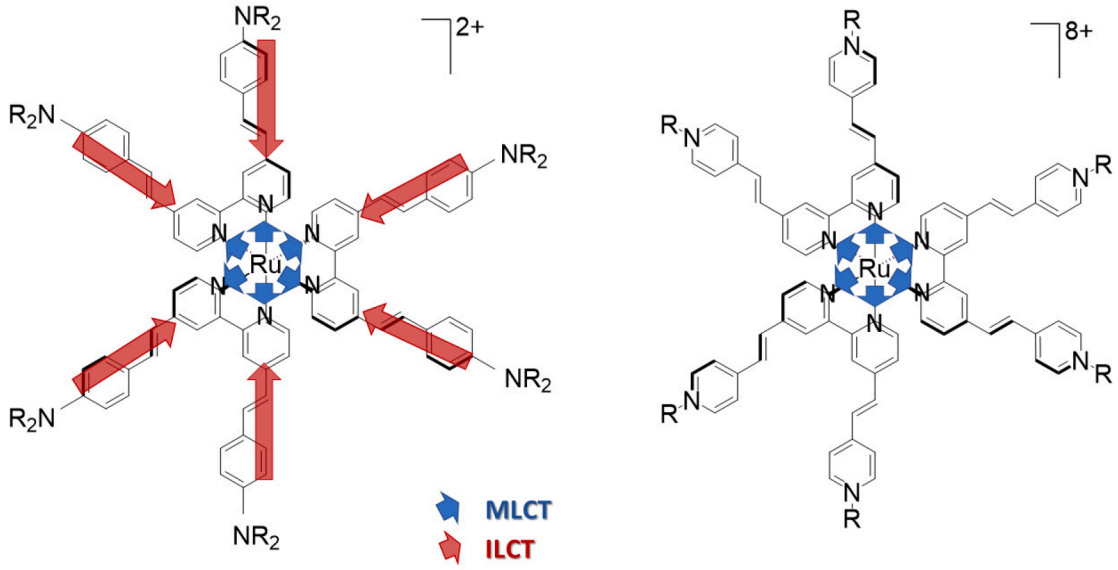

Fig. 12. ILCT (red arrows) and MLCT (blue arrows) directionalities within tris bipyridyl Ruthenium complexes in which the Ru (II) center is connected via π-conjugated bridges to *N*-dialkylamine or pyridinium end-groups: the ILCT transitions are directed from these end-groups to the central pyridyl groups, while the MLCT charge transfers occur from the metal center in the direction of the pyridyl groups. Therefore, the sum of the ILCT and MLCT contributions could result in non-coherent effects toward NLO properties [86].

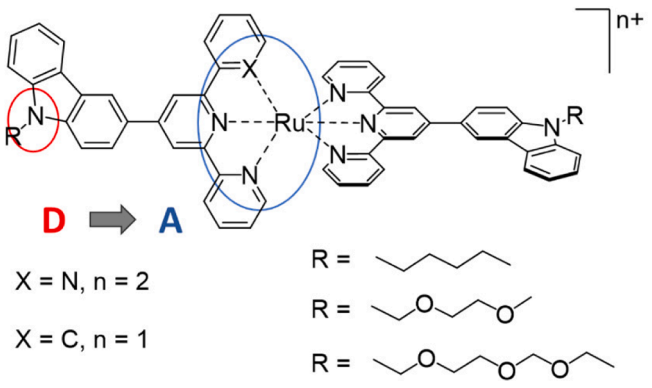

Fig. 13. Structures of 2, 2′: 6′, 2″-terpyridine (N^N^N), 6-phenyl-2, 2′-bipyridine (N^N^C) Ru (II) complexes studied by Xiao et al. [88].

effects between the ligands surrounding the metal center. In this way, J.-P. Malval et al. explored the impact of dimensionality on enhancing two-photon absorption in a range of homo- and heteroleptic bipyridyl $[RuL_n(bpy)_{3-n}]^{2+}$ complexes. These complexes featured 4,4′-substituted 2,2′-bipyridine ligands L, incorporating stilbenyl units with electron-rich arylamine moieties such as triphenylamine (L^T), carbazolyl (L^C) and diphenylaminofluorenyl (L^F) (Fig. 15) [92]. The ccordination with Ru^{2+} led to a substantial increase in the TPA cross-sections, by over six-fold compared to the free ligands and the corresponding homoleptic complexes. Additionally, the introduction of more π-extended stilbenyl-bipyridines resulted in elevated σ_{TPA} values, reaching up to 1465 ± 220 GM for $[Ru(L^T)_3]^{2+}$. These authors suggested that the significant enhancement in TPA resulted from a synergistic effect, which would combine the efficient increase in intramolecular charge transfer per branch with cooperative interbranch couplings throughout the entire multipolar structure. If $[Ru(L^T)_3]^{2+}$ demonstrated the highest TPA performance among its counterparts, the TPA performance of the carbazole series showed a similar trend but with a considerably weaker TPA increase. Finally, One of the most remarkable results concerns the diphenylaminofluorenyl series, where TPA performance rapidly reaches saturation for n = 2 and 3. In a more recent study supported by theoretical calculations [91], these authors concluded that elongating the π-conjugated system or strengthening the donor effect of peripheral moieties in the ligands promotes intraligand charge transfer as the primary factor driving TPA transitions. However, the number of π-extended ligands surrounding the metal is not the only factor to explain the TPA response of complexes, as suppressive or cooperative effects can arise from the contributions of metal–ligand charge transfer and ligand–ligand charge transfer, depending on the orientations of ILCT, MLCT and LLCT transitions.

The previous studies allowed key parameters of Ru (II) polypyridyl complexes in terms of TPA to be established. The number and the synergy of charge transfers obviously lead to significant increase in the intrinsic TPA properties for these compounds. In parallel, the importance of $[Ru(bpy)_3]^{2+}$-like complexes originates essentially from three key photophysical processes, namely initial photon absorption, rapid intersystem crossing and relaxation to the ^{3}MLCT triplet excited state [75,93,94]. These photophysical events can benefit from undeniable advantages resulting from the synthetic flexibility and facile functionalization of these complexes [72,75,95–99] while the high stability of polypyridyl ruthenium complexes favors their utilization in practical applications. The specific advantages of two-photon excitation – *i.e.* 3D spatial resolution, low photodamage, deeper penetration – applied to Ru (II) polypyridyl complexes have given rise to extensive research across various fields, including micro-fabrication [100–102], biological imaging or sensing [17,49,103,104], and photodynamic therapy [19–22]. An exhaustive overview of these applications lies well outside the scope of this review. We have chosen to limit ourselves to some examples that we considered to be particularly relevant. Key elements of these fields of research will be outlined to show how a combination with Ru (II) polypyridyl complexes with high TPA cross-sections could be an added bonus for these fields.

3. d^6 Ru (II) polypyridyl complexes as reliable tools for advanced materials processing

3.1. Two-photon induced microfabrication

Two-photon excitation is extensively utilized for building three-dimensional microscopic structures with sub-micrometer resolution

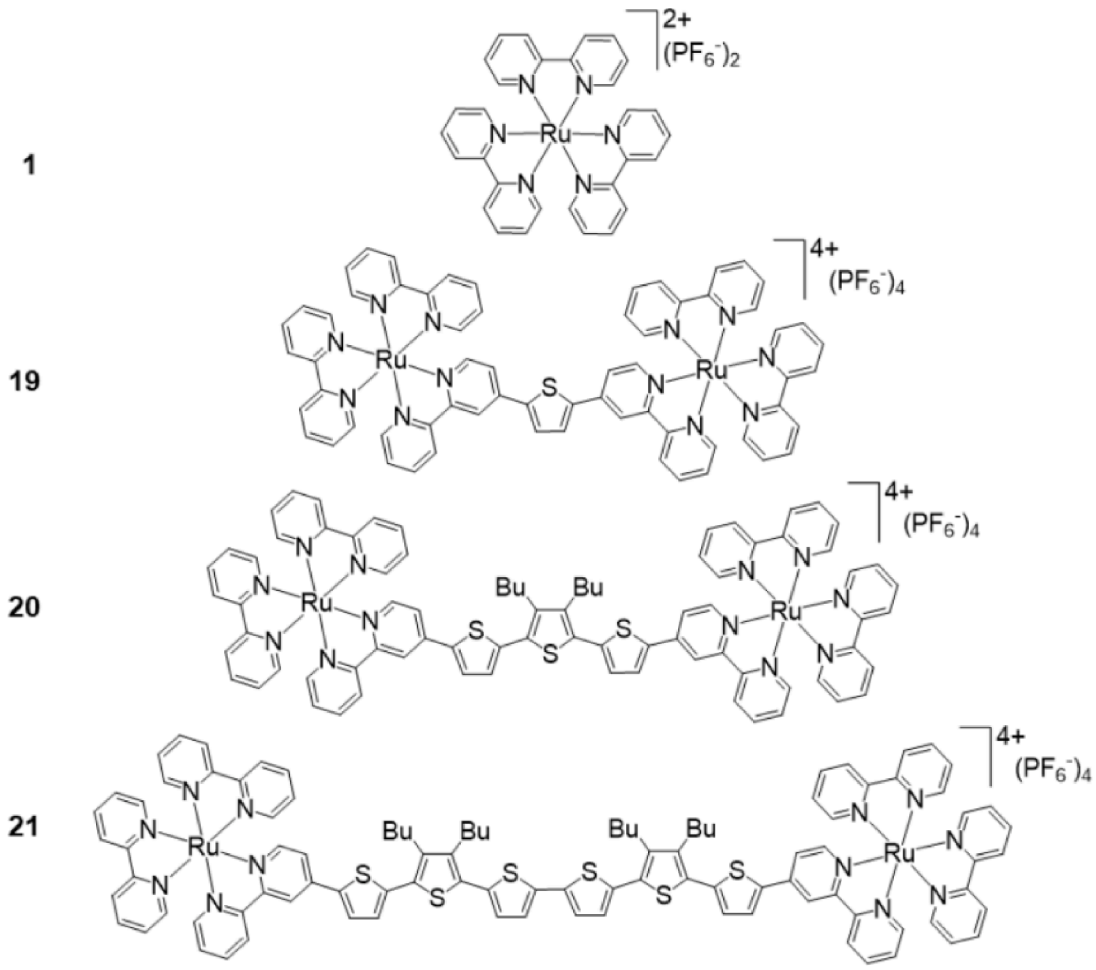

Fig. 14. Structures of $[Ru(bpy)_3][PF_6]_2$ (**1**) and dinuclear bridged complexes $[(bpy)_2Ru\text{-}bpy\text{-}nT\text{-}bpy\text{-}Ru(bpy)_2][PF_6]_4$ (**19–21**). *n*T: oligothiophene bridges with 1, 3 or 6 thiophene rings [90].

[105]. The most common method is the photopolymerization, where a pulsed laser with femtosecond-to-picosecond duration focuses into a photocurable resin. In order to create 3D micrometer-sized structures, precise sub-micrometer resolution is necessary when adjusting the displacement of the laser focal point in the resin, where the two-photon excitation triggers a programmable radical or cationic polymerization process. One definitive advantage of two-photon induced photopolymerization (TPIP) lies thus in its high spatial control, resulting from the precision of the photoactivated polymerization. On the other hand, the use of long wavelength excitation sources enables penetration at several tens of micrometers into the resin and limits thermal or photochemical side reactions, as the resin both above and below the focus is constantly exposed to low intensity, while the controlled displacement of the irradiation focal point allows the structure to be plotted (Fig. 16) [4,105].

The photocurable resin comprises two essential elements: the two-photon initiator and the monomeric resin [107,108]. Efficient two-photon absorption photo-initiators are required in order to achieve high writing speeds, a low polymerization threshold, and consequently, high quality structures. In addition to maximized TPA cross-sections, the efficiency of the photo-initiators depends on critical factors: minimum emission quantum yield (ϕ_F), high triplet quantum yield (ϕ_T), rapid initiation and appropriate solubility in the resin. From this point of view, coordination complexes used as photo-initiators offer wide opportunities for the fabrication of functional microstructures [109]. Several parameters can be taken in account: *i)* the absorption properties, encompassing both their absorption range and molar extinction coefficients. These features play a crucial role in minimizing the photo-initiator content. *ii)* the charge transfer nature at the excited state which contributes to enhance two-photon absorption [110]. *iii)* microsecond-to-millisecond range excited state lifetimes. By extending the excited state lifetime of photo-initiators, *i.e.* allowing longer time for the excited species to interact with the other components of the resin, the polymerization efficacy is enhanced. *iv)* their tunable electrochemical properties can be a key parameter for accelerating polymerization, by adjusting the photo-initiator's redox potential to favor redox reactions within the resin. Thus, using ruthenium polypyridyl complexes as photo-initiators for polymerization is well established [111–116]. In particular, the initiating system based on tris(2′-2′-bipyridine)dichloro-ruthenium (II) hexahydrate and sodium persulfate [117] has attracted wide interest in regenerative medicine and bioprinting [118–120]. This is related to its high molar absorptivity in the visible light range, enabling effective curing with a relatively low concentration of initiators [118].

In spite of these advantages, the number of reports of ruthenium polypyridyl complexes as photo-initiators in the field of two-photon microfabrication is rather limited. Most examples under this approach relate to the photo-induced polymerization of pyrroles [121–125]. Yamada et al. demonstrated the multiphoton-sensitized polymerization of pyrrole, using $[Ru(bpy)_3]^{2+}$ as a two-photon photo-initiator [126]. This approach was based on the photo-induced excitation of tris(2,2′-bipyridyl) ruthenium complex $[Ru(bpy)_3]^{2+}$ in presence of methyl viologen, which enables to generate $[Ru(bpy)_3]^{3+}$, a strong oxidant [127]. The resulting spatially localized oxidation power allowed the initiation of polymerization sequence of pyrrole. Multi-photon

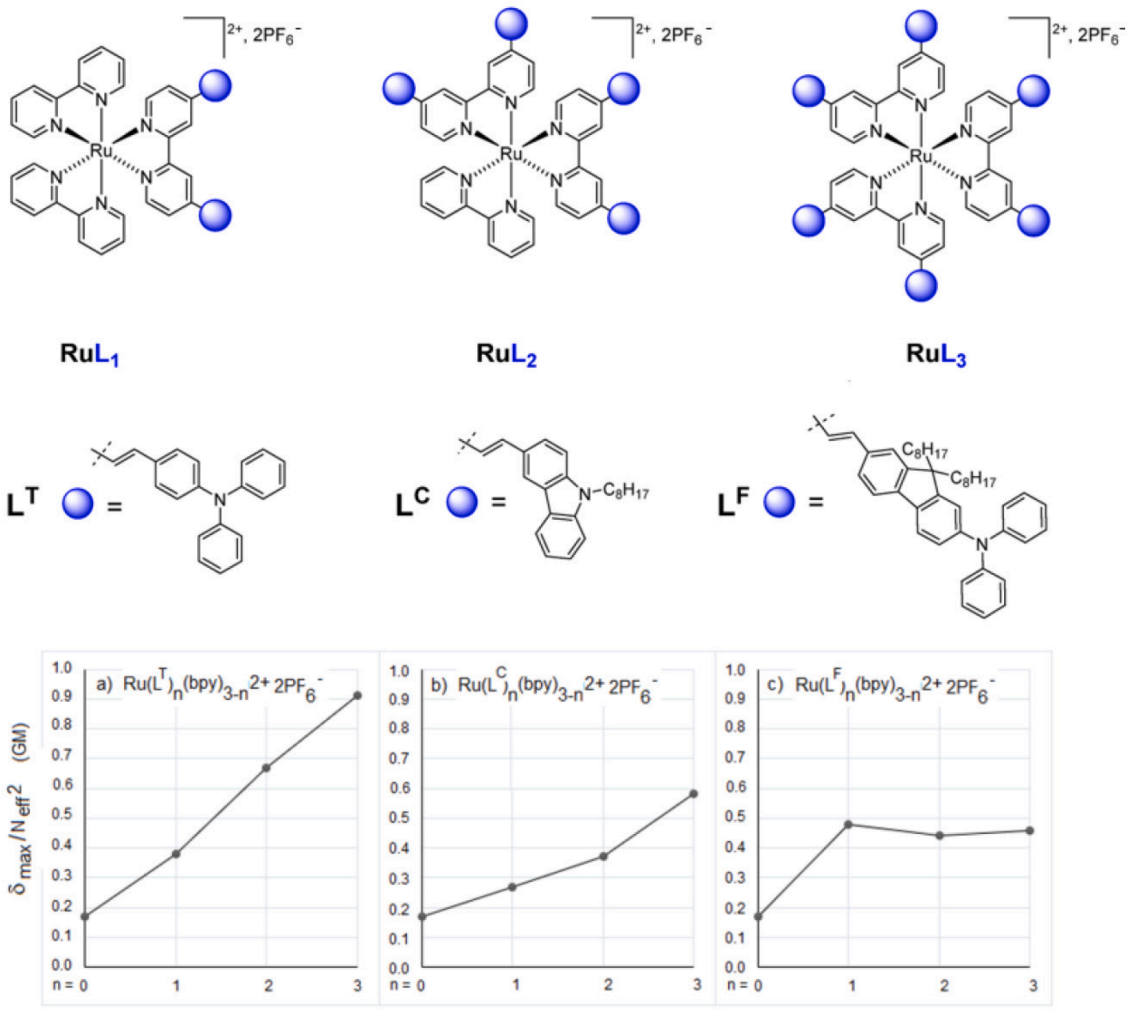

Fig. 15. Top: Illustration depicting both homoleptic and heteroleptic complexes $[RuL_n(bpy)_{3-n}]^{2+}$ (n = 0, 1, 2). Middle: Diagram showing the π-extending stilbenyl units present in bipyridines L^T, L^C, and L^F. Bottom: Graph illustrating the variation of intrinsic TPA cross-sections [83] as a function of the number of ligands, L^T (a), L^C (b), and L^F (c), in $[RuL_n(bpy)_{3-n}]^{2+}$ complexes. $Ru(bpy)_3^{2+}$ acting as a reference (n = 0). Adapted with permission from Ref. [91]. © 2022 The Authors. Licensee MDPI, Basel, Switzerland.

sensitized polymerization was only initiated at the focal point of a NIR femtosecond pulsed laser, resulting in the fabrication of conducting polymer-based 3D microstructures, with much higher patterning resolution (under 500 nm) than one-photon processes.

Similarly, employing $[Ru(bpy)_3^{2+}]$ as a photosensitizer enabled the multi-photon sensitized polymerization of polythiophenes [128]. This led to the fabrication of 3D poly-(3,4-ethylenedioxythiophene) (PEDOT) conductive micropatterns. However, photopolymerization of 3,4-ethylenedioxythiophene (EDOT) was unfeasible using this method due to its higher oxidation potential (+1.15 V vs. Ag/Ag^+) compared to $[Ru(bpy)_3^{2+}]$ (+0.62 V vs. Ag/Ag^+). Conversely, bis-EDOT, a dimeric compound of 3,4-ethylenedioxythiophene, proved suitable for this multi-photon photopolymerization method thanks a lower oxidation potential (+0.55 V vs. Ag/Ag^+). These differences are related to the fact that the photo-polymerization only occurs if the one electron transfer from $[Ru(bpy)_3^{2+}]$ to the ethylene-dioxythiophene species is exergonic.

In parallel to these studies, Stephan et al. explored the fabrication of gold microstructures using thin films of polystyrene sulfonate in its acidic form as a support [129]. These host polymer and ion-exchange materials enabled tetrachloroauric acid ($HAuCl_4$) to be homogeneously dispersed in the formulation, without reacting with the matrix. Photodeposition of gold was obtained upon a two-photon irradiation at 740 nm of $[Ru(bpy)_3]^{2+}$ used as the photo-initiator. Two-photon excitation of this dye generated the triplet excited state of $[Ru(bpy)_3]^{2+}$, which displays appropriate reducing properties towards the gold ions. This approach, which works at low laser powers, minimizes local heating, ensuring the creation of high-quality metal deposits on 3D structure surfaces. Additionally, nanoparticles formed during writing are directly immobilized in the polymer network, enhancing the stability of fabricated metallic microstructures.

The same research team reported on creating biocompatible and bioactive gelatin methacryloyl–collagen matrices through covalently linking ruthenium complexes [130]. These matrices were designed to continuously monitor oxygen levels (pO_2) at a cellular level. They utilized a two-photon polymerization 3D micro printer to construct these matrices. Strengthening the matrices involved increasing the cross-linking density with Gelatin methacryloyl (GelMA), which contained additional methacrylate photo-polymerizable groups. During two-photon polymerization, unsaturated methacryloyl groups formed covalently cross-linked hydrogels in the presence of dichloro-tris(1,10-phenantroline)ruthenium (II) as a photo-initiator. These unsaturated groups became covalently linked to the collagen fiber during the photo-initiated polymerization reactions. The resulting GelMA collagen matrices with covalently linked ruthenium complexes were utilized for directly monitoring local pO_2 during cell activity and tumor mass formation. The ruthenium complex served as a bio-optical oxygen probe, enabling quantitative measurement and imaging of oxygen levels through phosphorescence quenching [131].

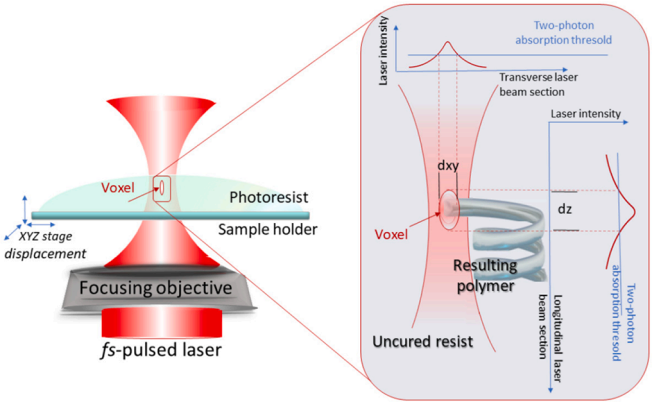

Fig. 16. Schematic representation of a two-photon induced microfabrication process illustrating how a spot, narrower than the width of the laser beam and located inside the resin, can undergo polymerization: a liquid photoresist is drop-cast onto a glass coverslip, which can be displaced in X, Y, or Z by a piezo system. The polymerization is initiated in the focal region, the voxel, of a photosensitive resin capable of cross-linking photoresist. As TPA is a non-linear process, the probability of absorption outside the voxel is low. Consequently, the reaction propagation is limited, which enables fine resolution Moving around the voxel results in the creation of intricate 3D structures that can be isolated after development. Laser operating at visible or near-infrared wavelengths enables to build mechanically stable structures with feature sizes ranging from 200 to 300 nm [106].

Based on their investigations on a range of $[RuL_n(bpy)_{3-n}]^{2+}$ heteroleptic complexes (Fig. 15), J.-P. Malval et al. developed a 'one pot' two-photon polymerization process for the photostructuration of ruthenium-based materials at the µm scale [132]. This approach was based on the design of two stilbenyl π-conjugated ruthenium-based two-photon photo-initiators $[Ru(bpy)_2L]^{2+}$ complexes (Fig. 17) [92].

These complexes demonstrated both high two-photon absorption cross-sections: $\sigma_{TPA} = 312 \pm 47$ GM for $[Ru(bpy)_2L^T]^{2+}$ and 597 ± 90 GM for $[Ru(bpy)_2L^F]^{2+}$ at λmax ~ 800 nm and ~850 nm respectively. Additionally, they exhibited efficient quantum yields allowing the generation of reactive species to promote monomer cross-linking. Their two-photon excitation in the presence of acrylate resins rapidly generated emissive photopolymerized microdots. Interestingly, the photopolymerization process also involved the opening of the stilbenyl double bonds within the ruthenium-based photo-initiators. As a result, these ruthenium complexes covalently integrated into the polymer network, while their photophysical and electrochemical properties were preserved. These results represent an interesting step towards the development of ultrasensitive analytical tools; indeed, this 'one-pot' approach was applied for the direct integration of electrochemiluminescent materials onto electro-active surfaces through 2D-patterning. The spectra of these materials align with the luminescence of $[Ru(bpy)_2L]^{2+}$ by-products formed during the two-photon fabrication process [132].

3.2. Two-photon-absorbing ruthenium complexes for NIR light-driven photocatalysis

While ruthenium polypyridyl complexes have found extensive application in one-photon induced photocatalysis [68,133], their use as TP photocatalysts remains virtually unexplored to date. This is likely due to the necessity of employing high-power lasers as the primary light source in most cases. Consequently, the potential of such catalysts remains underestimated. meanwhile, even if visible-light photocatalysis is a powerful synthetic tool using UV/visible photons presents inherent limitations, including limited penetration into reaction media, potential absorption competition with involved species, and incompatibility with light-sensitive functionalities. As a result, the exploration of photocatalysis powered by near-infrared light, particularly through two-photon photocatalysts, has been envisaged to circumvent most of these challenges associated with UV/visible light irradiation. Recent progress indicates that two-photon absorption can occur even with low-power light sources like light-emitting diodes (LEDs), expanding its practical usability. On the other hand, the development and synthesis of two-photon absorption-based photocatalysts, comprising organic chromophores and metal complexes, opened new opportunities for these photocatalysts [134].

C. Turro, Y. Sun, and colleagues described a series of ruthenium polypyridyl complexes coordinated by ligands featuring extended π-conjugation [135]. This structural design endowed these complexes with two-photon absorption capability. It was observed that these complexes populated identical excited states upon excitation at both 480 and 800 nm wavelengths. Demonstrating excellent photocatalytic performance under NIR light irradiation, these complexes facilitated various organic transformations similarly to one-photon-absorbing photosensitizers under visible-light irradiation. Energy-transfer and photo-redox reactions, along with metalla-photoredox C–C coupling reactions aided by a transition metal co-catalyst, were successfully investigated. Notably, the high photocatalytic activity in the coupling of amines involving singlet oxygen ($^1O_2$) prompted exploration into various NIR light-driven $^1O_2$ reactions, utilizing O_2 as a sustainable oxidant. This methodology was applied to the $^1O_2$-driven enhancement of biomass-derived chemicals, such as 5-hydroxymethylfurfural, into value-added fine chemicals like maleic acid anhydride or 5-hydroxy-4-keto-2-pentenoic acid, achieving an impressive overall conversion rate of 92 %.

Another study carried out by the Sun group looked at a heterogeneous photocatalyst by integrating a two-photon-absorbing ruthenium

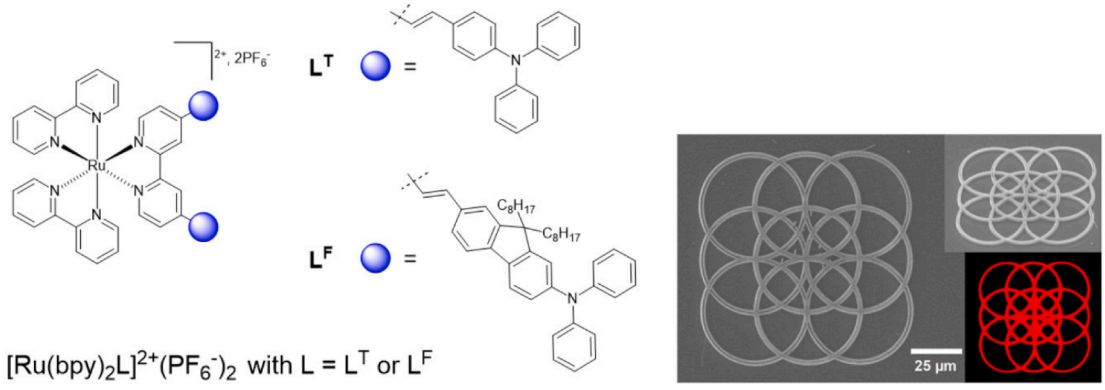

Fig. 17. Left: schematic drawing of the heteroleptic complexes $[Ru(bpy)_2L]^{2+}$ complexes and π-extending stilbenyl units in bipyridines L^T and L^F ligands. Right: Scanning electron microscope captures images of a two-photon polymerized 2D microstructure, alongside its corresponding epiluminescence image. Adapted from Ref. [132] © 2022 The Authors with permission from the Royal Society of Chemistry.

complex into a metal organic framework (MOF) [136]. It was expected that this design would not only preserve the TPA performance of the photocatalyst, but also enable it to be easily recycled thanks to the heterogeneous nature of the hybrid MOF-Ru system. The framework MOF-253, comprising aluminum oxide clusters and 5,50-dicarboxyl-2,20-bipyridyl ligands, was chosen as the scaffold to support the TP photocatalyst. Photocatalyst embedding was achieved by coordinating the ruthenium complex to the external bipyridyl sites of coordination of MOF-253. Using this hybrid photocatalyst, which operates through a TPA process under 740 nm light irradiation, five representative organic reactions were successfully conducted. These included energy transfer reactions, reductive and oxidative reactions, net redox neutral reactions, and atom transfer radical polymerization (ATRP) of acrylates. The potential for reuse and recovery of the MOF-Ru heterogeneous photocatalyst was assessed through recycling experiments, helped by the easy separation of the photocatalyst via centrifugation. Overall, these authors have developed a heterogeneous photocatalyst with two-photon absorption capability, effective under low-power infrared light. This opens avenues for utilizing low-energy light efficiently and enables practical recycling of the two-photon photocatalyst.

3.3. Two-photon induced photo-uncaging in the field of materials

A fully different approach relies on the properties of Ru (II) polypyridyl complexes as photocages. Several studies have focused on exploring these properties for applications in material sciences, such as surface modification [137,138], light-driven machines [139] or regulation of hydrogel properties [140] although most studies focused on applications in biology [141–143]. These strategies are supported by the capability of specific Ru (II) polypyridyl complexes, characterized by distorted octahedral geometries, to undergo ligand loss induced by light irradiation. This loss is attributed to the population of low-lying metal-centered excited states (^{3}MC) [144], which exhibit a pronounced anti-bonding nature [145,146].

Upon light irradiation, metal-to-ligand charge transfer triplet excited states (^{3}MLCT) are generated, which convert into low-lying triplet metal-centered (^{3}MC) states, or d–d states (Fig. 18). These excited states exhibit significant dissociative properties, leading to the substitution of a ligand by a solvent molecule. A conventional strategy to enhance the presence of the ^{3}MC states and improve the efficiency of ligand release involves incorporating bulky ligands into the coordination sphere [144,148–154]. This approach is effective because bulky ligands reduce the ligand field, thereby decreasing the overlap between Ru d orbitals and the lone pairs of pyridine nitrogen, thus rendering the ^{3}MC states more accessible.

Even if these fundamentals result from studies of one-photon processes, it was established that Ru (II) polypyridyl complexes can also be involved in two-photon induced photocleavage of caged systems, following the same photochemistry as one-photon mechanisms (Fig. 18) [147]. Studies by Etchenique et al. [148,149] on the use of two-photon light-cleavable [Ru(bpy)$_n$]-like complexes has additionally prompted the development of a technique for directly measuring the two-photon action cross-section of TP absorbers [155]. This experimental approach uses a conventional two-photon microscopy configuration for both uncaging and detection, enabling the determination of absorption/action cross-sections with the sole requirement of having a diffraction-limited microscope system. Even action cross-sections as low as hundredths of GM, nearing the lower limit for biological applications, can be accurately determined using laser sources commonly employed for two-photon imaging. Noteworthy, this method can be extended to non-fluorescent photo-triggers by utilizing a microscope along with an attached optical fiber-CCD spectrometer. This procedure was tested with a TP active ruthenium-based caged serotonin [Ru(bpy)$_2$(PMe$_3$)(5HT)]Cl$_2$ (RuBi-5HT, bpy = 2,2′-bipyridine, PMe$_3$ = trimethylphosphine, 5-HT = 5-hydroxytryptamine (serotonin) **22**, which was previously employed to administer serotonin in rodent brains *via* blue light in the single-photon mode. (Fig. 19) [156]. A direct photolysis measurement of the absorption cross-section of RuBi-5HT reported a value close to 1.4 GM at 777 nm, which is consistent with the value obtained using conventional two-photon excitation fluorescence ($\sigma_{TPA} = 1.40 \pm 0.09$ GM). Additionally, an effective action cross-section of 0.04 GM was determined at the same wavelength.

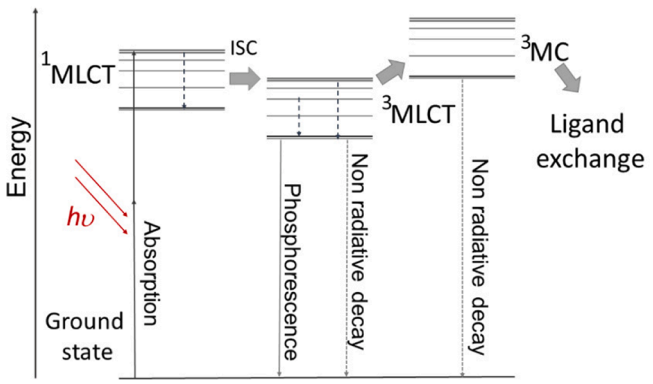

Fig. 18. Schematic Jablonski diagram illustrating the electronic transitions leading to two-photon induced ligand labilization in [Ru(bpy)$_3$]$^{2+}$-like complexes: the triplet ^{3}MLCT band may undergo deactivation via emission, non-radiative pathways, or the population of the non-bonding ^{3}MC state, potentially resulting in the destabilization of a ligand. Key steps: *i)* two-photon photoexcitation, *ii)* intersystem crossing (ISC), *iii)* radiative deactivation, *iv)* internal conversion, *v)* cleavage reaction and ligand exchange. This simplified Jablonski diagram overlooks structural deformations and thus provides only a limited depiction of the system [147].

3.4. Two-photon photosensitive functionalized surfaces

Because of its ability to operate remotely and with high spatiotemporal precision, two-photon excitation emerges as an appealing noninvasive method for controlling surface functionalities, with promising applications in lithography, photopatterning, bio-interfaces, and microfluidics [157]. A. Del Campo et al. exploited the high spatiotemporal resolution provided by two-photon excitation of a light-cleavable caged aminosilane [Ru(bpy)$_2$(PMe$_3$)(APTSi)](PF$_6$)$_2$ complex (APTSi = 3-aminopropyltriethoxysilane), attached to silica surfaces to control functions of these silica surfaces (Fig. 20, left) [158]. Both single-photon (460 nm) and two-photon (900 nm) irradiations resulted in the removal of the cage and the generation of reactive amine groups. The two-photon uncaging of Ru units attached to the silica surface layer was achieved by scanning the surface at 900 nm in the presence of water. The resulting photogenerated free amine groups were available for subsequent chemical modification and were reacted with a fluorescent dye (Alexa-Fluor 488 carboxylic acid succinimidyl ester) specifically targeting free amine groups, thus labeling the surface's free amino groups. A fluorescent pattern, displaying bright (uncaged) and dark (caged) areas mirroring the mask's shape, was visualized using a fluorescent microscope (Fig. 20, right). These findings highlight the feasibility of chemical lithography via the uncaging of surface-bound Ru cages through two-photon processes. Furthermore, the authors demonstrated that the uncaging process can be site-selective, while the ratio of uncaged areas depends on the dose and can be regulated by adjusting laser intensity or exposure time.

3.5. Two-photon photoreactive polymeric materials

The potential of two-photon light-cleavable [Ru(bpy)$_3$]$^{2+}$-like complexes as constituents for advanced photoreactive polymeric materials was also demonstrated by U. Monkowius et al. [159]. These authors developed photodegradable metalla-supramolecular gels responsive to both visible light in a single-photon process and near-infrared radiation

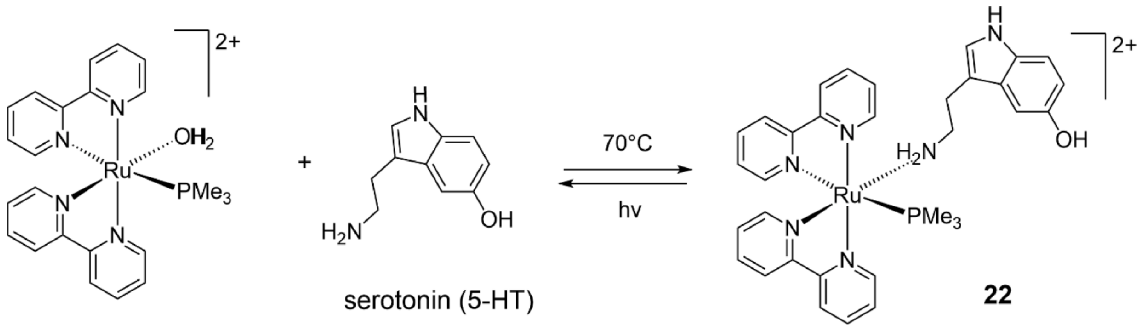

Fig. 19. Complexation of serotonin with $[Ru(bpy)_2(PMe_3)(H_2O)]^{2+}$ (forward) and one-step light-triggered removal of serotonin 5-HT (backward) [156].

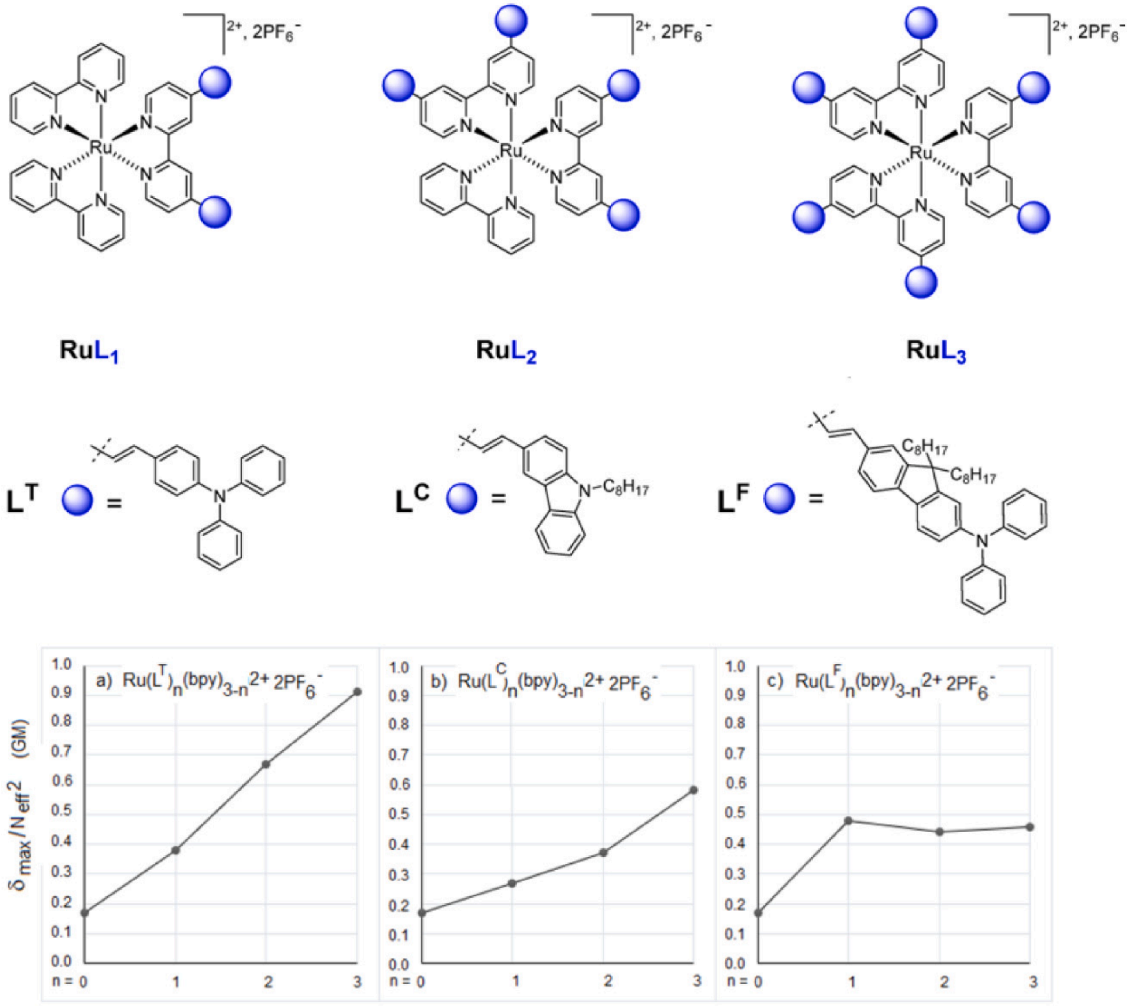

Fig. 20. (a) Structure of a Ru (II) complex silane-modified surface and (b) fluorescence micrograph depicting a surface labeled with AlexaFluor 488 after exposure to femtosecond-laser patterning at 900 nm. Each square correlates with a precise laser intensity and irradiation time. The fluorescence intensity reveals the surface density of the dye, serving as a measure of the extent of the uncaging reaction for a given two-photon dose. The inset shows the emission profile for squares irradiated at a same laser intensity but different times. Adapted with permission from Ref. [158]. Copyright 2012 American Chemical Society.

(800 nm) in a two-photon process, by using a bipyridine ruthenium complex with pendant amines $[Ru(bpy)_2(4\text{-(aminomethyl) pyridine})_2]^{2+}$. This complex rapidly formed stable gels by reacting covalently with a hexamethylene diisocyanate prepolymer. While stable in the dark, the gels were rapidly degraded by visible light (>395 nm). These polypyridyl ruthenium complexes with pendant amines are also light-cleavable under pulsed NIR-laser irradiation at 800 nm. Degelation occurred rapidly in the sole irradiated regions, offering an opportunity for spatiotemporal micropatterning by high-frequency pulsed multiphoton irradiation (Fig. 21).

4. Two-photon activation of d^6 Ru (II) polypyridyl complexes: potential biomedical applications

4.1. Two-photon photo-triggers for biologically-active compounds

Parallel to the incursions in the field of advanced materials, most reports have focused on bioimaging and therapeutic applications, taking

advantage of the fact that Ru (II) polypyridyl complexes showed promising bactericidal, bacteriostatic and anti-cancer activity [73,99,142,160,161] and can be applied in various biological and cellular contexts, such as bioimaging, biomolecular imaging, and phototherapy [72]. The first reports on their utilization for two-photon bioimaging and PDT have highlighted the significant benefits of two-photon excitation, despite the prevalent use of dyes with limited TPA cross-sections [104]. This interest stems from the many advantages that transition metal complexes offer, including: *i)* readily adjustable chemical and photophysical properties; *ii)* large Stokes shifts facilitating precise discrimination between excitation and emission wavelengths, which also prevent self-absorption-induced fluorescence quenching; *iii)* high emission quantum efficiencies and long emission lifetimes, thereby minimizing background autofluorescence interference; and *iv)* emissive properties responsive to variations in the local environment. Of course, achieving deep-tissue photoactivation necessitates extending the absorption profile of photosensitizers (PS) to encompass the therapeutic wavelength range of 650–900 nm. This is an expected advantage of biphotonic activation. In addition, the use of two-photon (TP) irradiation maintains excitation localization deep within complex biological tissues, enabling higher spatiotemporal resolution within these tissues.

Various approaches for improving the permeability of the Ru (II) polypyridyl complexes have been explored, with particular emphasis on adjusting their lipophilicity, charge, and solubility. These factors play a crucial role in influencing the penetration and accumulation of the complexes in the cells. For instance, in the course of a study of fluorinated ruthenium (II) complexes for two-photon PDT (Fig. 22a), Chao et al. demonstrated that the complexes could traverse the extracellular matrix of human cervical HeLa cancer cells.[3] They observed that two-photon excitation with long wavelengths (700–900 nm) achieved deeper tissue penetration compared to one-photon excitation. Specifically, the penetration depth of two-photon-excited luminescence for the Ru (II) complexes in HeLa Multicellular Tumor Spheroids (MCTS)[4] was approximately 200 μm, compared to the approximately 70 μm depth achieved with one-photon excitation [162].

4.2. Ru (II) polypyridyl complexes for TP-induced sensing and bioimaging

Bioimaging with two-photon-induced luminescence stands out as particularly suitable for *in vivo* sensing, primarily because of remarkable benefits, including deep tissue penetration, minimal phototoxicity, high excitation selectivity, and limited photobleaching area [163]. In this context, Ru (II) polypyridyl complexes can play a key role as alternative probes to steady-state or nanosecond bioimaging and biosensing thanks to elevated quantum yields, large Stokes shifts and extended emission lifetimes [71,72]. In addition, the emission properties of these complexes are sensitive to changes in the environment, including variations in oxygen levels, viscosity, and pH [164–168]. Finally, as shown by some of the examples below, an anticipated molecular design allows these complexes to localize in specific cell organelles (subcellular structures with one or more specific functions to perform in the cell) [169].

C.-T. Poon et al. were among the first to use a Ru (II) polypyridyl complex for two-photon tumor-imaging [170]. These authors described the synthesis and study of a Ru (II) polypyridyl compound appended with a porphyrin, **23** (Fig. 23, left). This design was expected to heighten both TPA cross-section and cellular penetration. A σ_{TPA} cross-section of 178.0 ± 26.8 GM was determined employing 100-fs laser pulses, at 800 nm, instead of 28 GM for the free tetraphenyl-porphyrin H_2TPP [171]. This improvement could be justified by the charge separation occurring between the porphyrin and the Ru (II)-polypyridyl unit, which arises from photo-induced electron transfer.

The uptake of **23** by human nasopharyngeal carcinoma HK-1 cells was examined using both flow cytometry and fluorometry. After incubation for 1 h, the fluorescence intensity of HK-1 cells treated with **23** was approximately 10 times higher than that of untreated cells. This intensity further increased by an additional 10-fold after incubation for 6 h, reaching a plateau after approximately 16–24 h. Compound **23** was then analyzed for its live cell imaging capabilities using two-photon microscopy. Upon excitation with an 800 nm laser, a strong red emission was observed in the cytoplasm (Fig. 23-right, a); compound **23** predominantly localized in lysosomes, with lesser localization in the endoplasmic reticulum, Golgi body, and mitochondria (Fig. 23-right, b–e).

Since this pioneering work, many efforts were devoted to directing the localization of two-photon absorber probes in living cells and tissues [21,104,131,172,173]. For instance, among recent studies, W. Zhang et al. outlined the design of a Ru (II) polypyridyl complex **Ru-NO$_2$** (Fig. 24a) as a two-photon phosphorescent probe suitable for the detection of glutathione S-transferases (GSTs) [174]. These studies specifically targeted the detection of GSTs because of their multifaceted physiological role in metabolism and detoxification: if GSTs play a putative role in safeguarding living cells against a broad range of harmful molecules, abnormal expressions of GSTs are often linked to drug resistance and more particularly drug-induced liver injuries [175]. **Ru-NO$_2$** was weakly luminescent because of a strong Photo-induced Electron Transfer (PeT) within this complex. After being reacted with glutathione (GSH), through a nucleophilic aromatic substitution (S_NAr) reaction, in the presence of GSTs, a new complex was generated, Ru-SG, which showed an intense red emission (Fig. 24). The luminescence lifetime of Ru-SG was determined to be 154.2 ns, meeting the criteria for time-gated luminescence imaging of GSTs in living cells. Before investigating the potential of **Ru-NO$_2$** for two-photon imaging of GSTs and tissues, the maximum σ_{TPA} cross-section values of **Ru-NO$_2$** and Ru-SG were determined to be 118 GM, at 752 nm, and 248 GM, at 765 nm, respectively. These features suggest that **Ru-NO$_2$** is well-suited for two-photon imaging of GSTs in deep tissues. The authors highlighted that experimental results regarding time-gated luminescence detection and luminescence imaging analysis of GSTs in Drug-induced Liver Injury (DILI) mouse sera and liver tissues indicated that **Ru-NO$_2$** could facilitate dynamic monitoring of GST fluxes. Consequently, it has the potential to contribute to future clinical applications, enabling early diagnosis and treatment monitoring of DILI.

Due to their emission lifetimes spanning from hundreds of nanoseconds to microseconds, Ru (II) polypyridyl complexes are well-suited for lifetime-based imaging methods like phosphorescent lifetime imaging microscopy (PLIM) and time-resolved emission imaging microscopy (TREM) [176]. These techniques effectively remove interference from biomolecular autofluorescence, which typically exhibits lifetimes ranging from picoseconds to a few nanoseconds [177]. Coupling these techniques with two-photon absorption is notably advantageous for live cell-based samples: it allows for the use of low-energy excitation wavelengths within the biological window, while the precise excitation of probes results in exceptional spatial resolution [71].

Thus, J. A. Thomas et al. explored dinuclear Ruthenium(II) complexes, Ru(II)(tpphz) 24 and 25 (Fig. 25) as PLIM probes for nuclear DNA in both live and fixed cells [178]. σ_{TPA} cross-sections, 142 GM for 24 and 108 GM for 25, were measured at 800 nm. These probes, which exhibit minimal emission in aqueous media, emit strong luminescence when bound to DNA. Upon two-photon excitation at 800 nm, they exhibited characteristic emission lifetimes exceeding 160 ns. Meanwhile a shorter-lived cytoplasmic emission was observed in live MCF–7 (a human breast cancer cell line) and HaCat (a long-lived, spontaneously immortalized human keratinocyte cell line) cells. The longer lifetime

[3] HeLa cells were the first human cell line to be established and have been widely used in laboratory studies, especially in research on viruses, cancer, and human genetics.

[4] MCTS are easy to handle heterogeneous cell aggregates that have been gradually accepted as valid 3D cancer models that lie between a cell monolayer and a solid tumor.

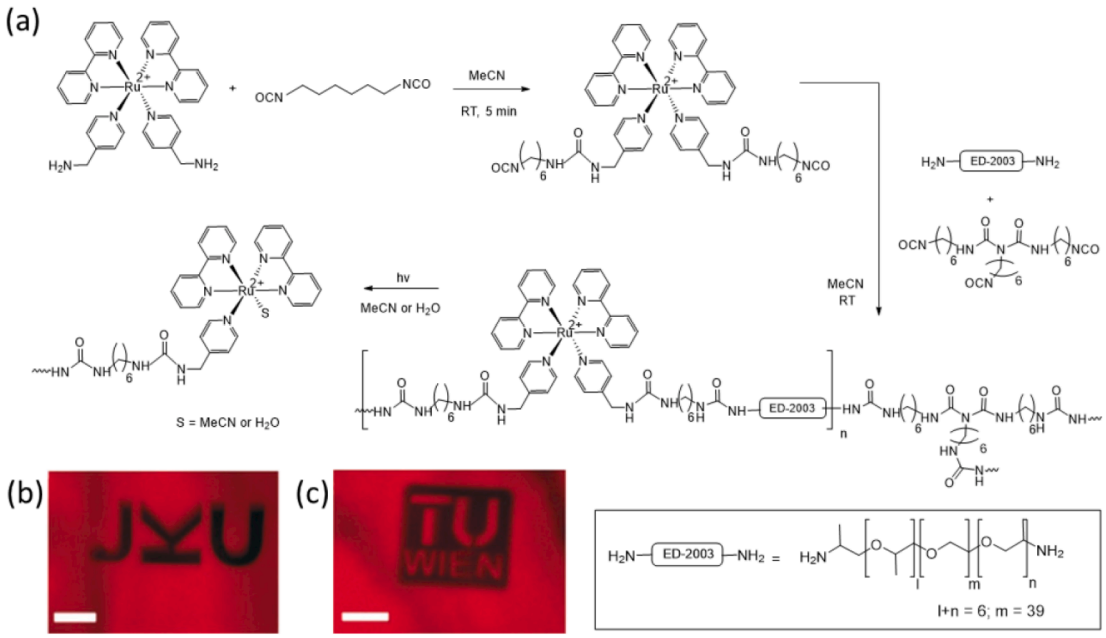

Fig. 21. (a) Synthesis and photoinduced cleavage of gels containing ruthenium developed by U. Monkowius et al. [159] (b, c) micropatternings obtained upon two-photon irradiation at 800 nm using a standard two-photon microfabrication setup. Scale bar = 100 μm. Adapted with permission from Ref. [159]. © 2017 The Authors. Published by Wiley-VCH Verlag GmbH.

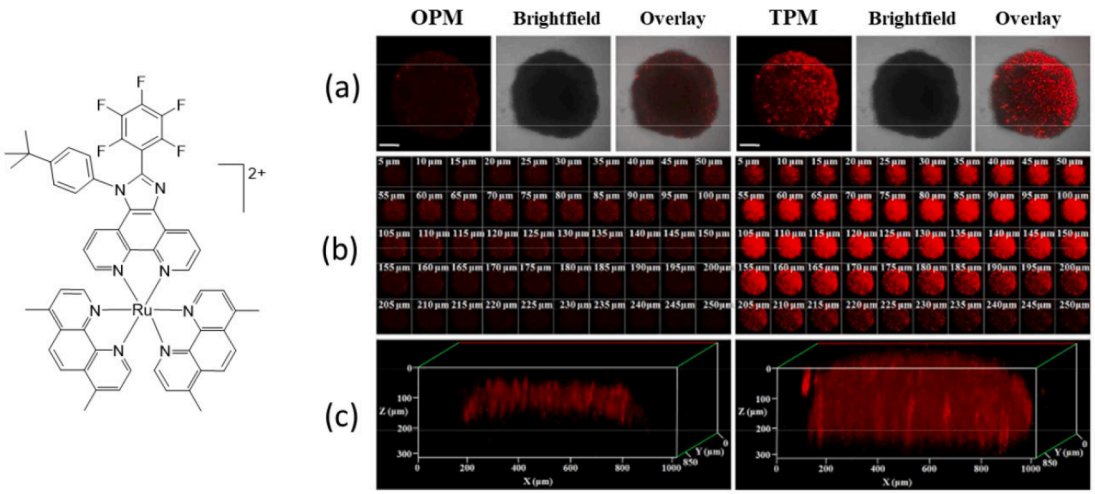

Fig. 22. Left: Structure of a fluorinated ruthenium (II) complex studied for two-photon PDT. Right: (a) One- and two-photon luminescent pictures of 3D tumor spheroids after incubation with this complex (10 μM) for 6 h. (b) Both one- and two-photon Z-stack images were acquired at intervals of 5 μm from the top to the bottom. (c) One- and two-photon Z-stack images of an undamaged spheroid acquired utilizing a 10 × objective. λ_{ex} = 458 nm (one-photon) or λ_{ex} = 825 nm (two-photon); λ_{em} = 630 ± 20 nm. Scale bar: 200 μm. Adapted with permission from Ref. [162]. © Copyright 2017 American Chemical Society.

depicted in the nucleus reveals a more effective shielding from surrounding water molecules in the DNA-bound sites compared to the cytoplasm. These observations highlight how lifetime imaging techniques, coupled with two-photon excitation, offer valuable insights with sub-micrometer spatial resolution.

Y. Zhang et al. reported on a series of taurine-modified polypyridyl Ru-complexes designed to explore lysosome-targeting [179]. These complexes demonstrated specific accumulation within lysosomes. Among them, the six taurine-modified Ru-complex **26** (Fig. 26) displayed the most intense emission. However, its two-photon absorption cross-section at pH = 4.5 was less than 20 GM at 800 nm. On the other hand, the two-photon excited emission property of 28 served as a in situ tool for non-invasive monitoring of cell uptake *in vivo*, particularly benefiting from enhanced tissue penetration under light.

X. Liang, X. Liu, M. S. Roberts et al. developed two-photon turn-on sensing probes 28–30 for *in vivo* imaging of oxidative stress with resolution at the single-cell level [180]. The Ru (II) complex served as the signaling unit and was coupled with responsive groups targeting glutathione (GSH), hydrogen peroxide (H_2O_2) and hypochlorous acid (HOCl) (Fig. 27). In these systems, the ^{3}MLCT resulting from the excitation of the tris-(2,2′-bipyridine) Ru (II) unit is corrupted so that the phosphorescent emission is quenched by an effective intramolecular photoinduced electron transfer (PeT) process. The responsive groups undergo quantitative cleavage when exposed to GSH, H_2O_2 or HOCl. As a consequence, the phosphorescent emission and lifetime are restored. By enabling the coupling of luminescence intensity and lifetime imaging, these Ru (II) probes ensure precise localization and measurement of Reactive Oxygen Species (ROS) and GSH changes within the liver [181].

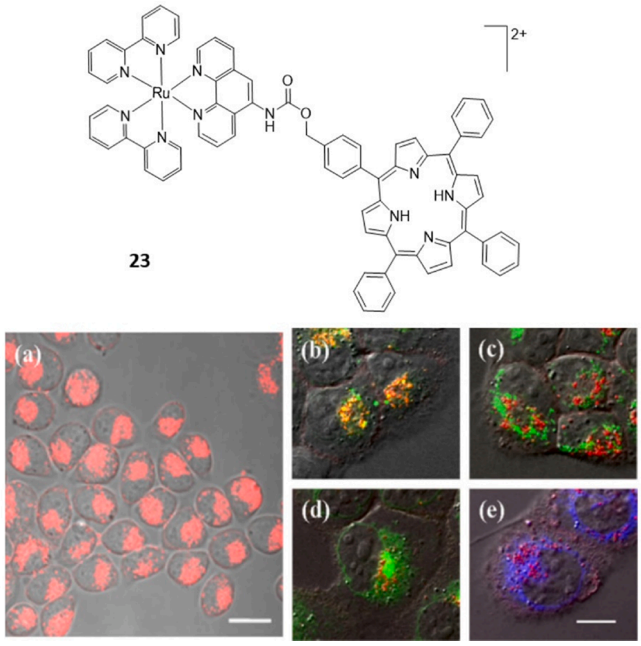

Fig. 23. Left: Chemical structure of the complex **23** [170]. Right (a) Two-photon confocal fluorescent imaging of HK-1 cells performed after a 24-hour incubation with compound **23** (8 μM). Scale bar = 20 μm. (b–e) Subcellular localization of **23** in HK-1 cells After a 24-hour incubation with compound **23** (8 μM). Cells were then stained with (b) lysosome probe Lyso-Tracker Green DND-26L7526 (50 nM), (c) mitochondria probe Mito-Tracker Green FM dye M7514 (50 nM), (d) Golgi probe BODIPY FL C5–ceramide complexed to BSA (5 μM) or (e) endoplasmic reticulum probe ER-Tracker Blue–White DPX dye (200 nM). Indicate overlapping fluorescent signals from compound **23** and the organelle probes. Scale bar = 10 μm. Adapted with permission from Ref. [170]. Copyright 2010, Elsevier.

The authors suggested that the high resolution and precision afforded by the dual-mode quantitative imaging approach for *in vivo* cellular oxidative stress could be used to determine the severity of heterogeneous diseases among cell populations and to assess their response to drugs.

H. Chao et al. developed switchable two-photon luminescent probes **30–32** (Fig. 28) by exploiting the redox properties of the quinone/hydroquinone pair to selectively and dynamically detect hypoxia[5] [182].

Under normoxia, compound **32** exhibited low luminescence even in the presence of NADPH. By contrast, under hypoxia, characterized by low oxygen levels, a noticeable increase (more than 80-fold) of the phosphorescent emission of **32** was observed. This increase stemmed from NADPH catalyzing the reduction of quinone derivatives specifically under hypoxic conditions. But not under normoxia [183]. This "off-on" luminescent switch was both fully reversible and reproducible. Furthermore, the sensitivity of compounds **30–32** to hypoxia was assessed using a two-photon excitation range extending from 750 to 1050 nm. The highest σ_{TPA} cross-section values were recorded at 800 nm, under hypoxic conditions, for the **30–32** complexes: these values were 147 GM for **30** + NADPH, 168 GM for **31** + NADPH, 196 GM for **32** + NADPH, using rhodamine B as a reference. These complexes proved highly effective in visualizing intratumoral hypoxia in A549 multicellular tumor spheroids (A549 being lung human carcinoma cells) and monitoring hypoxia-reoxygenation cycles in living zebrafish through two-photon luminescent imaging (Fig. 29).

[5] Hypoxia refers to a state of low oxygen tension, typically ranging from 1% to 5% O_2, commonly observed in the central regions of tumors owing to weak vascularization. Normoxia denotes oxygen tensions ranging from 10% to 21%, while hyperoxia indicates oxygen levels exceeding 21% [181].

Polypyridyl Ruthenium (II) complexes with simple chemical structures like those presented above may undergo rapid clearance from the body due to their small size, positive charge, and hydrophilic properties, thereby limiting their *in vivo* applicability [184]. C.-P. Tan, Z.-W. Mao et al. have addressed this issue by covalently linking Ru (II) complexes to carbon nanodots (CDs) for two-photon imaging of lysosome (Fig. 30) [185]. This approach was supported by the biocompatibility, non-toxicity, photostability, and tunability of carbon dots, which are macromolecules characterized by strong photoluminescence and high resistance to photobleaching [186,187].

CDs, **33** and **33**@CDs exhibit two-photon excited emissions, which make them suitable for live cell bioimaging and *in vivo* applications [185]. The σ_{TPA} cross-section of **33**@CDs in DMSO at 810 nm (1118 GM) significantly exceeds that of **33** (171 GM), an increase that could result from a fluorescence resonance energy transfer (FRET) from CD to **33** on two-photon excitation. To assess the penetration capability of **33** and **33**@CDs, A549 ranging from 400–500 μm were treated for 12 h with **33** or **33**@CDs. Examination using one- and two-photon microscopy shows that **33** and **33@CDs**, with average particle sizes about 66 and 80 nm respectively, can cross the extracellular matrix and accumulate in MCTSs. The images are much brighter for **33@CDs** than for **33**, which is consistent with the enhanced two-photon absorption and cellular uptake capacities of the modified carbon dots **33@CDs**.

One- and two-photon fluorescence imaging of one-day-old zebrafish embryos was conducted to study the potential of **33@CD** for imaging in living tissues. **33** and **33@CD** did no present obvious toxicity in zebrafish embryos within 6 days. Significantly high fluorescence intensities were noted with two-photon excitation in the zebrafish embryos, as opposed to one-photon excitation, indicating their ability to perform deep two-photon excited imaging, as well as their potential for *in vivo* applications.

4.3. Ru (II) polypyridyl complexes as two-photon-activatable therapeutic agents

Photodynamic therapy relies on the use of therapeutic agents, called photosensitizers (PS), which cause necrosis of the surrounding tissues, due to their cytotoxic activity in the excited state [188,189]. This non-invasive procedure is applied clinically for both oncological and non-oncological indications, such as the eye disease macular degeneration. Typically, it involves the production of highly reactive singlet oxygen ($^1O_2$) through interactions among a photosensitizer, light, and oxygen ($^3O_2$) (type II photoreactions) (Fig. 31). The excited photosensitizer can also directly interact with neighboring biomolecules through electron exchange or proton transfer, leading to the formation of radical intermediates. (type I photoreactions). Two-photon PDT (TP-PDT) has been suggested as a way to bring benefits to the established one-photon PDT in terms of penetration depth, spatial selectivity and lower photodamage to healthy tissues. Meanwhile, using current photosensitizers is not realistic as a clinical trials: the relatively small cross-sections TPA of the conventional sensitizers (e.g. $\sigma_{TPA} = 10$ GM for Photofrin® at ~ 800 nm) [190] necessitates laser powers near the tissue-damage threshold to be used. New photosensitizers with high TP cross-section values and long triplet state lifetimes are therefore in high demand to make TP-PDT an applicable therapeutic treatment [191,192].

In this context, Ru (II) polypyridyl derivatives constitute promising candidates for photodynamic therapy, which can be involved in the type I and type II photoreaction processes [73,184,193–196]. Their visible light absorption and reasonably long-lived triplet excited states that allow the effective production of $^1O_2$ are obvious advantages, also supported by clinical trials of **TLD1433** (Fig. 32) [197], a photosensitizer developed in the McFarland and Lilge laboratories, for a PDT treatment of bladder cancer with intravesical application. **TLD-1433** is presently under investigation in Phase II clinical trials in both the USA and Canada [198].

On the other side, the field of one-photon antibacterial

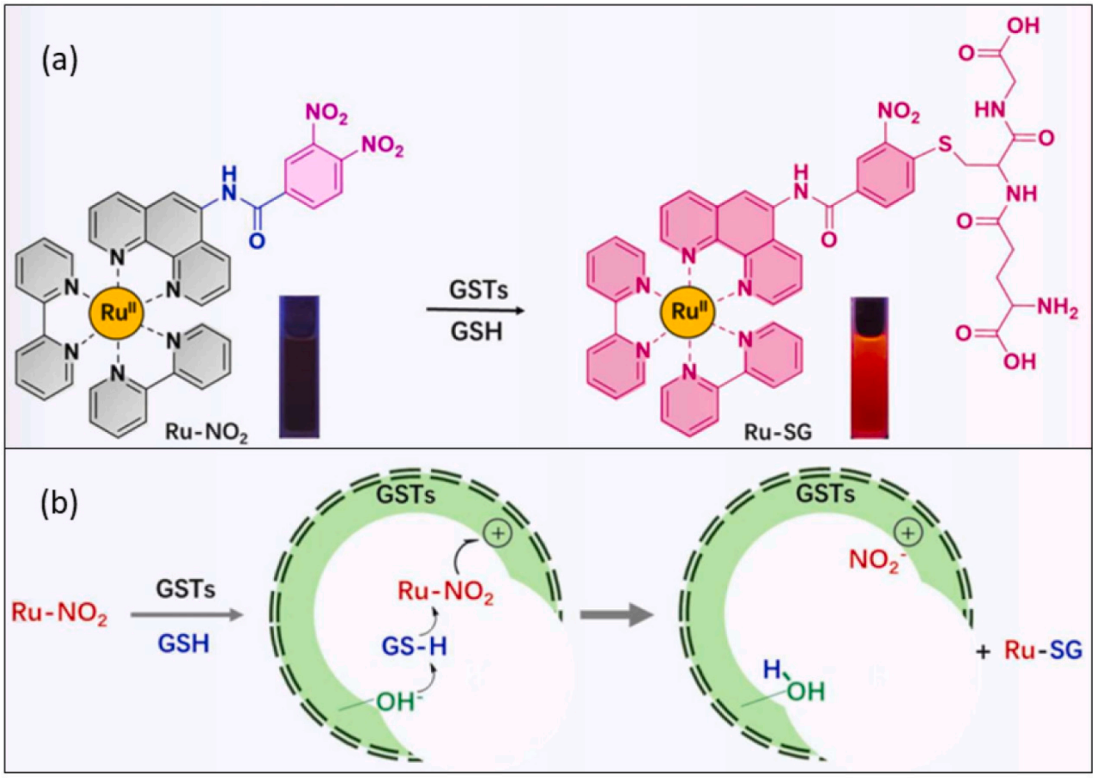

Fig. 24. (a) Synthetic route for producing **Ru-SG** by reacting **Ru-NO_2** with GSH in the presence of GSTs. Photographs of Ru-NO_2 and Ru-SG solutions highlighting their differences in terms of emission properties. (b) Schematic illustration by Zhang et al. of the GSTs-catalyzed **Ru-NO_2**-GSH reaction in living cells. Adapted with permission from Ref. [174]. Copyright 2022, Elsevier.

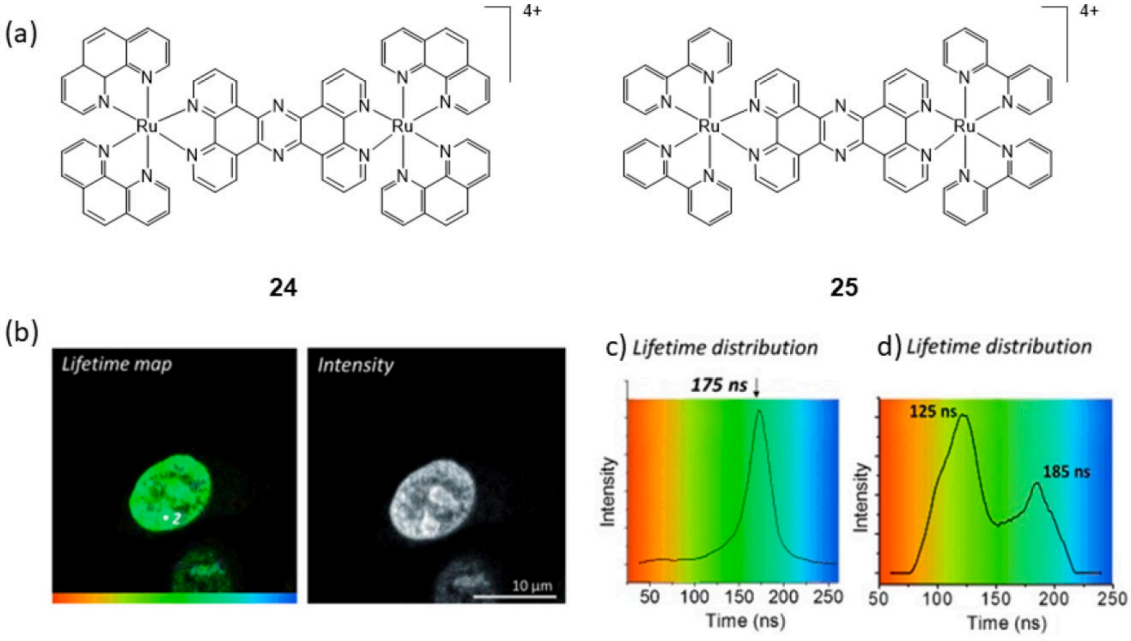

Fig. 25. (a) Structures of dinuclear complexes **24** and **25**. (b) Comparison of MCF-7 live cell pre-treated with complex **24** lifetime and intensity imaging. (c,d) Lifetime imaging of immobilized, permeabilized MCF7 cells pre-treated with complex 24 revealing different lifetimes in c) the nucleus and d) cytoplasm. Adapted with permission from Ref. [178]. Copyright 2014, Wiley-VCHGmbH.

photodynamic therapy (aPDT) has garnered significant interest due to its potential as a non-invasive treatment for bacterial infections, especially in an era of rising antibiotic resistance [199]. Despite this, there are few studies exploring the use of ruthenium(II) polypyridyl complexes in aPDT [200–202]. This technique, which precisely targets microbial cells, is particularly effective for treating surface-level infections. Additionally, two-photon induced antibacterial PDT could offer deeper tissue penetration and higher precision, making it a complementary approach for treating deeper infections while minimizing damage to surrounding healthy tissues. However, to the best of our

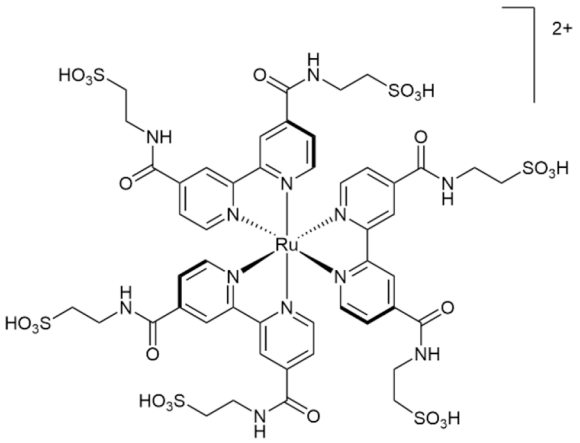

Fig. 26. Chemical structure of the six taurine-modified Ru-complex **26** designed by Y. Zhang et al. as a lysosome-specific photosensitizer for PDT targeting cancerous brain cells [179].

knowledge, the application of 2P-PDT in conjunction with ruthenium(II) polypyridyl complexes in antibacterial assays has not yet been reported [203,204]. This indicates how much research still needs to be conducted on ruthenium complexes within the field of two-photon photodynamic therapy.

Recent studies aim to develop strategies for adjusting ruthenium complexes to the requirements of TP-PDT. J. Guo, A. Ren and co-workers investigated the photophysical properties of a series of heteroleptic Ru (II) complexes containing pyrene units as two-photon sensitizers (Fig. 33) [205]. These studies were supported by density functional theory (DFT) and time-dependent density functional theory (TD-DFT) calculations that were conducted on the electronic structure, one- and two-photon absorption properties, type I/II mechanisms, triplet state lifetime, and solvation free energy. These data allowed their ability as TPA PSs to be evaluated. It was observed that incorporating pyrene groups led to a significant enhancement in the lifetime of the complex, while ethynyl linkers enhanced σ_{TPA} values. For instance, complex **34** has a large σ_{TPA} value (1376 GM) at 698.5 nm and a lifetime (136 μs), both values that support it as a potential candidate for TP-PDT.

Another strategy for improving the characteristics of complexes for infrared TP-PDT has recently been proposed by F. Gao et al. [206]. In this study, Ru (II) homoleptic complexes **36**–**38** with 3 distinct (*E*)-2-styryl-1*H*-imidazo[4,5-*f*][1,10]phenanthroline (sip) ligands (Fig. 34) were designed and compared to the parent heteroleptic complex $[Ru(bpy)_2(sip)]^{2+}$, **35** [207].

The σ_{TPA} values of the homoleptic complexes were 51–142 GM [206], which is not really different from that of the heteroleptic parent system (91 GM) [207]. At the same time, the introduction of two additional sip ligands significantly enhanced the $^1O_2$ quantum yield under infrared two-photon irradiation and the DNA photocleavage effect of the homoleptic complexes **36**–**38**: when subjected to 450 nm LED irradiation (50 mW.cm^{-2}), the $\Phi_{\Delta 450}$ values for complexes **36** and **38** were 0.59 and 0.49, respectively, compared to **35** (0.13). Furthermore, under 808 nm TP irradiation (100 mW.cm^{-2}) irradiation, **36** also demonstrated the highest $\Phi_{\Delta 808}$ value among these complexes. These complexes

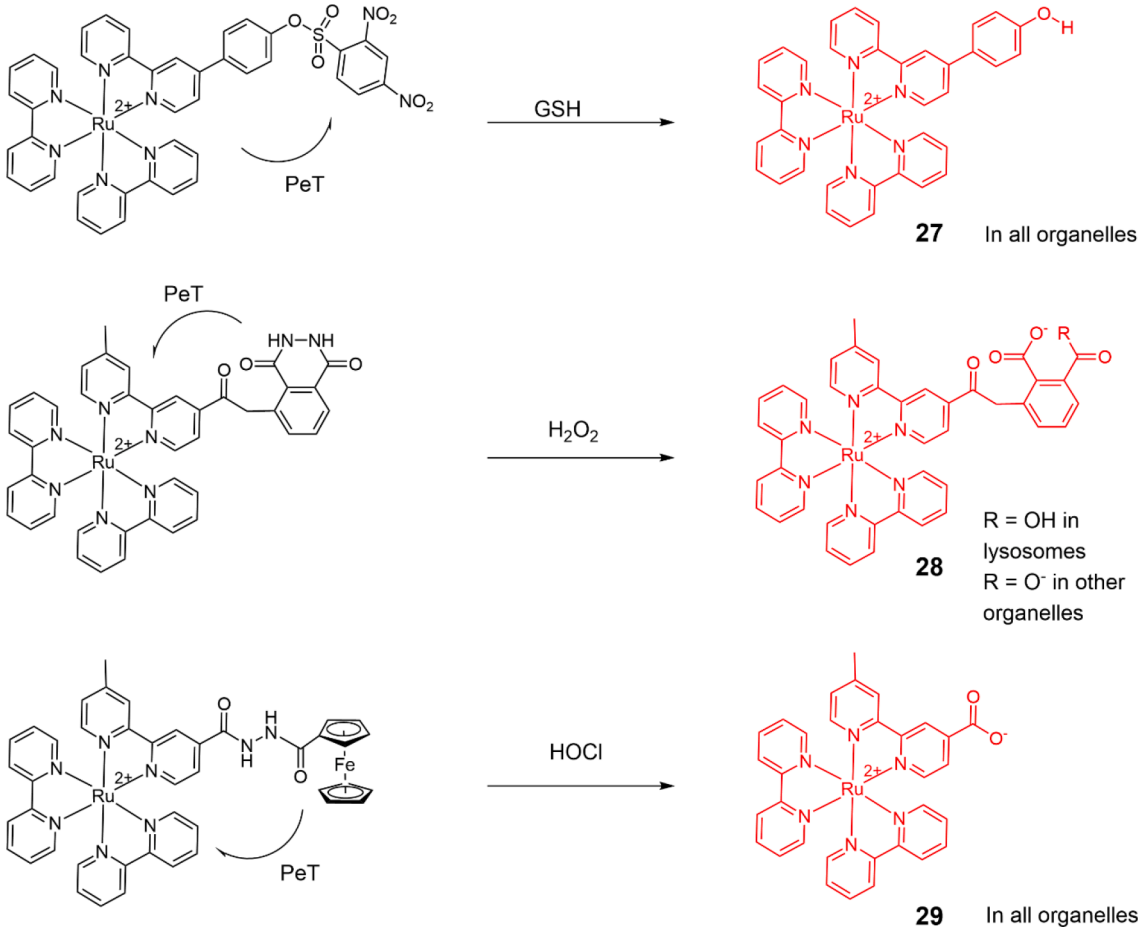

Fig. 27. Illustration of the reactions of **27, 28** and **29** with GSH, H_2O_2 or HOCl. The emission of the ruthenium complex is initially quenched because of a photo-induced electron transfer process (PeT). It is restored in presence of GSH, H_2O_2 or HOCl, the responsive groups being quantitatively cleaved. The carboxylate/carboxylic features of compound **29** are influenced by the pH levels within the organelle. Sodium and potassium serve as the counter-ions. [180].

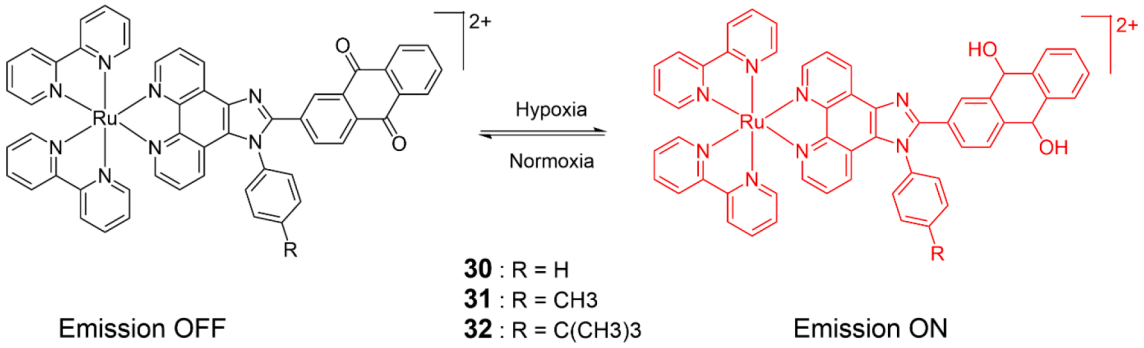

Fig. 28. Ruthenium (II) anthraquinone complexes **30**–**32** for two-photon luminescent hypoxia imaging [182].

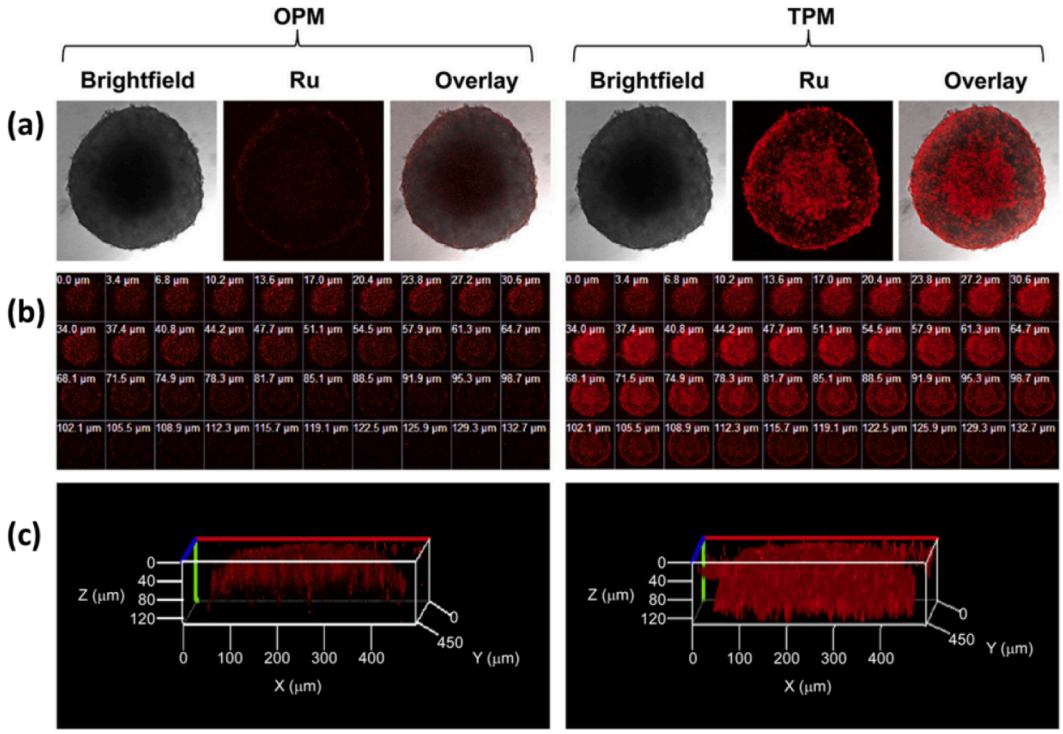

Fig. 29. (a) One- and two-photon luminescence images of 3D tumor spheroids following incubation with **32** (10 μM) for 6 h. (b) Z-stack images were captured at intervals of 3.4 μm from the top to bottom. (c) 3D Z-stack images of an intact spheroid, using a 10 × objective. λ_{ex} = 460 nm (one-photon), 800 nm (two-photon); λ_{em} = 560–680 nm. Adapted with permission from Ref. [182]. Copyright 2015, Elsevier.

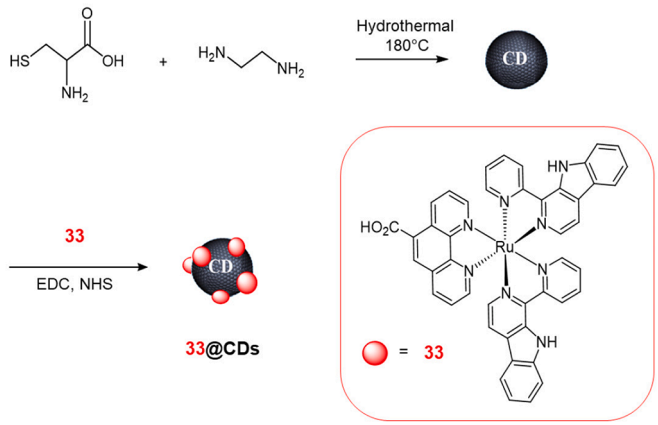

Fig. 30. Main steps for the preparation of covalently linked Ru (II) complex **33** to carbon nanodots (**33**@CDs) for two-photon imaging of lysosome [185].

specifically target the mitochondria rather than the nuclei, thereby producing intracellular singlet oxygen $^1O_2$ under visible or infrared light irradiation. Complex **36** exhibited highest efficacy in generating intracellular singlet oxygen $^1O_2$ and displayed strong cytotoxic effects *in vitro* on melanoma cells in humans.

The two-photon absorption cross-section of most PSs are too low to ensure an efficient TPA process at a low photon density. Up to now, two-photon excitation has been carried out by using intense laser irradiation that may cause irreparable damage to tissues and cells. In contrast to these approaches, F. Gao et al. envisaged the use of low-dose light irradiation using a low-power civil laser, offering the possibility of longer exposure times for the administration of higher doses of light, which would make it possible to treat larger or more deeply buried tumors during clinical trials. These authors synthesized dinuclear Ru (II) complexes featuring planar bridging ligands. These complexes exhibited outstanding two-photon absorption, efficient generation yields of singlet oxygen ($^1O_2$) and remarkable photothermal efficiency. They are therefore promising for dual photodynamic and photothermal therapy of melanoma tumors *in vivo* [208]. As a representative example, it was

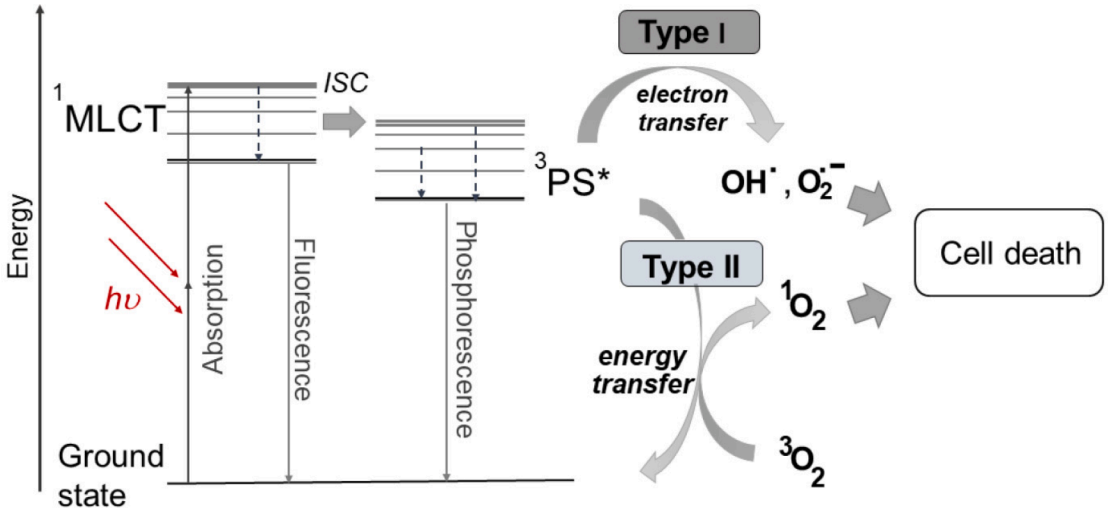

Fig. 31. Diagram illustrating two-photon excitation-triggered PDT via type I and type II mechanisms.

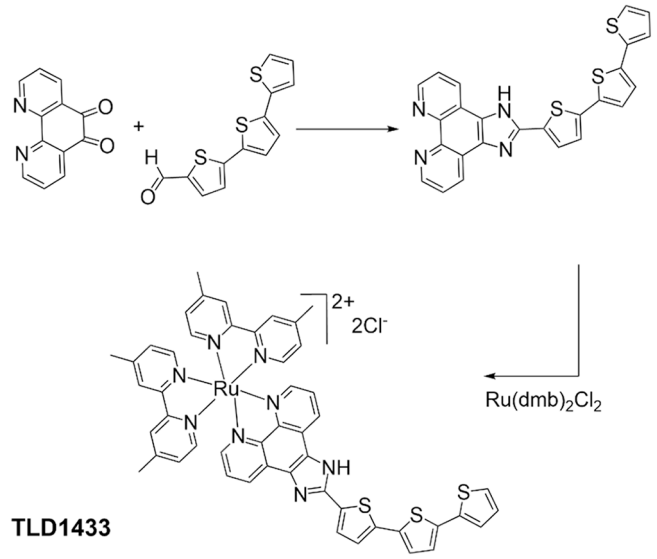

Fig. 32. Main steps of the synthesis of **TLD1433** [197] (dmb = 4,4′-dimethyl-2,2′-dipyridyl).

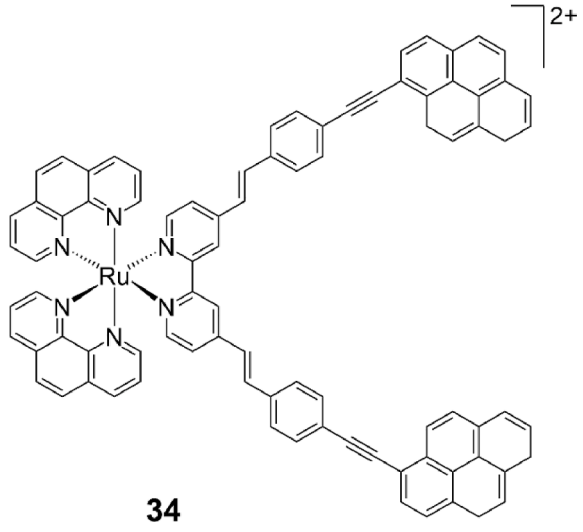

Fig. 33. Chemical structure of Ru-complex **34** [205].

observed that a *tert*-butyl-substituted complex was targeting the mitochondria without entering the nucleus, thereby considerably increasing its PDT while reducing its cytotoxicity in absence of light activation. It effectively inhibits the growth of melanoma tumors *in vivo* through synergistic two-photon photodynamic therapy (TP-PDT) and photothermal therapy (PTT). This occurs under low light doses (30 J.cm^{-2}) irradiation, using an 808 nm civil low-power laser (0.1 W.cm^{-2}). The characteristics of this complex would therefore make it a suitable candidate for the treatment of larger or more deeply buried tumors, turning it into a potential model for an innovative class of dual-function, low-power infrared-driven therapeutic agents for dual PDT/PTT therapy.

This report follows a number of studies, some of which are presented below, that underlined that beyond high cross-section values and long triplet state lifetimes, or $^1O_2$ quantum yield, other parameters also require consideration, particularly in terms of the internalization of the Ru (II) complexes in cells and their localization [196,209]. Actually, it quickly became apparent through seminal studies that one downside of Ru (II) polypyridyl-based two-photon photosensitizers is their poor selectivity toward cancer cells, leading to unintended phototoxic effects on healthy tissues [210].

G. Lemercier and P. Baldeck's research teams presented the first instance of a Ru (II) complex (**39**, Fig. 35) as a photosensitizer for two-photon photodynamic therapy, in 2009 [211]. The Ru (II) center was framed by three fluorene–phenanthroline ligands bearing hydrophilic triethylene glycol chains in order to ensure within biological mediums and ability to penetrate cell membrane. **39** exhibited a ^{3}MLCT state with a relatively long lifetime (500 ns in CH_3CN), while a maximum TPA cross-section $\sigma_{TPA} \approx 40$ GM, at 740 nm, was measured. Fluorescence imaging of rat brain tumor models (F98 glioma cells) revealed the internalization of **39** into the cytoplasmic vesicles. No discernible localization was observed within the nuclei. Single-cell TP irradiation experiments, at 740 nm, were achieved with variable irradiation powers (respectively 300, 200, 100 and 30 mW), for 5 min. In all instances, cell damage was exclusively observed in cells that were incubated with **39**.

Further to this pioneering work, W.-K. Wong et al. explored the TP-PDT properties of Ru (II) complexes with appended porphyrins through an ethynyl linker (Fig. 36) [212,213]. This approach was based on the fact that porphyrins and their analogues have been extensively studied as photosensitizers in anticancer PDT due to their tendency to accumulate more in tumor cells (approximately 2 to 5 times higher than in normal cells) and their capacity to cause oxidative damage to vital cell

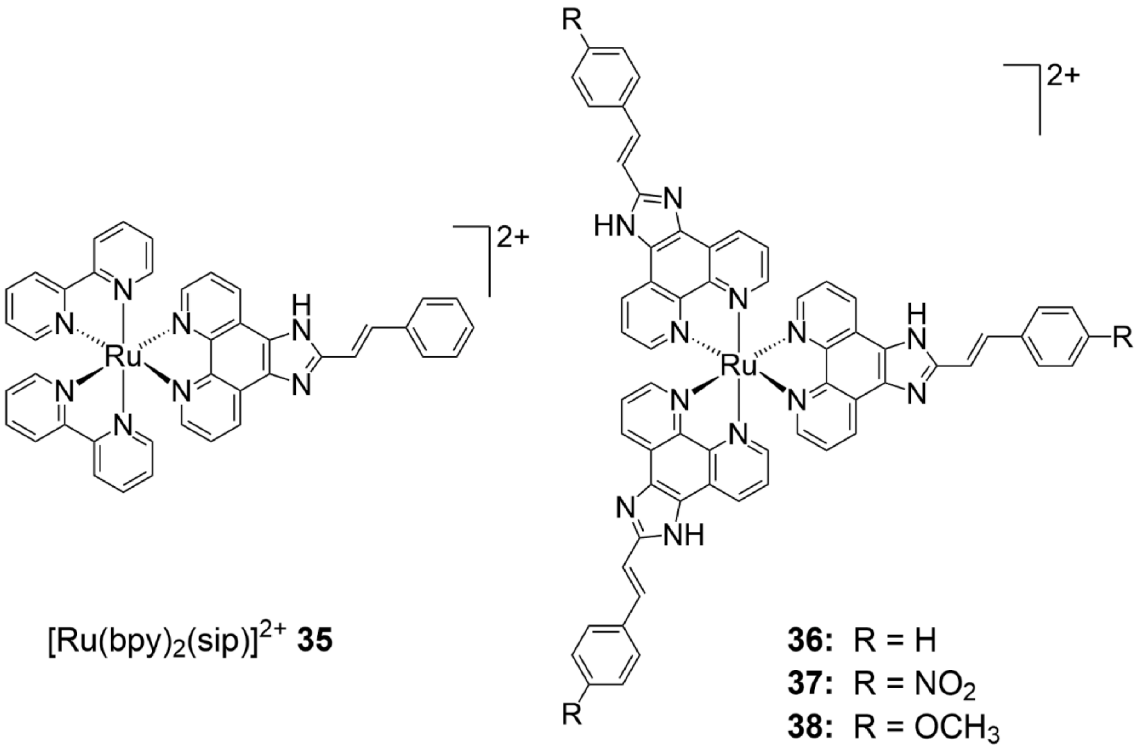

Fig. 34. Representative structures of Ru-sip-complexes **35–38** [206].

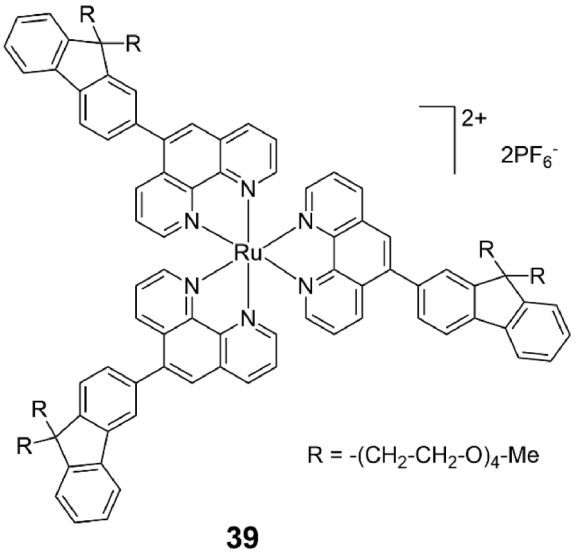

Fig. 35. (a) Chemical structure of 39 [211].

components like DNA, proteins, and membranes [214,215]. The complexes **40**–**42** differ because of the position of the ethynyl linker: the β-position for 40 and 41 and the meso position for 42 [212,213]. Zn(II) was chosen over other metal ions because Zn(II)-tetraphenylporphyrins usually exhibit higher $^1O_2$ quantum yields compared to those of free tetraphenylporphyrins and related metalated complexes [216]. **40**–**42** showed high Φ_Δ values: 0.66 (40), 0.76 (41) and 0.93 (42) in $CHCl_3$. The σ_{TPA} cross-sections of 40 and 41, assessed using the open-aperture Z-scan technique at 800 nm, were found to be 555 and 485 GM, respectively, while the *meso*-linked conjugate 42 exhibited a σ_{TPA} value of 1104 GM. The authors assumed that this enhancement arises from both the extended π-conjugation and the molecular polarization resulting from the asymmetrical (D–π–A) structure linking the porphyrin and Ru (II)-polypyridyl components.

The photocytoxicity studies of these three complexes in HeLa and HK-1 cells did not uncover any discernible organelle localization for **40** and **41** but showed mitochondria localization for **42**. After 5 min of pulsed two-photon excitation at 850 nm, HK-1 cells treated with **42** exhibited a 90 % phototoxicity, associated to morphological deformations or loss of integrity. At the same time, 70 % of HeLa cells displayed similar changes after exposure to **40** under continuous laser irradiation at 800 nm for 30 min. In contrast, no significant morphological alterations were observed with **41** under the indicated two-photon excitation conditions. Therefore, **42** exhibited a strong two-photon absorption cross-section, enabling the generation of singlet oxygen via both linear and two-photon excitation, alongside effective targeting of mitochondria for which it can be considered as a promising photodynamic therapy agent.

P. J. Stang, H. Chao et al. investigated a supramolecular strategy to modulate the characteristics of Ru (II) polypyridyl complexes as two-photon photodynamic therapy sensitizers. For instance, they designed the coordination-driven self-assembled heterometallic Ru–Pt metallacycle **43** (Fig. 37) [217]. This metallacycle exhibited near-infrared emission, strong TPA, and high efficiency in generating Reactive Oxygen Species (ROS), as the integration of the Ru (II) polypyridyl unit within a tetramethylammonium-decorated Pt (II)-based metallacycle promotes intersystem crossing. This highly charged supramolecular structure favors the internalization of the PS in cells. Thus, a dual localization in both the mitochondria and nuclei was observed.

The quantum yield of singlet oxygen (Φ_Δ) for **43** was determined to be 88 % relative to $[Ru(bpy)_3]^{2+}$ as a reference. The product of TPA cross-section σ_{TPA} and Φ_Δ, which indicates the efficacy of singlet oxygen generation, under two-photon excitation, was evaluated to be $\sigma_{TPA} \times \Phi_\Delta$ = 1,220 GM in **43**. This merit parameter, revealed that **43** is highly performant as a two-photon $^1O_2$ sensitizer. *In vitro* investigations demonstrated that the Ru–Pt metallacycle showed limited toxicity in absence of light, but upon photoexcitation, the intracellular generation of singlet oxygen by the metallacycle caused damage to both mitochondria and nuclei and, finally, led to cell death. *In vivo* studies with

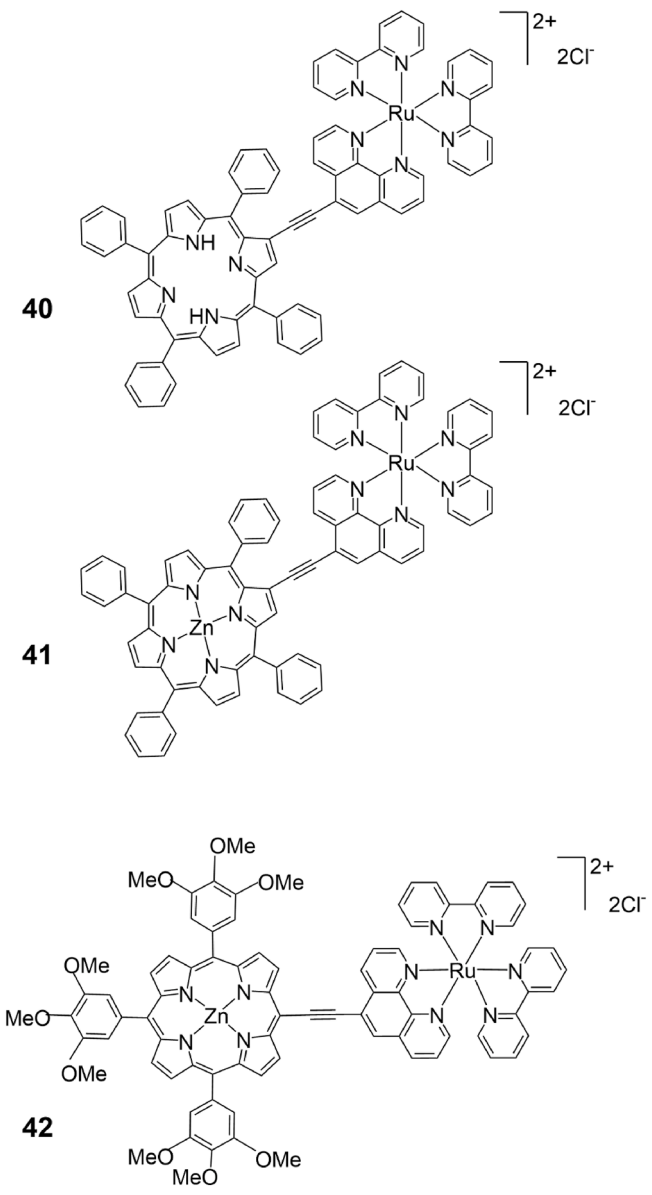

Fig. 36. Structures of Ru (II) complexes **40–42** with attached porphyrin moieties [212,213].

tumor-bearing mice revealed that **43** effectively eradicates cancerous tissues, even at low light doses, while exhibiting low systemic toxicity.

Later, the Karges group described asymmetrically substituted Ru (II) polypyridine complexes containing 1,10-phenanthroline and 4,7-diphenyl-1,10-phenanthroline as effective photosensitizers for both one- and two-photon PDT (Fig. 38) [218]. The complexes displayed effective two-photon absorption within the biological spectral range, the σ_{TPA} values being up to ≈ 1600 GM. Their efficacy was investigated in MultiCellular Tumor Spheroids (MCTSs) with an 800 μm diameter, simulating the pathological environment of clinically-relevant tumors. The complexes successfully penetrated the MCTSs and produced singlet oxygen within their hypoxic cores (Hypoxia, characterized by low oxygen levels, is a prevalent trait in many tumors, with varying severity across tumor types. This characteristic is obviously a source of complications with classical PDT regimes). After treatment, the MCTSs, even their large hypoxic cores, were completely eliminated. The authors finally indicated, on the basis of experimental models, that the 1,10-phenanthroline Ru (II) polypyridine complexes could serve as TP-PDT photosensitizers. For instance, compound **44b** (Fig. 38) effectively eliminated an adeno-carcinomic human alveolar basal epithelial tumor in a mouse model under excitation relevant for clinical applications, either one-photon (500 nm) or two-photon (800 nm).

4.4. Strategies for an anticipated localization of Ru-based TP-photosensitizers

Photodynamic therapy exhibits precise spatiotemporal selectivity within biological systems due to the short lifetime (<40 ns) and limited diffusion range (<20 nm) of singlet oxygen $^1O_2$ [219]. Hence, the PDT efficacy relies on the subcellular distribution of the Ru (II) polypyridyl photosensitizer (PS), attributable to the short lifetimes of the reactive oxygen species (ROS) generated upon PS excitation. Thus, controlling the localization of the Ru (II) polypyridyl complex in specific organelles (membrane, mitochondria, lysosomes, nuclei…) is essential for increasing the PDT outcome as it will determine the cell death mechanism [220]. Together with reducing side effects. Numerous studies on the penetration features of Ru (II) complexes in cells demonstrated that the efficiency of their cellular uptake, their intracellular positioning, even their mechanisms of toxicity can be modulated [142,221,222]. H. Chao, G. Gasser et al. illustrated these aspects by studying the intracellular localization and anticancer efficacy of the complexes **46** and **47**, which only differ by the presence of peripheral methoxy or hydroxy groups (Fig. 39) [223]. This study illustrated that functionalizing the dppz-ligands is decisive for both the uptake and localization of these complexes. The emission quantum yields of **46** (Φ_{em} = 2.8 %) and **47** (Φ_{em} = 1.7 %), in acetonitrile, and their respective maximum TPA cross-section values **46**: 245 GM) and **47**: 93GM) around 800 nm are similar to those of comparable Ru (II) polypyridyl complexes. Compound **46** exhibited longer phosphorescence emission lifetimes in aerated and degassed CH_3CN solutions (325 and 645 ns, respectively), compared to **47** (109 and 220 ns). The cellular localization of **46** and **47** in HeLa cells, investigated by confocal microscopy, showed that the more lipophilic complex, **46**, was uniformly localized in the HeLa cells, while **47** was predominantly detected at the membranes. The correlation between the cellular localization of complexes **46** and **47** and their respective PDT efficiency was then investigated. Significant differences in their biological properties were observed. **47** univocally confined to the outer shell of HeLa MCTSs cancer cell spheroids and did not induce oxidative damage to inner cells upon irradiation. By contrast, **46** penetrated into HeLa MCTSs where severe oxidative damage occurred, thus confirming its superior tissue penetration and higher efficiency in two-photon photodynamic therapy (TP-PDT) compared to **47** [223].

Two basic methods can be used to target specific organelles using metal complexes: one consists in adapting relevant properties (size, charge, shape of the ligands) of the metal complexes to meet the specific requirements of the targeted organelles; the other is the association of the metal center with an organelle-targeting moiety. Both approaches have been applied to polypyridyl ruthenium complexes.

Several studies have focused on targeting mitochondria. Indeed, mitochondria are pivotal in regulating cell death [224] and can be considered as potential anticancer drug targets [214]. Chao et al. described the synthesis and main features of 4,7-diphenyl-1,10-phenanthroline ruthenium (II) complexes incorporating a triphenylphosphonium moiety (Fig. 40) [141]. The phosphonium group was chosen because of its affinity for mitochondria, as lipophilic cationic units tend to accumulate in these organelles due to the large negative potential of the mitochondrial inner membrane [225]. The design of these amphiphilic ruthenium (II) complexes has proved to be efficient: they internalized and accumulated primarily into the mitochondrial region of HeLa cells. **48** (Fig. 40), which has a flexible triphenylphosphonium-functionalized arm, showed the highest affinity for mitochondria, as ascertained by Inductively Coupled Plasma Mass Spectrometry (ICP-MS). This complex also has the highest TP cross-section values (about 200 GM in the interval 810–830 nm) for this series of compounds. The TPE using the wavelength of 830 nm penetrates deeply into MCTS,

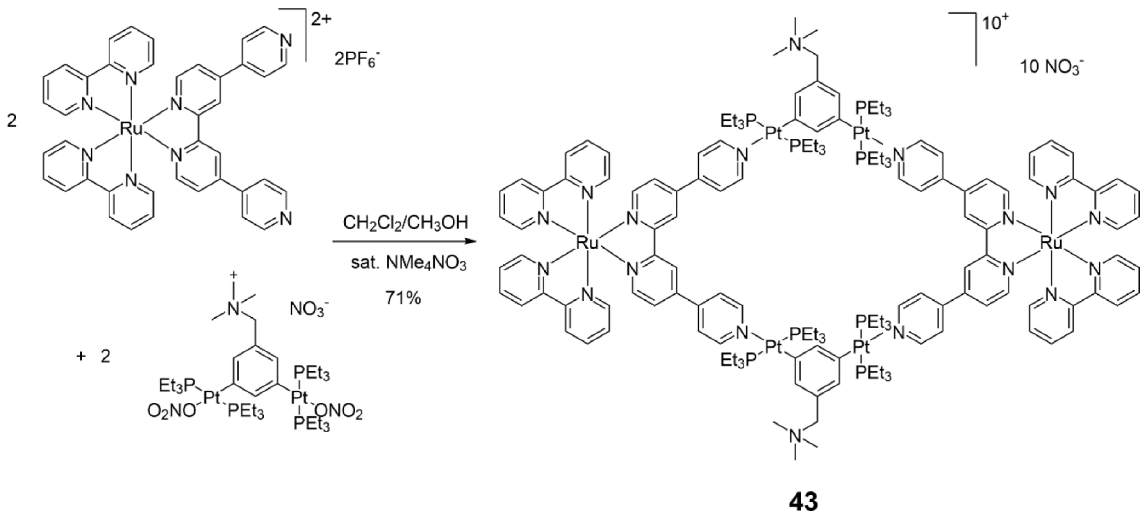

Fig. 37. Supramolecular synthesis of the Ru–Pt metallacycle 43 by P. J. Stang, H. Chao et al. [217].

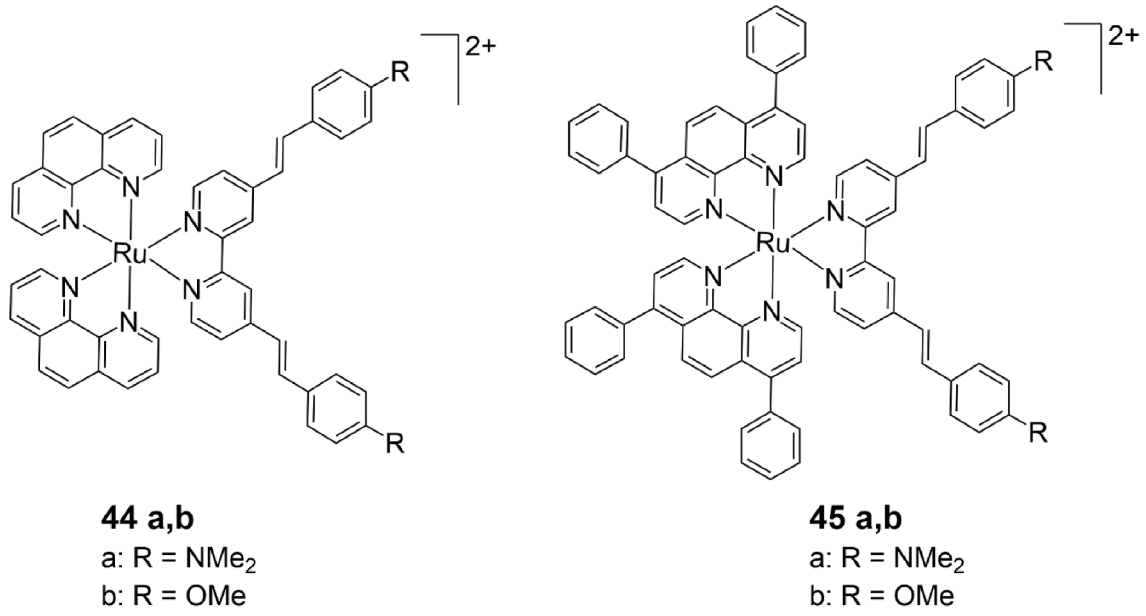

Fig. 38. Chemical structures of compounds investigated by Karges and co-workers [218].

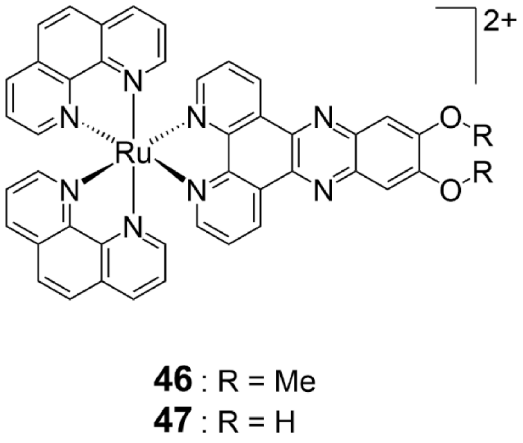

Fig. 39. Chemical structures of **46** and **47** which only differ by the presence of peripheral methoxy or hydroxy groups [223].

allowing the luminescence of **48** located at a depth greater than 100 μm to be detected. The photocytotoxicity of the complexes was examined with 3D HeLa multicellular spheroids, as screening models. The complexes demonstrated potent inhibition of Multicellular Spheroid (MCS) growth, with a gradual reduction in MCS volume post-irradiation, **48** showing the most pronounced inhibition. Conversely, the photocytotoxicity under two-photon excitation at 830 nm surpassed that under one-photon excitation at 450 nm, with respective IClight50 values[6] of 1.9 μM and 9.6 μM.

S. Rau, T. Weil et al. proposed a bio-inspired approach for the design of mitochondrial targeting PS on the basis of the synthesis of a HSA-Ruthenium conjugate (HSA = Human Serum Albumin) [226]. Triphenylphosphine groups were introduced to achieve mitochondrial targeting while blood plasma protein serum albumin was selected as a nano-

[6] The half-maximal inhibitory concentration (IC_{50}) denotes the amount of a drug required to inhibit a biological process by 50%, serving as a measure of potency for antagonist drugs in pharmacological research [220].

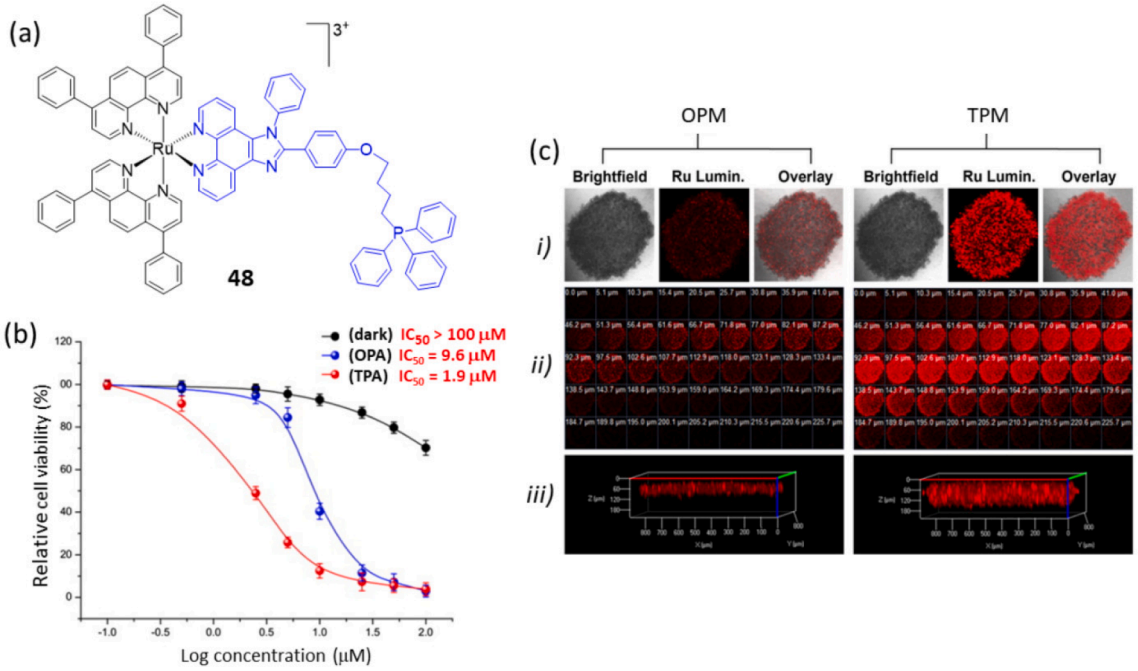

Fig. 40. (a) Molecular structure of compound **48**. (b) Cell viability plotted as a function of concentration of **48** incubed in 3D Multicellular Tumor Spheroids (MCTSs) following One-Photon Excitation (OPE, depicted in blue) or Two-Photon Excitation (TPE, depicted in red), as well as without light excitation (depicted in black). OPE involved irradiation with a LED (20 mW.cm^{-2}) at 450 nm for 10 min, while TPE entailed irradiation with a laser (100 mW, 100 fs) at 830 nm for 3 min per section of MCSs. (c) Comparison between One-Photon (458 nm) and Two-Photon (830 nm) excited Z-stack images of 3D HeLa MCTSs after 8 h-incubation with **48** (10 µM): *i)* from left to right: Brightfield; Luminescent emission of the Ru complex; Overlay. *ii)* Orthogonal projection microscopy (OPM) and two-photon microscopy (TPM) Z-axis scanning images acquired every 5.1 µm from the top to bottom of an intact 800 µm MCTS. *iii)* 3D Z-stack images via One-Photon (OP) and Two-Photon (TP) excitation of an intact spheroid. Adapted with permission from Ref. [141]. Copyright 2015, Elsevier.

transporter with the aim of minimally influencing cell uptake mechanisms and subcellular distribution patterns. The resulting nano-transporter, **49** (Fig. 41), exhibited an eightfold enhancement in singlet oxygen generation upon photo-irradiation (λ_{exc} = 470 nm) compared to its Ru (II) counterpart lacking mitochondria-targeting functionalities. It also exhibited excellent localization within mitochondria in HeLa cells. The conjugation of HSA to the Ru (II) did not alter its visible-light absorption features but the two-photon absorption cross-section (50 GM in water at 800 nm) of the conjugate was five times larger than that of the unmodified analogue. The high loading capacity of **49**, the efficient cellular uptake and localization within mitochondria, as well as its strong photosensitivity and capacity for $^1O_2$ generation collectively contributed to the effective two-photon-induced photocytotoxicity of this ruthenium complex. The authors suggest that the effective suppression of growth seen in an acute myeloid leukemia cell line, along with the selective elimination of leukemic cells over normal bone marrow cells, may provide a promising therapeutic window relying on **49** for treating acute myeloid leukemia [226].

Photosensitizers with the ability to target cellular organelles beyond mitochondria are also of great interest. In particular, lysosomes are other important organelles and have established roles in recycling cellular material, in cell growth, mitogenic signaling and promotion of metastasis, for instance. On the other hand, a disturbance of the lysosomal integrity, leading to permeabilization of the lysosomal membrane and the subsequent hydrolases release into the cytosol, can trigger cell death [228]. With this in mind, H. Chao, G. Gasser et al. synthesized highly charged ruthenium complexes (Fig. 42) with the expectation that these highly charged complexes will not localize in either the mitochondria or the nucleus. Instead, they are expected to selectively accumulate in lysosomes *via* endocytosis [229]. Tertiary ammonium groups were introduced into the core structure of $[Ru(bpy)_3]^{2+}$ to enhance both the water solubility and the binding affinity of complexes **50**–**52** to negatively charged cell membranes. This strategy proved successful: **50**–**52** localized within the lysosomes by endocytosis in HeLa cells as ascertained by ICP-MS. Upon extending the irradiation time, **50** diffused from the lysosomes to the cytoplasm, subsequently migrating to the nucleus and nucleoli. These lysosome localized photosensitizers showed outstanding quantum yields of $^1O_2$ generation in methanol (0.92–0.99) and D_2O (0.49–0.67), together with a low dark cytotoxicity. They exhibited σ_{TPA} cross-sections ranging from 185 to 250 GM, which facilitated two-photon-induced photosensitization in multicellular spheroids, resulting in necrocytosis in both HeLa cells and HeLa MCTSs at low light doses (800 nm, 10 J.cm^{-2}).

Although PSs can effectively penetrate tumor cells, the most effective photodynamic reactions typically take place primarily on the surface of the tumors because of a limited light penetration. In addition, low irradiation intensities in the deeper layers of the tumor can display tumorigenic effects, leading to the emergence of resistance to treatment. The development of photosensitizers with the ability to induce cell death at both high and low light intensities is therefore an appealing area of research. In this context, H. Chao et al. reported on the synthesis and features of five fluorinated Ru (II) polypyridyl complexes (**53**–**57**) (Fig. 43) for two-photon PDT [162], taking in account that the affinity for cell membranes can be enhanced through fluorination of the compounds (see also Fig. 22 and the relevant discussion). The highest two-photon action cross-section values for **53**–**57** were estimated to 163–191 GM units at 825 nm. Their ability to produce $^1O_2$ in HeLa MCTSs under two-photon laser light (360 J.cm^{-2}) and one-photon surface light (12 J.cm^{-2}) was confirmed. The cellular localization of the complexes was subsequently examined by two-photon confocal laser scanning microscopy. After a 0.5 hr incubation time with HeLa cells, complexes **53**–**57** were detected on the cytomembranes, outside of the cells. By contrast, after 4 h incubation, they localized both on the cytomembranes and inside, thus on the mitochondria. After irradiation with a two-photon laser, a notable alteration in the morphology of the HeLa cells was depicted and blisters were observed. The mitochondria

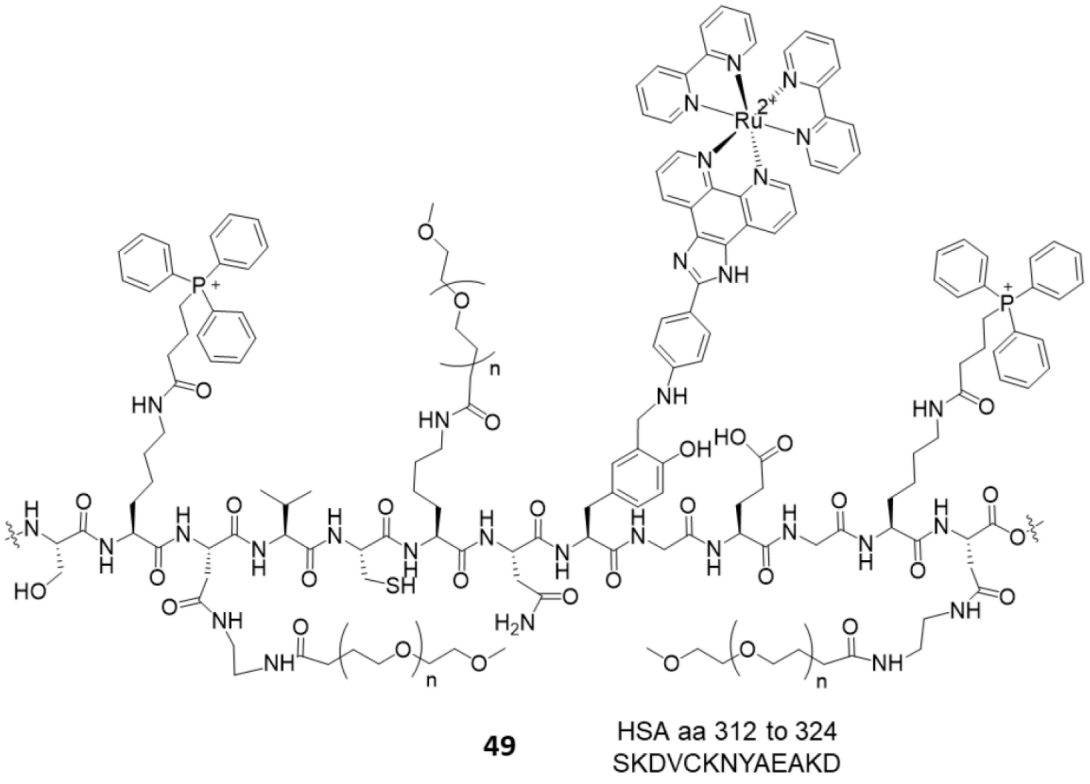

Fig. 41. Ru (II) PS linked to human serum albumin **49** and to HSA aa 312 to 324 [226,227].

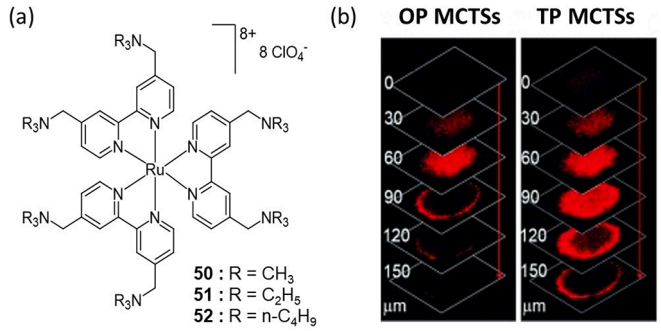

Fig. 42. (a) Chemical structures of complexes **50**–**52**. (b) HeLa cells evolution upon treatment with compound **50** following two-photon irradiation (at 800 nm) for varying period of times, showing the penetration of this PS in lysosomes by endocytosis and the cell necrocytosis upon two-photon excitation. Adapted with permission from Ref. [229]. Copyright © 2015 WILEY-VCH Verlag GmbH & Co. KGaA.

and cytomembranes of the cancer cells were eliminated simultaneously and HeLa cells were destroyed effectively by the complexes, regardless of whether the cells were arranged in a monolayer or formed multicellular spheroids. In view of its highest phototoxicity index in the series, compound **56** was used in two-photon PDT for *in vivo* treatment of tumor xenografts. This study highlighted its effective hindrance of tumor growth. According to the authors, these results make it possible to envisage an efficient TP-PDT method for anticancer therapy involving simultaneous ablation of two critical sites within cancer cells—cytomembranes externally and mitochondria internally—using a single photosensitizer.

Photosensitizers for therapeutic approaches against tumors also focused on materials that preferentially localize in the cell nucleus. This targeting is intended to disrupt the replication system, selectively impacting cancer cells Indeed, targeting the DNA replication mechanism

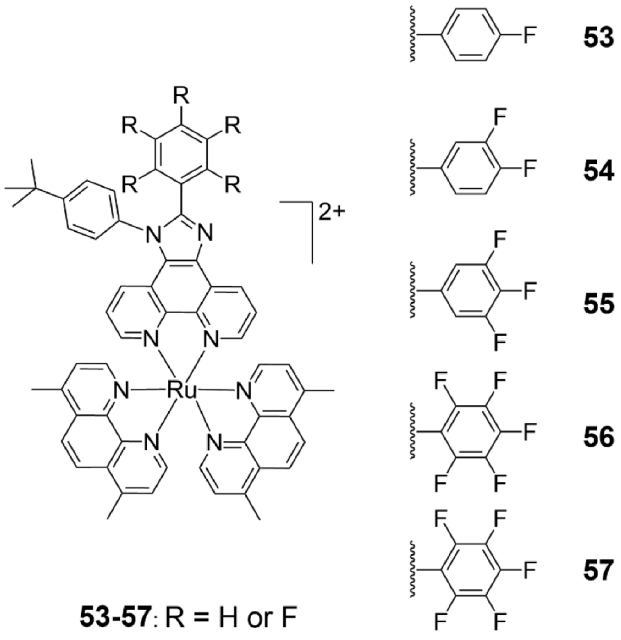

Fig. 43. Structures of fluorinated complexes **53–57** [162].

has been shown to affect cancer cells more severely than normal tissues, as cancer cells proliferate and replicate at a significantly accelerated rate compared to healthy, normal cells [230]. J. A. Thomas, S. MacNeil, J. W. Haycock et al. reported on a dinuclear Ru (II) complex [{Ru(TAP$_2$)}$_2$(tpphz)]$^{4+}$ (TAP = 1,4,5,8-tetraazaphenanthrene, tpphz = tetrapyrido[3,2-*a*:2′,3′-*c*:3″,2″-*h*:2‴,3‴-*j*]phenazine) **58** (Fig. 44) [231]. The [{Ru(TAP$_2$)}$_2$(tpphz)]$^{4+}$ complex binds with high affinity to duplex and quadruplex DNA structures. Moreover, it displays the ability to directly damage biomolecules without the mediation of singlet oxygen

or others ROS. Indeed, both duplex and quadruplex DNA structures quench its excited state leading to guanine radical cations as photo-oxidization products within the DNA. As the emission properties of **58** are suitable for optical microscopy applications, it was possible to directly track its penetration into cells, showing its primary localization within the nucleus. The σ_{TPA} cross-section of $[\{Ru(TAP_2)\}_2(tpphz)]^{4+}$ was evaluated to 90 GM at 850 nm, compared to Rhodamine B. Optimal emission outputs from the internalized complex were detected with two-photon excitation within the range of 850–900 nm. Preclinical spheroid models containing healthy, hypoxic and necrotic layers and C8161 human melanoma cell lines offered improved insights into the efficacy of this dinuclear photosensitizer in terms of penetration, light penetration, responsiveness to dosage within a lifelike tumor microenvironment, highlighting the potential of **58** for the selective treatment of melanoma.

Chao and co-workers designed the bimetallic ruthenium (II) azo PS **59** (Fig. 45) [232] to enhance penetration in cancer cells, taking in account that intracellular concentration of GSH in cancer cells is noticeably elevated compared to that in normal cells [233]. The azo group is designed to quench the phosphorescent emission of the Ru-azo dinuclear complex **59**. Interestingly, the reduction of the azo group within **59**, by glutathione, afforded the formation of the dinuclear complex **60** with a hydrazo unit. This reaction results in the restoration of a luminescence signal while the capacity of the complex **60** to generate ROS is activated. The level $^1O_2$ generation of the hydrazo complex **60** was 20 times higher than that of the azo complex **59**, which validates the design of **59** as a GSH-activatable potential prodrug for PDT. The cell studies highlighted that both **59** and **60** permeate MCTSs and aggregate within the mitochondria of cancer cells. **60** showed a σ_{TPA} of 210 GM at 810 nm, in MeOH. Its phototoxicity on incubated HeLa MCTSs, induced by TP irradiation at 810 nm, was also established with an $IC_{50\ light}$ of 5.7 μM and a phototoxicity index (PI = $[IC_{50\ dark}]/[IC_{50\ light}]$) of 19. **60** effectively promoted the generation of singlet oxygen in MCTS cells and hindered cancer growth. As for it, MCTSs treated with the azo complex **59** stopped their growth two days following TP irradiation, validating the significance of this type of TP-activated photosensitizers.

As previously indicated, a second strategy to enhance the selectivity of Ru (II) polypyridyl-based photosensitizers involves conjugating them with targeting groups (such as folic acid, biotin, or glucose) that can bind to specific receptors on cancer cell membranes, favoring their preferential localization and function at the tumor site. Such groups are generally bound to ruthenium by a spacer (via the second coordination sphere of the ligands) and rarely attached directly in the first coordination sphere. J. Fan et al. reported on a tamoxifen modified Ru (II) polypyridyl complex **61** (Fig. 46) that consists of two complementary functional subunits: a tamoxifen-containing ligand provided specific targeting of estrogen receptor (ER) while the Ru (II) polypyridyl moiety, similar to **62**, served for monitoring cellular uptake and localization and as TP-photosensitizer [234]. The highest σ_{TPA} cross-section of 61 was 180 GM at 830 nm. Photo-cytotoxicity assays indicated that 61 exhibits increased cell uptake and photo-cytotoxicity to MCF-7 (ER-positive) breast cancer cells by inducing lysosome damage, in contrast to the control compound **62** lacking the tamoxifen moiety.

With the aim of identifying new therapeutic tools against resistant cancers, Y. Chen, H. Chao et al. synthesized a biotin-containing Ru (II) complex (**Ru-Biotin**, Fig. 47) as a photosensitizer [235]. Biotin, also referred to as vitamin H or B8, is required for cell growth. As a consequence, cancer cells exhibit a greater demand for biotin compared to normal cells. Hence, biotin appears as a promising vitamin based site-directing agent for diagnostic and targeted anticancer drug delivery [236]. The synthesis of **Ru-Biotin** was carried out by using a biotin–phenanthroline ligand resulting from the coupling of 5-amino-1,10-phenanthroline with an acyl chloride derivative of biotin [237]. Ru-Biotin exhibited a maximum σ_{TPA} values of 140 GM at 820 nm in methanol, determined by the TPEF method. It was established that introducing biotin lightly increases the cytotoxicity of the complex in the dark, but above all, it notably improves the distinction between cancerous and normal cells. In particular, Ru-Biotin displayed substantial accumulation within A549R cancer cells overexpressing biotin receptors (A549R are derived cisplatin resistant A549 cells). When exposed to two-photon excitation at 820 nm, Ru-Biotin exhibited potent photocytotoxicity against cancer cell lines and showed a very low IC50 value (3.3 μM) towards A549R cells. The observed distinct levels of photocytotoxicity against cancerous and non-cancerous cell lines may be attributed to differences in the cellular uptake levels of the Ru (II)-Phenanthroline–Biotin complex. Together with the $\sigma_{TPA} \times \phi_\Delta$ merit of 122.0, this underlines the efficiency of Ru-Biotin as a two-photon $^1O_2$ sensitizer.

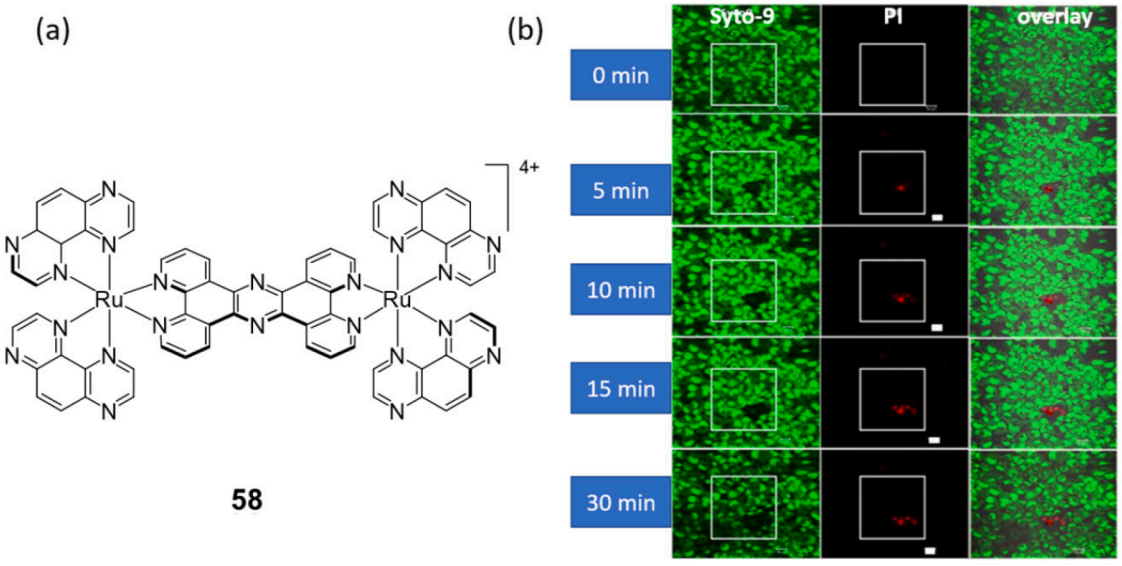

Fig. 44. (a) Structure of $[\{Ru(TAP_2)\}_2(tpphz)]^{4+}$, **58**. (b) Two-Photon photo-toxicity of **58** in human melanoma cells incubed with 100 μM **58** following irradiation at 900 nm (10 mW, 30 min) inside the limits of the white square. Left column: live cells imaged with Syto-9 (2 μM); Right column: dead cells imaged with Propidium iodide (500 nM). Recorded at intervals of 0, 5, 10, 15 and 30 mins (scale bar = 20 μm). Adapted with permission from Ref. [231]. Copyright ©2020 American Chemical Society.

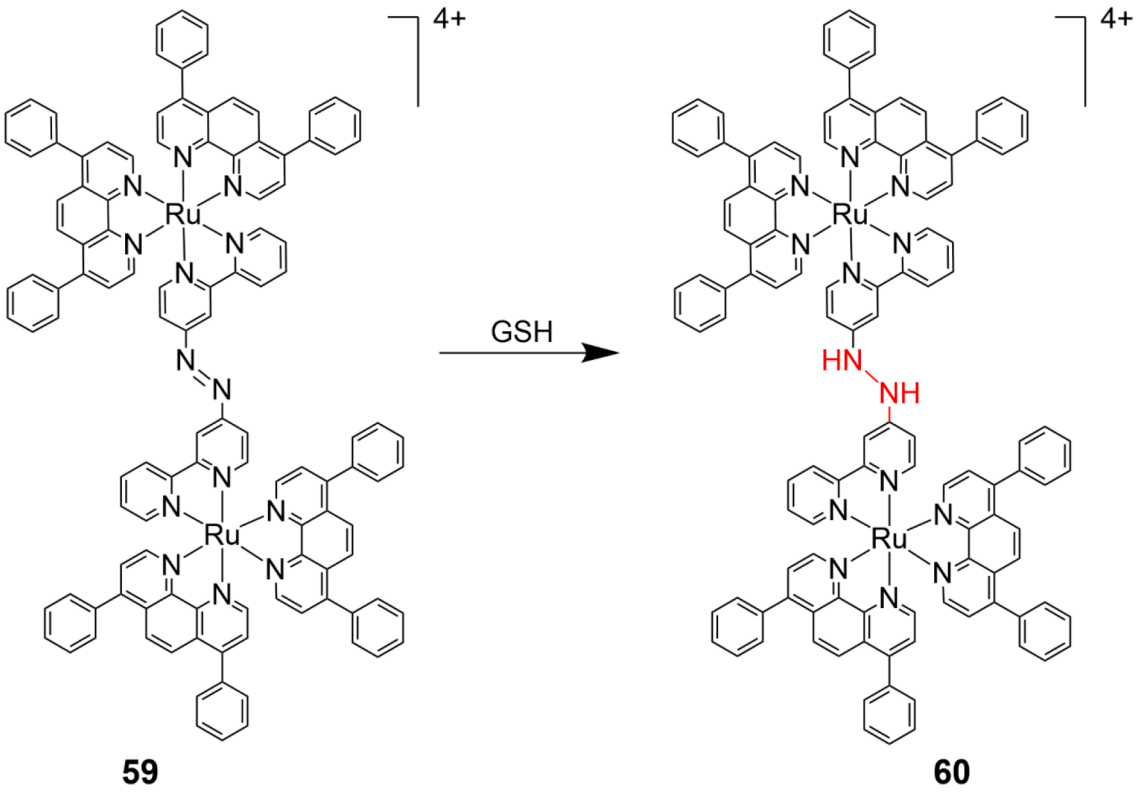

Fig. 45. Reduction reaction of the Ru-azo complex **59** by GSH leading to **60** [232].

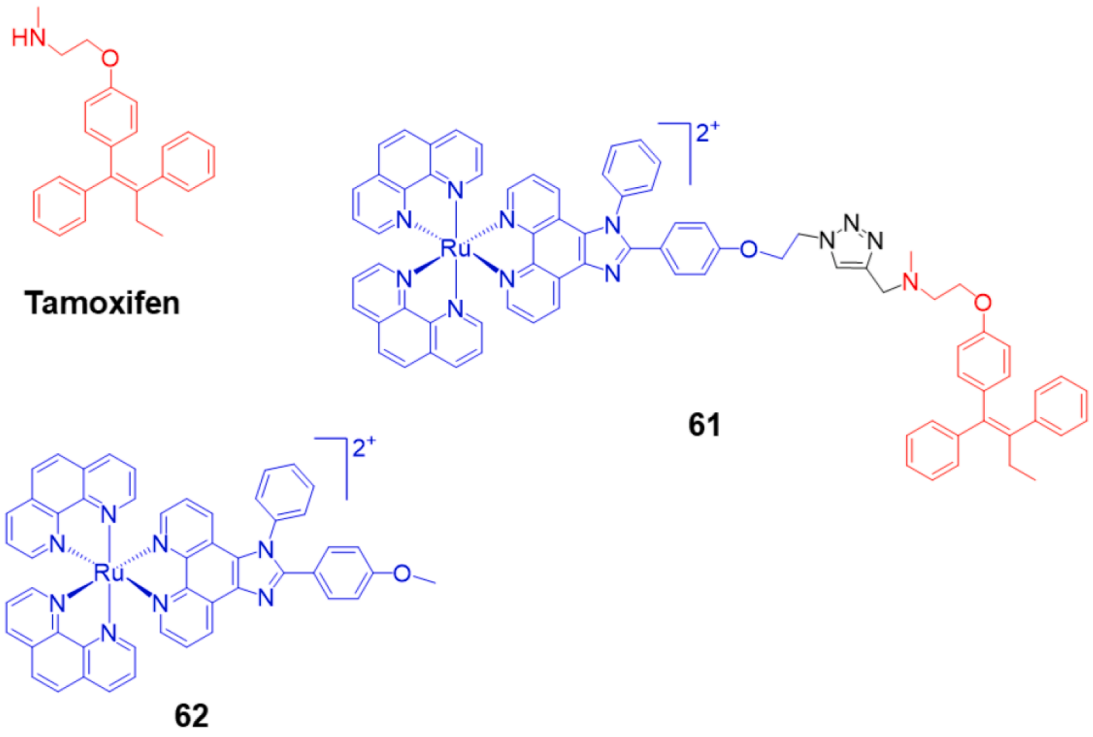

Fig. 46. Chemical structures of the tamoxifen-containing Ru (II) polypyridyl complex **61**, a control compound **62** and tamoxifen [234].

Overexpressed glucose transporters (GLUTs) favor increased glucose uptake in cancer cells and thus, become promising targets for tailored cancer therapies. Keeping this in view, the Chao group investigated on series of glucose appended to Ru (II) polypyridyl complexes **63**–**66** denoted as $[Ru(dip)_2(N^N\text{-glucose})]^{2+}$ (dip = 4,7-diphenyl-1,10-phenanthroline) (Fig. 48) [238]. These glucose-appended Ru (II) complexes demonstrated increased penetration in several cancerous cell lines and localized in their mitochondria. In particular, the complex 64 successfully eliminated a HeLa tumor xenograft through a multi-stage in vivo two-photon PDT assay, which allows tumors to be re-enriched with

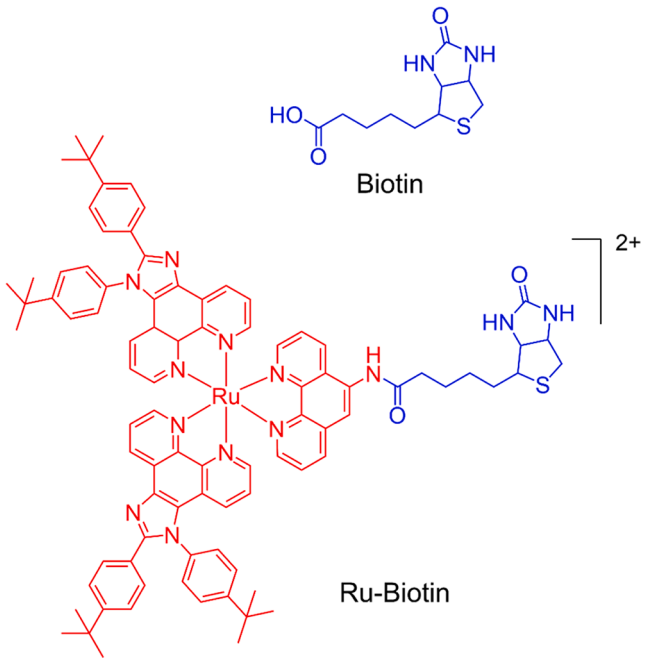

Fig. 47. Chemical structure of a biotin-modified Ru (II) complex developed by Y. Chen, H. Chao et al. as a photosensitizer for tumor-targeted PDT [235].

oxygen, increasing the efficacy of PDT in hypoxic conditions.

Further, Zhao et al. developed a ruthenium (II) phenanthroline complex linked with a cyclic tripeptide, Arg-Gly-Asp (RGD). This complex operates as a two-photon activatable PDT sensitizer for ablating tumors, specifically targeting the mitochondria of tumor cells abundant in integrin αvβ3 [239]. The maximum TPA value of the resulting Ru-conjugate was 63.5 GM at 820 nm. *In vitro* and in vivo experiments confirmed its selectivity towards integrin $\alpha_v\beta_3$-rich tumor cells, cellular penetration, together with its PDT anticancer efficacy under TP irradiation.

D. Luo, H. Chao and co-workers developed an alternative bio-orthogonal approach based on a copper-catalysed azide–alkyne click reaction between ruthenium (II) complexes bearing an alkyne termini, and an azide-labeled monosaccharide, the tetraacetylated N-Azidoacetyl-mannosamine, that provides a highly specific tool for studying glycoproteins [240]. Thanks to this bio-orthogonal labelling, these authors realize effective tumor-specific photodynamic therapy against triple-negative breast cancer cells. With outstanding singlet oxygen quantum yield and TPA cross-section, the specific bio-orthogonally labelled ruthenium (II) complex exerted an antitumor reaction by affecting cell membranes. Its efficacy as a two-photon photosensitizer was validated in both monolayer and 3D multicellular tumor spheroids. Consequently, the design of bio-orthogonal two-photon photosensitizers using Ru (II) complexes represents a new alternative for developing effective photodynamic therapy.

4.5. Ru (II) polypyridyl complexes in two-photon photoactivated chemotherapy[7]

Photoactivated chemotherapy (PACT) offers a promising alternative to photodynamic therapy approaches. It entails deactivating pro-drug molecules through a protective group that can be eliminated upon light exposure (“uncaging”). Ideally, the non-irradiated PACT agent should exhibit minimal biological activity and low toxicity, whereas this PACT agent should manifest potent biological activity, upon irradiation. Once the bond is cleaved by light, the generated product becomes toxic to the cancer cells. PACT can thus be defined as a noninvasive method of activating a drug with a good spatial and temporal control [241–246]. Ruthenium (II) complexes with the ability to undergo ligand exchange due to a distorted octahedral geometry have significant potential as metal-based PACT compounds, thanks to their favorable photophysical features, good structural stability under physiological conditions and stable redox states [247–250]. An engaging characteristic of Ru (II) polypyridyl complexes is the relative ease with which various ligands can be combined around the metal center. This flexibility makes it possible to adjust both the photo-physical features and the composition of the caged molecule [143,149,251]. These properties can be used to release toxins *in situ*, thereby contributing to the lethality of phototherapy [252,253]. Here again, the wavelength required to trigger light activation is a crucial factor, as it can limit therapeutic applications if the light cannot penetrate deeply into dense tissue. Ideally, light should be employed within the window where biological materials are most transparent, (600–900 nm), to activate the photodissociation of one ligand from the coordination sphere and, as a consequence, promote targeted cytotoxic processes [254]. Low energy NIR irradiations as applied in two-photon excitation processes could help minimize potential light-induced photodamage while ensuring improved light penetration depths. This is crucial since at shorter wavelengths, light penetration is typically restricted by the absorption and scattering effects of biological tissue [252]. In light of this, Ru (II) polypyridyl complexes were extensively studied as photorelease complexes for therapeutic applications [143,144,246,251,252]. The general aspects have been the subject of recent and fully detailed reviews [253,255], which reveal how the combination TP-PACT with Ruthenium (II) complexes was little explored, apart from mechanistic studies [147,256].

R. Etchenique et al. were the first to illustrate the feasibility of using ruthenium bipyridyl complexes as two-photon photo-triggers for biologically-active substances, employing very low-energy IR photons, under physiological conditions [257]. Two-photon uncaging of 4-aminopyridine (4AP), a K^+ channel inhibitor, from the ruthenium bipyridyl complex $[Ru(bpy)_2(4AP)_2]Cl_2$ (RuBi-4AP) **67** (Fig. 49) was observed upon one-photon irradiation at 360 nm as well as two-photon irradiation at 720 nm. It led to the photocleavage of $[Ru(bpy)_2(4AP)_2]Cl_2$ yielding free 4-aminopyridine together with the non-fluorescent aquo complex $[Rubpy_2(H_2O)(4AP)]^{2+}$. Even if the action cross-section for the uncaging of 4AP cannot be precisely quantified, the authors provided an estimated range in the order of 0.01 to 0.1 GM at 800 nm, based on NMR-TPE coupled experiences [257].

This approach has been extended to a range of photon uncaging neurotransmitters such as RuBi-Gluta **68** (Fig. 49) [258], from which glutamate (Gluta) can be released by two-photon activation at about 800 nm [259]. As for the aminopyridine, these photoexcited ruthenium–bipyridyl complexes quickly afford clean and fast photorelease of the caged bioactive molecules. Two-photon induced uncaging of RuBi-Gluta presented a spatial precision that approximated the dimensions of a typical dendritic spine,[8] [260] making it suitable for optical mapping of glutamatergic receptors [259].

More recently, R. Yuste, R. Etchenique et al. studied the two-photon induced uncaging of a RuBi-dopamine (Dopa) complex RuBi-Dopa **69** (Fig. 49) for studying the dopaminergic signal transmission in dendritic spines considered to be the primary receptacles for stimulatory information within the brain [261]. A two-photon irradiation of 4 ms directly adjacent to the head of the spines resulted in the removal of dopamine from the RuBi-Dopa complex, together with a fast increase of the Ca^{2+} levels within the spinal columns. This observation suggests the photo-availability of dopamine via two-photon excitation and implies the

[7] The term photoactivated chemotherapy only applies to therapies in which the photo-activatable drug molecules incorporate a d-block element, as opposed to organic based photosensitizers [237].

[8] Dendritic spines typically do not surpass a size of 1000 nm [261].

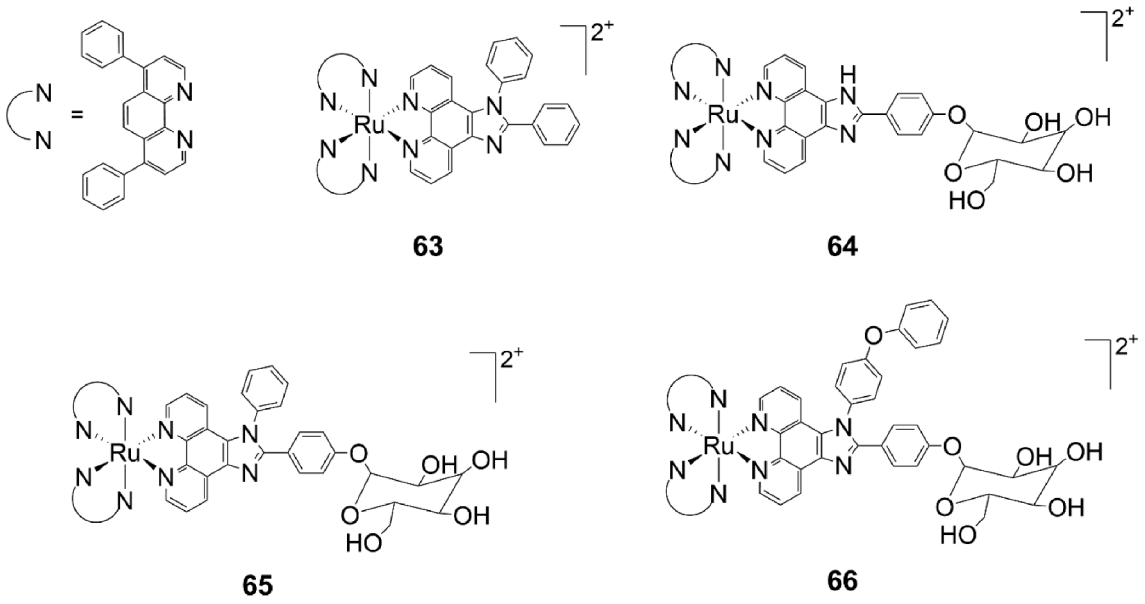

Fig. 48. Structures of glucose-appended Ru (II) polypyridyl complexes $[Ru(dip)_2(N^{\wedge}N\text{-glucose})]^{2+}$ (dip = 4,7-diphenyl-1,10-phenanthroline) **63–66** [238].

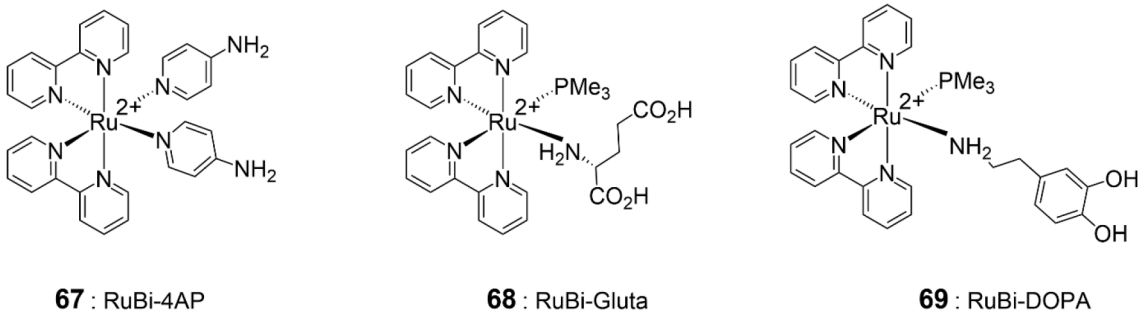

Fig. 49. Ruthenium polypyridyl complexes for two-photon induced photo-triggered uncaging [257,259,261].

existence of functional dopamine receptors on the spines. The resulting calcium imaging allowed these functional dopamine receptors to be mapped with high spatial resolution in brain tissue in a non-invasive manner.

Zhou et al. used a pyrene-modified-terpyridine (tpy-Py) as a sterically demanding bidentate ligand with the aim to design a Ru (II) polypyridine complex **70** (Fig. 50), which would exhibit both photodynamic therapy (PDT) and photoactivated chemotherapy (PACT) capabilities [262]. The uncoordinated pyridine participates to the distortion of the octahedral geometry, facilitating the dissociation of tpy upon irradiation. The presence of the pyrene group imparts the complex with a pyrene-based $^3\pi\pi$ state characterized by low energy and long lifetime, promoting singlet oxygen generation. An efficient energy transfer from tpy-Py to the Ru (II)-based metal-to-ligand charge transfer transitions leads to the quenching of tpy-Py fluorescence in complex **70**. However, the luminescent emission is restored upon photo-dissociation, both in an aqueous environment and within cancer cells. Complex **70** shows a σ_{TPA} cross-section about 300 GM at 800 nm. Its toxicity against A549 cells and A549R 3D multicellular spheroids (3D MCSs) under two-photon irradiation was evaluated and demonstrated potent anticancer activity against both hypoxic and cisplatin-resistant cancer cells upon near-infrared irradiation [262].

Achieving two-photon excitation of Ru (II)-based photoactivated chemotherapy agents within the biological window requires the design of complexes displaying high TPA cross-sections. Otherwise, TPA would require unsafe high-intensity laser excitation. X. Wang, Q. Zhou et al. circumvented this obstacle by designing supramolecular nanoparticles

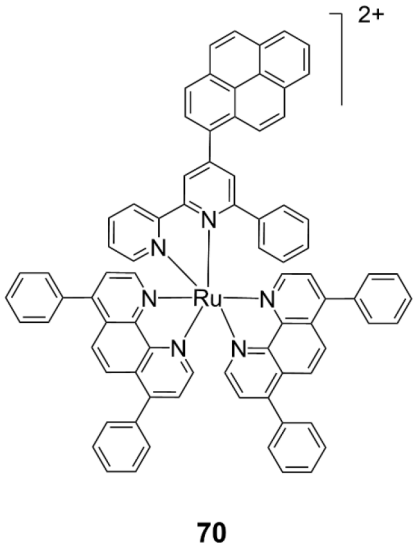

Fig. 50. Structure of the photoactivatable Ru (II) polypyridyl complex **70** [262].

(labeled as **Ru-PEG**) (Fig. 51) [263]. This design was based on a poly (ethylene glycol) (PEG) modified $[Ru(dip)_2(py\text{-}SO_3)]^+$ nano-assemblies (dip = 4,7-diphenyl-1,10-phenanthroline, py-SO_3 = pyridine-2-

sulfonate). These authors established that **Ru-PEG** underwent photoinduced dissociation and released $[Ru(dip)_2(H_2O)_2]^{2+}$, a cytotoxic species [264]. This photocage system was combined with 1,3-phenylenebis (pyren-1-ylmethanone) (BP), to form a supramolecular **Ru-PEG-BP** nano-assembly, chosen for its intense emission over the wavelengths where **Ru-PEG** strongly absorbs, together with an outstandingly high two-photon absorption cross-section value, which had been previously reported by these authors to be $\sigma_{TPA} = 2.8 \times 10^5$ GM [263].

The photo-induced cytotoxicity of the **Ru-PEG-BP** nanoparticles against human lung cancer A549 cells, as well as cisplatin resistant A549R cells and 3D MCTSs cancer model[9]was examined, showing that the Ru (II) based PACT nanoparticles effectively eliminate cancer cells via an oxygen-independent mechanism. This occurs upon 470 nm one-photon irradiation for 30 min or 810 nm two-photon irradiation (1 W. cm^{-2}) for various durations (ranging from 0 to 30 min). However, **Ru-PEG** showed minimal impact under identical conditions, likely due to its comparatively low two-photon absorption capability [263]. The cytotoxicity induced by two-photon excitation of **Ru-PEG-BP** nanoparticles has been attributed to the concerted effect of two-photon excitation of BP and effective Förster resonance energy transfer (FRET) from BP to **Ru-PEG**, which led to an efficient two-photon induced ligand dissociation of $[Ru(dip)_2(H_2O)_2]^{2+}$. This enables the PACT activity of **Ru-PEG-BP** upon two-photon excitation within the 650–900 nm phototherapeutic range. This approach therefore would represent a practical means of developing near-infrared activated PACT theranostic systems.

Regardless of the mode of action (PDT or PACT) in which the polypyridyl Ru (II) complexes are involved, the previous examples illustrate how important it is to rationalize the design of Ru (II)-based PS to provide sufficient presence in cancerous tissue, specifically, and limit systemic toxicity and peripheral photo-induced damage. Crucial inquiries, such as the localization within biological systems and systemic toxicity of ruthenium polypyridyl compounds, continue to be raised, as there are insufficient *in vivo* preclinical studies, leaving much yet to be understood. These general limits opened the way for the development of nanomaterials in which Ru (II) polypyridine complexes can be integrated [265]. Incorporating the metal complexes into polymeric materials, often referred as nanoparticles, presents a promising approach to overcome the pharmacological constraints of molecular agents while offering cancer-selective benefits. Indeed, polymeric nanomaterials are highly suitable for medical imaging, diagnosis, theranostics, and drug delivery, thanks to their tunable characteristics, such as their high surface area, properties at the interface, water solubility, and multifunctionality [266–268]. In this context, the construction of nanomaterials containing polypyridyl Ru (II) units as TP-photosensitizers with high cross-section values attract current attention to address the limitations of the Ru (II) complexes in terms of size, solubility, renal clearance and ability to target desired locations [20,269–272].

For instance, Karges et al. reported the incorporation of the heteroleptic Ru (II) polypyridine complex, $[Ru(2,2'\text{-bipyridine})_2((E,E')\text{-}4,4'\text{-Bis}[p\text{-}(N,N\text{-methoxy})\text{styryl}]\text{-}2,2'\text{-bipyridine})]^{2+}$ into polymeric nanoparticles featuring terminal biotin groups (Fig. 52) [273]. They achieved this by using a commercially available polymer known as 1,2-distearoyl-*sn*-glycero-3-phosphoethanolamine-N-[biotin(polyethyleneglycol)-2000], ($DSPE\text{-}PEG_{2000}$-biotin) in its ammonium salt form. Quantitative analysis revealed a roughly 20-fold increase in accumulation within the sodium multivitamin transporter-overexpressed adeno-carcinomic human lung (A549) cancer cells in comparison to human lung fibroblast non-cancerous cells. These nanoparticles demonstrated negligible toxicity in the absence of light but displayed increased cytotoxicity towards cancerous A549 cells relative to human non-cancerous pulmonary fibroblast cells when subjected to one-photon irradiation (500 nm) or two-photon irradiation (800 nm, 100 fs, 10.1 J/cm^2). Interestingly, a substantial 8.7-fold increase in accumulation within an A549 tumor-bearing mouse model was observed compared to the unformulated complex when equivalent amounts of the Ru (II) polypyridine complex were administered intravenously. Under clinically relevant one-photon (500 nm) or two-photon (800 nm) excitation conditions, these nanoparticles almost entirely eradicated tumors within the mouse model.

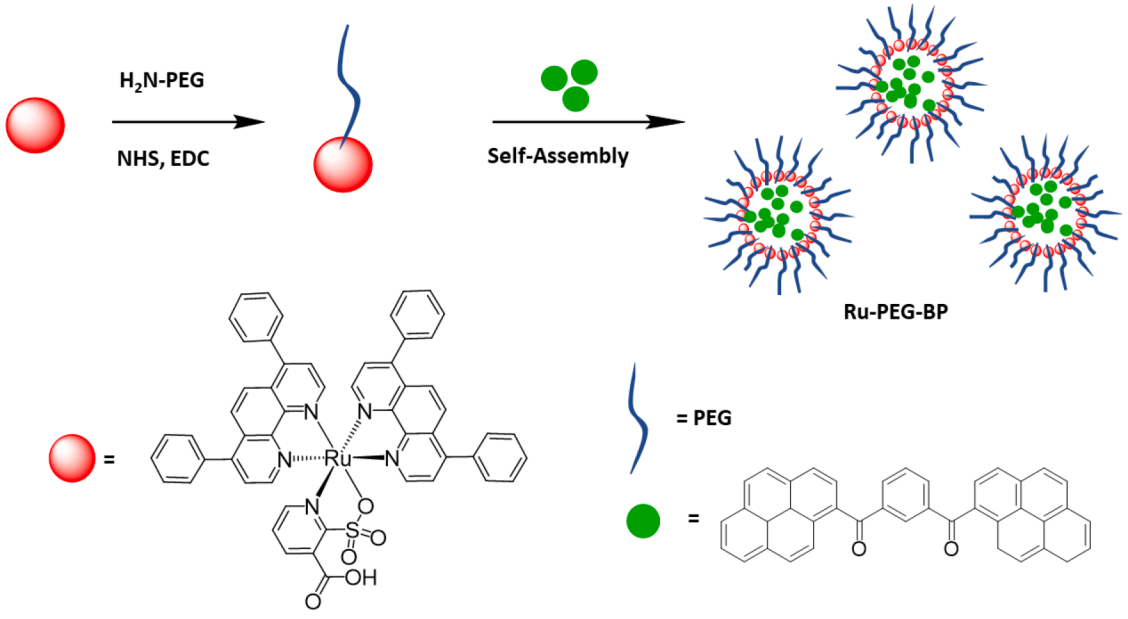

Fig. 51. Main steps for the preparation of a supramolecular **Ru-PEG-BP** nano-assembly [263].

Among other strategies, Ru (II) polypyridyl complexes have additionally been integrated onto the surface of inorganic nanomaterials. These functional nanomaterials can be succinctly described as three main classes of supports: metal–organic frameworks (MOFs),

[9] MCTS are considered more judicious than conventional cell monolayers for drug screening, as they can replicate *in vivo* pathophysiological conditions more accurately [182].

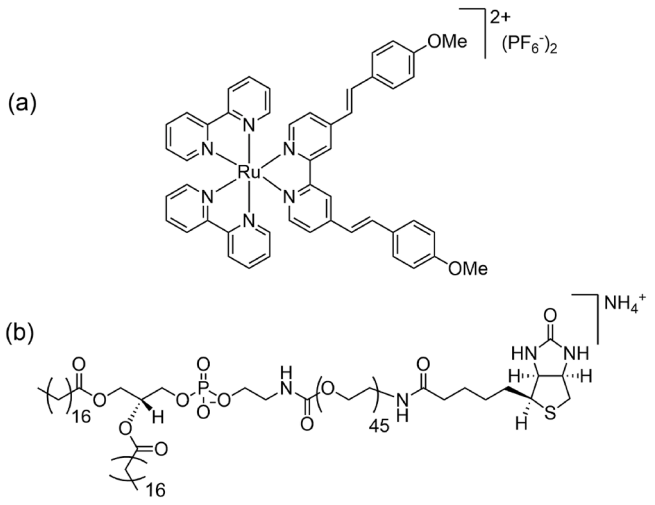

Fig. 52. Structures of (a) the PS [Ru(2,2′-bipyridine)$_2$((*E,E*′)-4,4′-bis[p-methoxystyryl]-2,2′-bipyridine)]$^{2+}$. (b) DSPE-PEG$_{2000}$-biotin: 1,2-distearoyl-*sn*-glycero-3-phosphoethanolamine-*N*-[biotin (poly(ethyleneglycol))-2000] [273].

carbonaceous nanomaterials, inorganic nanomaterials [274]. However, it should be kept in mind that the particle size, complexity and concerns regarding their metabolism, biodegradability and biosafety of these nanosystems remain areas of concern to be overcome [275–277].

In 2016, F. Cunin et al. reported that a Ru (II) complex, [Ru(5-Fluo-Phen)$_2$(5-E-Phen)]$^{2+}$, (5-Fluo-Phen) = 5-dihexylfluorene-1,10-phenanthroline and (5-E-Phen) = 5-ethynyl-1,10-phenanthroline, covalently bonded to the surface of porous silicon nanoparticles (pSiNP-Ru-PEG-Man) (Man = Mannose; PEG = polyethylene glycol) significantly increased the TP-PDT efficacy of these nanoparticles [278]. The PEG chain was introduced to enhance both biocompability and dispersibility; the mannose moiety was attached to this platform to facilitate tumor targeting. The in vitro photodynamic impact of various formulations, including pSiNPs, pSiNP–Ru, pSiNP–Ru–PEG and pSiNP–Ru–PEG–Man was assessed on MCF-7 cells. Results indicated a significant enhancement in the photodynamic effect of pSiNP–Ru compared to free Ru (II) complex and bare pSiNPs in terms of two-photon photodynamic therapy efficiency. Two-photon imaging confirmed successful endocytosis of the photosensitizer-functionalized materials by MCF-7 cells. The extension of PEG chains improved nanoparticle dispersion, potentially extending circulation time in the bloodstream. Mannose was efficient to target tumor cells, as confirmed by comparing the uptake of pSiNP-Ru-PEG-Man with that of pSiNP-Ru-PEG. Notably, cancer cell viability decreased to 36 % for pSiNPs functionalized with the Ru (II)-photosensitizer, indicating its ability to induce cytotoxic singlet oxygen and reactive oxygen species upon two-photon excitation. Furthermore, cancer cell viability was reduced by 13 % in cells treated with pSiNP–Ru–PEG–Man, underscoring the capacity of the Ru (II) complex in enhancing the efficacy of the pSiNP material for photodynamic therapy.

Considering that nanohybrids have been acknowledged for their enhanced efficacy in killing cancer cells in comparison to free photosensitizers, C.-P. Tan, Z.-W. Mao, et al. applied their **33@CDs** nanohybrids, comprising carbon nanodots covalently linked to Ru (II) complexes (refer to Fig. 30), for two-photon photodynamic therapy targeting cancer cells [185]. The efficacy of TP-PDT was evaluated for both **33** and **33@CDs** in two-dimensional cell cultures and multicellular tumor spheroid models (MCTSs). **33** and **33@CDs** showed low toxicity to MCTS in the absence of light. However, under two-photon irradiation, they exhibited significantly heightened toxicity. After being subjected to an 810 nm two-photon irradiation, MCTSs treated with either **33** or **33@CDs** displayed notably reduced green emission, alongside noticeable alterations in cell structure such as cell shrinkage and the emergence of numerous white blood cells. The IC_{50} values recorded for TP-PDT were as low as 12.0 μM (PI > 8.3) for **33** and 2.2 μM (PI > 45.4) for **33@CDs**, respectively. The enhanced photocytotoxicity of **33@CDs** in comparison to **33** can ascribed to their larger two-photon absorption cross-section and superior cellular uptake of ruthenium.

Ultimately, nanocarriers can fulfill a far more significant role beyond mere support for the photosensitizer. For instance, Zhang et al. introduced Ru (II) complex-functionalized single-walled carbon nanotubes (**Ru@SWCNTs**, depicted in Fig. 53), wherein the carbon nanotubes facilitate the integration of two-photon photodynamic therapy TP-PDT and photothermal therapy PTT [279]. Photothermal therapy involves artificially raising tissue temperatures to induce apoptosis or enhance cellular susceptibility to chemotherapy or radiotherapy. By combining PDT and PTT, this approach has the potential to enhance therapeutic outcomes beyond what could be achieved with separate PDT or PTT treatments [280]. Carbon nanotubes are recognized for their ability to convert light energy into heat [281]. In this case, they served dual roles as agents for photothermal therapy and as a platform for hosting the Ru (II) photosensitizers **71** and **72** (Fig. 53), both of which possess notably high two-photon absorption cross-sections (494 and 428 GM, respectively). The authors utilized heteroleptic ruthenium complexes comprising π-extended planar ligands, to favor π–π stacking interactions with carbon nanotubes [282]. The photothermal conversion efficacy of the **Ru@SWCNTs** was observed to be 40 % greater than that of SWCNTs by themselves. Upon irradiation with 808 nm light, temperature increases ranging from 36 to 38 °C were recorded, which are sufficient for conducting photothermal therapy against cancer. Alongside these temperature increases, the Ru (II) photosensitizers **71** and **72** were released upon irradiation with 808 nm light at 0.25 W.cm^{-2} and subsequently generated $^1O_2$ in HeLa cells upon two-photon irradiation at 808 nm.

A follow-up imaging study of incubated HeLa cells revealed that **Ru@SWCNTs**. Localized within lysosomes. Both pare carbon nanotubes and Ru (II) complexes (up to 200 μg/mL) exhibited minimal toxicity in the absence of light. However, when exposed to light, both **Ru@SWCNTs** and carbon nanotubes induced cell death, with the combined treatment resulting in a substantial decrease in cell viability. These findings were validated in both multicellular spheroids and an *in vivo* mouse model, confirming their relevance across various experimental settings.

A recent study by the Karges and Chao groups exploits an original route for integrating Ru (II) polypyridine two-photon photosensitizers via coordination synthesis to graphitic carbon nitride nanosheets (Fig. 54) [283]. This study is based on the fact that graphitic carbon nitride nanosheets have the ability to generate ROS by themselves within a hypoxic environment. Indeed, an earlier study by Chao's group revealed that **Ru-g-C_3N_4** exhibited extensive promise as a theranostic agent in cancer treatment [284]. Compared with pure g-C_3N_4, the nanosheets obtained demonstrated increased water solubility, enhanced absorption of visible light, and heightened biocompatibility. These results suggested that coordinating PS with g-C_3N_4 graphitic carbon nitride nanosheets serve as a method to enhance the photophysical properties of photosensitizers. The **Ru-g-C_3N_4** conjugates exhibited absorption patterns characteristic of a Ru (II) polypyridine complex, with a metal–ligand charge-transfer transition observed around 450 nm. Upon excitation at 450 nm, these metal complexes emitted red light with luminescence quantum yields ranging from 0.56 % to 1.21 %. Luminescence lifetimes increased from 738-1141 ns under normoxic conditions (21 % O_2) to 1721–2161 ns under hypoxic conditions (1 % O_2), indicating the photosensitizer's reactivity with oxygen. These conjugates displayed strong two-photon absorption, with **Ru3-g-C_3N_4**, for example, showing a σ_{TPA} value of 34,209 GM at 800 nm. They efficiently generated reactive oxygen species (ROS) including $^{\bullet}O_2^-$, $^{\bullet}OH$, and $^1O_2$. Additionally, the conjugates could catalytically convert H_2O/H_2O_2 into O_2, providing a self-sustaining ROS generation system independent of cellular oxygen levels. This ability to produce oxygen and ROS under hypoxic conditions holds promise for addressing the challenge of

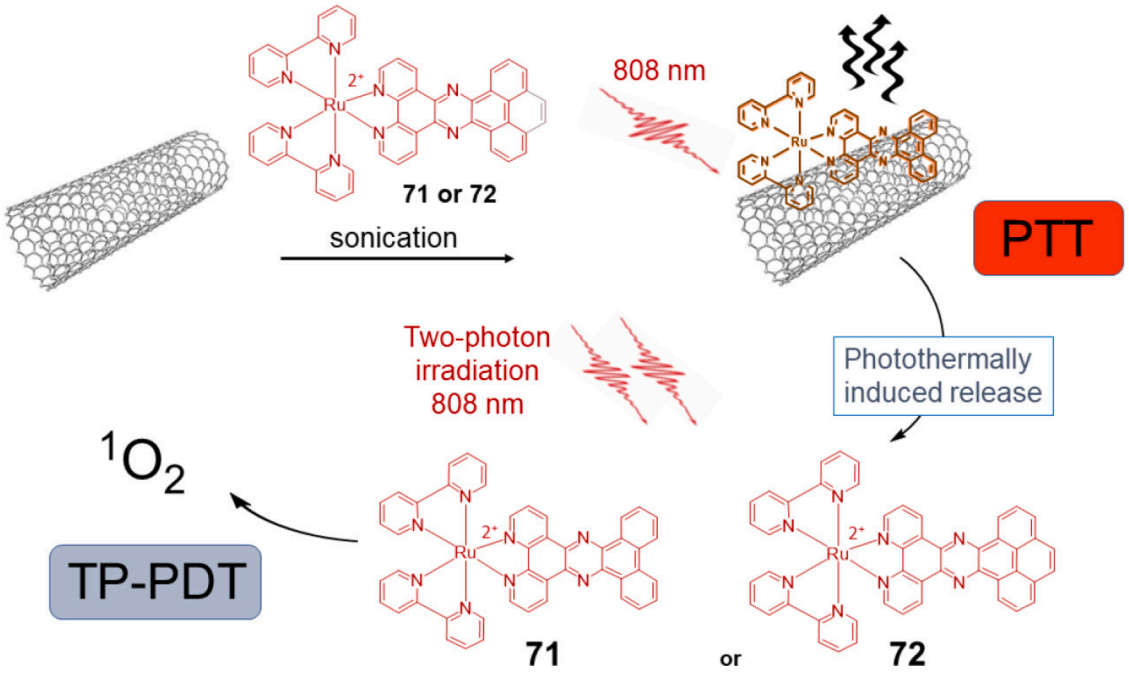

Fig. 53. Schematic illustration of **Ru@SWCNTs** for dual two-photon photodynamic therapy (TP-PDT) and photothermal therapy (PTT) upon exposure to irradiations at 808 nm [279].

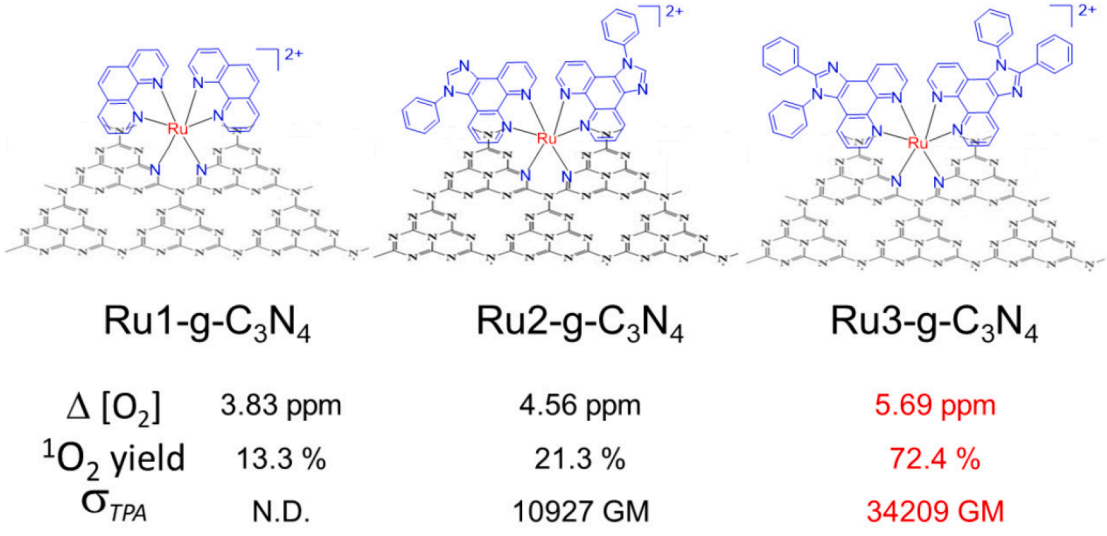

Fig. 54. Chemical structures of the Ru-g-C_3N_4 conjugates studied by the Karges group [283].

treating hypoxic solid tumors in photodynamic therapy.

To improve its pharmacological features, **Ru3-g-C_3N_4** was encapsulated within the amphiphilic DSPE-PEG_{2000}-NH_2 polymer setting up the nanoformulation **RuCN@PEG**. This nanomaterial demonstrated preferential accumulation within mitochondria and the endoplasmic reticulum. Upon exposure to either one- or two-photon irradiation (at 450 nm and 800 nm, respectively), **RuCN@PEG** death in both monolayer cells and multicellular tumor spheroids, via a combination of programmed cell death pathways including apoptosis, paraptosis, ferroptosis, and damage to immunogenic cells mechanisms. Further evaluation of its therapeutic potential involved intravenous administration into a mouse model with malignant melanoma. Under two-photon irradiation using an 800 nm laser, **RuCN@PEG** significantly suppressed tumor growth, affecting both primary and distant secondary tumors in the melanoma model by activating the immune system. This approach holds promise for the treatment of recurrent and metastatic or disseminated tumors, one of the most challenging areas of cancer therapy.

5. Overview and future outlook

The photophysical properties of Ru (II) polypyridyl complexes have captivated considerable interest in various fields of research**.** Their advantages include reliable methodologies for the preparation of complexes with reliably anticipated structures and tunable photophysical parameters, along with the ability to modify ligand affinities and include labile ligands. These complexes exhibit intriguing photophysical attributes, such as readily accessible excited triplet states. A substantial number of them serve as efficient emitters even under ambient conditions, displaying satisfactory emission quantum yields and remarkable

photostability. This attention is renewed by the possibility of making these compounds activatable in the two-photon mode, a property that expands their relevance to applications requiring precise in-depth penetration of light. The intrinsic photophysical characteristics of two-photon active polypyridyl Ru (II) complexes, combined with their structural adaptability, pave the way for interdisciplinary research spanning from their design and synthetic chemistry to fundamental photophysics, functional materials engineering, bio-imaging, and in-cell phototherapies.

Fundamental studies showed that octupolar ruthenium complexes with bistyryl-substituted bipyridyl ligands can display TPA cross-sections two to three times higher than that of the parent complex $[Ru(bpy)_3]^{2+}$. Generally, ligands with extended π-conjugation in the coordination sphere of the metal lead to increased TPA cross-section in the NIR region. Recognized approaches consist of amplifying the charge transfers within the complexes or favorizing their octupolar geometry. These solutions also seem applicable for heteroleptic systems, which would make it possible to combine several functional ligands around a unique $[Ru(bpy)_3]^{2+}$-like heart. Other solutions were explored, that focused on the functional aspects of the polypyridyl complexes rather than on the optimization of these complexes in the multiphoton regime. They consist in surrounding the complex by means of matrices or nanoplatforms that assume specific functions, such as two-photon imaging, chemo-photodynamic synergistic therapy or dual-drug loading, to name just a few. These approaches were more specifically directed towards biological or therapeutic objectives but could find an echo in the design of functional materials.

With their long-lived phosphorescence characteristics, polypyridyl ruthenium (II) complexes offer numerous advantages for luminescence imaging within living, intact cells and biological tissues. At the same time, the development of two-photon time-dependent luminescence analysis using these complexes as probes is expected to enable precise quantitative detection and visualization of active substances or organelles within biological samples. Additionally, TP-photosensitizers based on polypyridyl Ru (II) complexes show promise for potential therapeutic applications, an approach exemplified by TLD1433, which is currently undergoing human clinical trials for bladder cancer. These complexes can be made very efficient at generating singlet oxygen or other ROS in specific components or organelles during irradiation. Their conjugation with nanomaterials or peptides improves their efficacy and enables selective phototoxicity against cancer cells. However, challenges such as low water solubility, synthetic difficulties, short ROS lifetimes, and lack of tumor-targeting capabilities need resolution for the development of highly effective and selective anti-cancer treatments. Additionally, most of current TP excitations rely on high-power laser irradiations, posing tissue damage risks. Therefore, a key challenge is to develop TP-photosensitizers with sufficiently high cross-sections to ensure simultaneous absorption of two photons at low photon densities. Finally, despite promising preclinical performances, the lack of *in vivo* studies in this research area limits the assessment of their full potential.

Using ruthenium (II) polypyridyl complexes for encapsulating molecules has yielded promising outcomes. The study of complexes combining multi-phototherapeutic activities could open up new prospects as the design of these molecular systems continue to evolve. This approach may find inspiration in the many studies devoted to imaging and TP-PDT, in which the design of polypyridyl Ru (II)-based TP-photosensitizers will undoubtedly provide guidance for such developments. Of course, many more *in vivo* studies are required to uncover the complete capabilities of these bioconjugates. Regarding the risks linked to their therapeutic application, the precisely targeted activation of these prodrugs should enable a reduction in overall toxicity and side effects.

At this stage, it should be noted that studies on advanced materials (electrochromic or memory materials, photon harvesting and photocatalysts, etc.) appear very much underexplored given the properties of the TPA-polypyridyl ruthenium complexes. Current studies are focusing on the use of complexes *per se*. Their association with well-defined architectures, metal–organic and covalent–organic frameworks, supramolecular assemblies or carbon dots could certainly extend the research areas, generating unprecedented structural and functional possibilities.

There is no doubt that further exploration of ruthenium polypyridyl-based TP-photosensitizers will have a positive impact in a number of areas, such as advanced optical and electronic devices, photocatalysis, biology and medicine. The design of functionalized materials for precise specifications in terms of physicochemical or biological characteristics, photo- and electrochemical properties makes this highly engaging, with the potential for numerous emerging other applications. In conclusion, the continued study and advancement of innovative ruthenium polypyridyl-based TPA materials are expected to offer great potential to address a variety of challenges while stimulating innovations in fundamental research, technological and clinical applications.

Declaration of competing interest

The authors declare that they have no known competing financial interests or personal relationships that could have appeared to influence the work reported in this paper.

Data availability

No data was used for the research described in the article.

References

[1] M. Göppert-Mayer, Über Elementarakte mit zwei Quantensprüngen, Ann. Phys. 401 (1931) 273–294, https://doi.org/10.1002/andp.19314010303.
[2] M. Rumi, S. Barlow, J. Wang, J.W. Perry, S.R. Marder, Two-photon absorbing materials and two-photon-induced chemistry, in: Photoresponsive Polym. I, Springer-Verlag Berlin, Berlin, 2008, pp. 1–95.
[3] S. Maruo, O. Nakamura, S. Kawata, Three-dimensional microfabrication with two-photon-absorbed photopolymerization, Opt. Lett. 22 (1997) 132–134, https://doi.org/10.1364/OL.22.000132.
[4] A. Selimis, V. Mironov, M. Farsari, Direct laser writing: principles and materials for scaffold 3D printing, Microelectron. Eng. 132 (2015) 83–89, https://doi.org/10.1016/j.mee.2014.10.001.
[5] J. Chang, J. He, M. Mao, W. Zhou, Q. Lei, X. Li, D. Li, C.-K. Chua, X. Zhao, Advanced material strategies for next-generation additive manufacturing, Materials 11 (2018) 166, https://doi.org/10.3390/ma11010166.
[6] M. Vaezi, H. Seitz, S. Yang, A review on 3D micro-additive manufacturing technologies, Int. J. Adv. Manuf. Technol. 67 (2013) 1721–1754, https://doi.org/10.1007/s00170-012-4605-2.
[7] X. Zhou, Y. Hou, J. Lin, A review on the processing accuracy of two-photon polymerization, AIP Adv. 5 (2015) 030701, https://doi.org/10.1063/1.4916886.
[8] S. O'Halloran, A. Pandit, A. Heise, A. Kellett, Two-photon polymerization: fundamentals, materials, and chemical modification strategies, Adv. Sci. 10 (2023) 2204072, https://doi.org/10.1002/advs.202204072.
[9] D.A. Parthenopoulos, P.M. Rentzepis, Three-dimensional optical storage memory, Science 245 (1989) 843–845, https://doi.org/10.1126/science.245.4920.843.
[10] C.C. Corredor, Z.-L. Huang, K.D. Belfield, Two-photon 3D optical data storage via fluorescence modulation of an efficient fluorene dye by a photochromic diarylethene, Adv. Mater. 18 (2006) 2910–2914, https://doi.org/10.1002/adma.200600826.
[11] A.S. Dvornikov, E.P. Walker, P.M. Rentzepis, Two-photon three-dimensional optical storage memory, Chem. Eur. J. 113 (2009) 13633–13644, https://doi.org/10.1021/jp905655z.
[12] J. Lott, C. Ryan, B. Valle, J.R. Johnson III, D.A. Schiraldi, J. Shan, K.D. Singer, C. Weder, Two-photon 3D Optical data storage via aggregate switching of excimer-forming dyes, Adv. Mater. 23 (2011) 2425–2429, https://doi.org/10.1002/adma.201100458.
[13] D.L.N. Kallepalli, A.M. Alshehri, D.T. Marquez, L. Andrzejewski, J.C. Scaiano, R. Bhardwaj, Ultra-high density optical data storage in common transparent plastics, Sci. Rep. 6 (2016) 26163, https://doi.org/10.1038/srep26163.
[14] M. Imhof, D. Rhinow, N. Hampp, Two-photon polarization data storage in bacteriorhodopsin films and its potential use in security applications, Appl. Phys. Lett. 104 (2014) 081921, https://doi.org/10.1063/1.4867164.
[15] S. Pascal, S. David, C. Andraud, O. Maury, Near-infrared dyes for two-photon absorption in the short-wavelength infrared: strategies towards optical power limiting, Chem. Soc. Rev. 50 (2021) 6613–6658, https://doi.org/10.1039/D0CS01221A.
[16] S. Abdallah, R. Mhanna, J. Cabrera-González, R. Núñez, A. Khitous, F. Morlet-Savary, O. Soppera, D.-L. Versace, J.-P. Malval, Reversible optical data storage via two-photon micropatterning of *o*-carboranes-embedded switchable materials,

Chem. Mater. 35 (2023) 6979–6989, https://doi.org/10.1021/acs.chemmater.3c01249.
[17] V. Juvekar, H.W. Lee, D.J. Lee, H.M. Kim, Two-photon fluorescent probes for quantitative bio-imaging analysis in live tissues, TrAC Trends Anal. Chem. 157 (2022) 116787, https://doi.org/10.1016/j.trac.2022.116787.
[18] D. Kim, H.G. Ryu, K.H. Ahn, Recent development of two-photon fluorescent probes for bioimaging, Org. Biomol. Chem. 12 (2014) 4550–4566, https://doi.org/10.1039/C4OB00431K.
[19] J.D. Bhawalkar, N.D. Kumar, C.-F. Zhao, P.N. Prasad, Two-photon photodynamic therapy, J. Clin. Laser Med. Surg. 15 (1997) 201–204, https://doi.org/10.1089/clm.1997.15.201.
[20] Y. Shen, A.J. Shuhendler, D. Ye, J.-J. Xu, H.-Y. Chen, Two-photon excitation nanoparticles for photodynamic therapy, Chem. Soc. Rev. 45 (2016) 6725–6741, https://doi.org/10.1039/C6CS00442C.
[21] F. Bolze, S. Jenni, A. Sour, V. Heitz, Molecular photosensitisers for two-photon photodynamic therapy, Chem. Commun. 53 (2017) 12857–12877, https://doi.org/10.1039/C7CC06133A.
[22] B. Gu, W. Wu, G. Xu, G. Feng, F. Yin, P.H.J. Chong, J. Qu, K.-T. Yong, B. Liu, Precise two-photon photodynamic therapy using an efficient photosensitizer with aggregation-induced emission characteristics, Adv. Mater. 29 (2017) 1701076, https://doi.org/10.1002/adma.201701076.
[23] Y. Duo, Y. Yang, T. Xu, R. Zhou, R. Wang, G. Luo, B. Zhong Tang, Aggregation-induced emission: An illuminator in the brain, Coord. Chem. Rev. 482 (2023) 215070, https://doi.org/10.1016/j.ccr.2023.215070.
[24] G.C.R. Ellis-Davies, Two-photon microscopy for chemical neuroscience, ACS Chem. Neurosci. 2 (2011) 185–197, https://doi.org/10.1021/cn100111a.
[25] M. Rumi, S. Barlow, J. Wang, J.W. Perry, S.R. Marder, Two-photon absorbing materials and two-photon-induced chemistry, in: S.R. Marder, K.-S. Lee (Eds.), Photoresponsive Polym. I, Springer Berlin Heidelberg, Berlin, Heidelberg, 2008: pp. 1–95. https://doi.org/10.1007/12_2008_133.
[26] K.D. Belfield, S. Yao, M.V. Bondar, Two-photon absorbing photonic materials: from fundamentals to applications, in: S.R. Marder, K.-S. Lee (Eds.), Photoresponsive Polym. I, Springer Berlin Heidelberg, Berlin, Heidelberg, 2008: pp. 97–156. https://doi.org/10.1007/12_2007_126.
[27] P. Kim, S. Ham, J. Oh, H. Uoyama, H. Watanabe, K. Tagawa, H. Uno, D. Kim, Shape-dependent two-photon absorption in two-dimensionally extended benzoporphyrin arrays, Phys. Chem. Chem. Phys. 15 (2013) 10612, https://doi.org/10.1039/c3cp50166c.
[28] V. Singh, P.R. Kharangarh, P. Kumar, D. Singh, A. Sanjay, S.K. Ghosh, Measurements of third-order optical nonlinearity using Z-scan technique: A review, Bahal, India (2019) 140035, https://doi.org/10.1063/1.5122548.
[29] C. Xu, W.W. Webb, Measurement of two-photon excitation cross sections of molecular fluorophores with data from 690 to 1050 nm, J. Opt. Soc. Am. B 13 (1996) 481, https://doi.org/10.1364/JOSAB.13.000481.
[30] S. de Reguardati, J. Pahapill, A. Mikhailov, Y. Stepanenko, A. Rebane, High-accuracy reference standards for two-photon absorption in the 680–1050 nm wavelength range, Opt. Express 24 (2016) 9053, https://doi.org/10.1364/OE.24.009053.
[31] R. Medishetty, J.K. Zaręba, D. Mayer, M. Samoć, R.A. Fischer, Nonlinear optical properties, upconversion and lasing in metal–organic frameworks, Chem. Soc. Rev. 46 (2017) 4976–5004, https://doi.org/10.1039/C7CS00162B.
[32] D.A. Oulianov, I.V. Tomov, A.S. Dvornikov, P.M. Rentzepis, Observations on the measurement of two-photon absorption cross-section, Opt. Commun. 191 (2001) 235–243, https://doi.org/10.1016/S0030-4018(01)01121-X.
[33] M. Drobizhev, N.S. Makarov, S.E. Tillo, T.E. Hughes, A. Rebane, Two-photon absorption properties of fluorescent proteins, Nat. Methods 8 (2011) 393–399, https://doi.org/10.1038/nmeth.1596.
[34] M. Sheik-Bahae, A.A. Said, T.-H. Wei, D.J. Hagan, E.W. Van Stryland, Sensitive measurement of optical nonlinearities using a single beam, IEEE J. Quantum Electron. 26 (1990) 760–769, https://doi.org/10.1109/3.53394.
[35] M. Falconieri, Thermo-optical effects in Z-scan measurements using high-repetition-rate lasers, J. Opt. Pure Appl. Opt. 1 (1999) 662–667, https://doi.org/10.1088/1464-4258/1/6/302.
[36] M. Samoc, A. Samoc, B. Luther-Davies, M.G. Humphrey, M.-S. Wong, Third-order optical nonlinearities of oligomers, dendrimers and polymers derived from solution Z-scan studies, Opt. Mater. 21 (2003) 485–488, https://doi.org/10.1016/S0925-3467(02)00187-8.
[37] M. Rumi, J.W. Perry, Two-photon absorption: an overview of measurements and principles, Adv. Opt. Photon. 2 (2010) 451, https://doi.org/10.1364/AOP.2.000451.
[38] M. Kauert, P.C. Stoller, M. Frenz, J. Rika, Absolute measurement of molecular two-photon absorption cross-sections using a fluorescence saturation technique, Opt. Express 14 (2006) 8434, https://doi.org/10.1364/OE.14.008434.
[39] P. Chandra Jha, Y. Wang, H. Ågren, Two-photon absorption cross-sections of reference dyes: a critical examination, ChemPhysChem 9 (2008) 111–116, https://doi.org/10.1002/cphc.200700397.
[40] M. Pawlicki, H.A. Collins, R.G. Denning, H.L. Anderson, Two-photon absorption and the design of two-photon dyes, Angew. Chem. Int. Ed. 48 (2009) 3244–3266, https://doi.org/10.1002/anie.200805257.
[41] M. Rumi, J.E. Ehrlich, A.A. Heikal, J.W. Perry, S. Barlow, Z. Hu, D. McCord-Maughon, T.C. Parker, H. Röckel, S. Thayumanavan, S.R. Marder, D. Beljonne, J.-L. Brédas, Structure−property relationships for two-photon absorbing chromophores: bis-donor diphenylpolyene and bis(styryl)benzene derivatives, J. Am. Chem. Soc. 122 (2000) 9500–9510, https://doi.org/10.1021/ja994497s.
[42] D. Beljonne, W. Wenseleers, E. Zojer, Z. Shuai, H. Vogel, S.J. Pond, J.W. Perry, S. R. Marder, J.-L. Brédas, Role of dimensionality on the two-photon absorption response of conjugated molecules: the case of octupolar compounds, Adv. Funct. Mater. 12 (2002) 631–641, https://doi.org/10.1002/1616-3028(20020916)12:9<631::AID-ADFM631>3.0.CO;2-W.
[43] C. Katan, S. Tretiak, M.H.V. Werts, A.J. Bain, R.J. Marsh, N. Leonczek, N. Nicolaou, E. Badaeva, O. Mongin, M. Blanchard-Desce, Two-photon transitions in quadrupolar and branched chromophores: experiment and theory, J. Phys. Chem. B 111 (2007) 9468–9483, https://doi.org/10.1021/jp071069x.
[44] Z.J. Liu, T. Chen, B. Liu, Z.L. Huang, T. Huang, S.Y. Li, Y.X. Xu, J.G. Qin, Two-photon absorption of a series of V-shape molecules: the influence of acceptor's strength on two-photon absorption in a noncentrosymmetric D-pi-A-pi-D system, J. Mater. Chem. 17 (2007) 4685–4689, https://doi.org/10.1039/b707909e.
[45] O. Mongin, L. Porrès, M. Charlot, C. Katan, M. Blanchard-Desce, Synthesis, fluorescence, and two-photon absorption of a series of elongated rodlike and banana-shaped quadrupolar fluorophores: A comprehensive study of structure-property relationships, Chem. Eur. J. 13 (2007) 1481–1498, https://doi.org/10.1002/chem.200600689.
[46] C. Andraud, R. Fortrie, C. Barsu, O. Stéphan, H. Chermette, P.L. Baldeck, Excitonically coupled oligomers and dendrimers for two-photon absorption, in: Photoresponsive Polym. II, Springer, 2008: pp. 149–203. https://link.springer.com/chapter/10.1007/12_2008_158.
[47] F. Terenziani, C. Katan, E. Badaeva, S. Tretiak, M. Blanchard-Desce, Enhanced two-photon absorption of organic chromophores: theoretical and experimental assessments, Adv. Mater. 20 (2008) 4641–4678, https://doi.org/10.1002/adma.200800402.
[48] M. Albota, Design of organic molecules with large two-photon absorption cross sections, Science 281 (1998) 1653–1656, https://doi.org/10.1126/science.281.5383.1653.
[49] C. Le Droumaguet, O. Mongin, M.H.V. Werts, M. Blanchard-Desce, Towards "smart" multiphoton fluorophores: strongly solvatochromic probes for two-photon sensing of micropolarity, Chem. Commun. (2005) 2802, https://doi.org/10.1039/b502585k.
[50] I. Ledoux, J. Zyss, Multipolar engineering of molecules and materials for quadratic nonlinear optics, C. R. Phys. 3 (2002) 407–427, https://doi.org/10.1016/S1631-0705(02)01332-4.
[51] S. Di Bella, Second-order nonlinear optical properties of transition metal complexes, Chem. Soc. Rev. 30 (2001) 355–366, https://doi.org/10.1039/b100820j.
[52] I.C. de Silva, R.M. de Silva, K.M. Nalin de Silva, Investigations of nonlinear optical (NLO) properties of Fe, Ru and Os organometallic complexes using high accuracy density functional theory (DFT) calculations, J. Mol. Struct. (THOECHEM) 728 (2005) 141–145, https://doi.org/10.1016/j.theochem.2005.02.092.
[53] S. Di Bella, C. Dragonetti, M. Pizzotti, D. Roberto, F. Tessore, R. Ugo, Coordination and organometallic complexes as second-order nonlinear optical molecular materials, in: H. Le Bozec, V. Guerchais (Eds.), Mol. Organomet. Mater. Opt., Springer, Berlin Heidelberg, Berlin, Heidelberg, 2010, pp. 1–55, https://doi.org/10.1007/978-3-642-01866-4_1.
[54] B.J. Coe, Developing iron and ruthenium complexes for potential nonlinear optical applications, Coord. Chem. Rev. 257 (2013) 1438–1458, https://doi.org/10.1016/j.ccr.2012.06.025.
[55] P.G. Lacroix, I. Malfant, C. Lepetit, Second-order nonlinear optics in coordination chemistry: An open door towards multi-functional materials and molecular switches, Coord. Chem. Rev. 308 (2016) 381–394, https://doi.org/10.1016/j.ccr.2015.05.015.
[56] X. Xue, H. Wang, Y. Han, H. Hou, Photoswitchable nonlinear optical properties of metal complexes, Dalton Trans. 47 (2018) 13–22, https://doi.org/10.1039/C7DT03989A.
[57] I. Ledoux, J. Zyss, J.S. Siegel, J. Brienne, J.-M. Lehn, Second-harmonic generation from non-dipolar non-centrosymmetric aromatic charge-transfer molecules, Chem. Phys. Lett. 172 (1990) 440–444, https://doi.org/10.1016/0009-2614(90)80135-Z.
[58] J. Zyss, I. Ledoux, Nonlinear optics in multipolar media: theory and experiments, Chem. Rev. 94 (1994) 77–105, https://doi.org/10.1021/cr00025a003.
[59] M.C. Wolff, N. van Steerteghem, K. Clays, J. Heck, Unexpected high second-order nonlinear optical activity of metal complexes with three-branched hexadentate 2,2′-bipyridine ligands, Chem. - Eur. J. 24 (2018) 14901–14905, https://doi.org/10.1002/chem.201801189.
[60] C. Dhenaut, I. Ledoux, I.D. Samuel, J. Zyss, M. Bourgault, H. Le Bozec, Chiral metal complexes with large octupolar optical nonlinearities, Nature 374 (1995) 339–342, https://doi.org/10.1038/374339a0.
[61] H. Le Bozec, T. Renouard, Dipolar and non-dipolar pyridine and bipyridine metal complexes for nonlinear optics, Eur. J. Inorg. Chem. 2000 (2000) 229–239. https://chemistry-europe.onlinelibrary.wiley.com/doi/abs/10.1002/(SICI)1099-0682(200002)2000:2<229::AID-EJIC229>3.0.CO;2-A.
[62] W.-H. Lee, H. Lee, J.-A. Kim, J.-H. Choi, M. Cho, S.-J. Jeon, B.R. Cho, Two-photon absorption and nonlinear optical properties of octupolar molecules, J. Am. Chem. Soc. 123 (2001) 10658–10667, https://doi.org/10.1021/ja004226d.
[63] O. Maury, H. Le Bozec, Molecular engineering of octupolar NLO molecules and materials based on bipyridyl metal complexes, Acc. Chem. Res. 38 (2005) 691–704. https://pubs.acs.org/doi/10.1021/ar020264l.
[64] C. Feuvrie, O. Maury, H. Le Bozec, I. Ledoux, J.P. Morrall, G.T. Dalton, M. Samoc, M.G. Humphrey, Nonlinear optical and two-photon absorption properties of octupolar tris(bipyridyl)metal complexes, Chem. A Eur. J. 111 (2007) 8980–8985, https://doi.org/10.1021/jp0735381.
[65] B.J. Coe, J.A. Harris, B.S. Brunschwig, I. Asselberghs, K. Clays, J. Garín, J. Orduna, Three-dimensional nonlinear optical chromophores based on metal-to-

ligand charge-transfer from ruthenium(II) or iron(II) centers, J. Am. Chem. Soc. 127 (2005) 13399–13410, https://doi.org/10.1021/ja053879x.
[66] B.J. Coe, Switchable nonlinear optical metallochromophores with pyridinium electron acceptor groups, Acc. Chem. Res. 39 (2006) 383–393, https://doi.org/10.1021/ar050225k.
[67] B.J. Coe, S.P. Foxon, M. Helliwell, D. Rusanova, B.S. Brunschwig, K. Clays, G. Depotter, M. Nyk, M. Samoc, D. Wawrzynczyk, Heptametallic, Octupolar nonlinear optical chromophores with six ferrocenyl substituents, Chem.- Eur. J. 19 (2013) 6613–6629, https://doi.org/10.1002/chem.201204453.
[68] C.K. Prier, D.A. Rankic, D.W.C. MacMillan, Visible light photoredox catalysis with transition metal complexes: applications in organic synthesis, Chem. Rev. 113 (2013) 5322–5363, https://doi.org/10.1021/cr300503r.
[69] A. Hagfeldt, G. Boschloo, L. Sun, L. Kloo, H. Pettersson, Dye-sensitized solar cells, Chem. Rev. 110 (2010) 6595–6663, https://doi.org/10.1021/cr900356p.
[70] L.-C.-C. Lee, K.-K.-W. Lo, Luminescent and photofunctional transition metal complexes: from molecular design to diagnostic and therapeutic applications, J. Am. Chem. Soc. 144 (2022) 14420–14440, https://doi.org/10.1021/jacs.2c03437.
[71] K.Y. Zhang, Q. Yu, H. Wei, S. Liu, Q. Zhao, W. Huang, Long-lived emissive probes for time-resolved photoluminescence bioimaging and biosensing, Chem. Rev. 118 (2018) 1770–1839, https://doi.org/10.1021/acs.chemrev.7b00425.
[72] J. Shum, P.-K.-K. Leung, K.-K.-W. Lo, Luminescent ruthenium(II) polypyridine complexes for a wide variety of biomolecular and cellular applications, Inorg. Chem. 58 (2019) 2231–2247, https://doi.org/10.1021/acs.inorgchem.8b02979.
[73] C. Mari, V. Pierroz, S. Ferrari, G. Gasser, Combination of Ru(II) complexes and light: new frontiers in cancer therapy, Chem. Sci. 6 (2015) 2660–2686, https://doi.org/10.1039/C4SC03759F.
[74] E. Boros, P.J. Dyson, G. Gasser, Classification of metal-based drugs according to their mechanisms of action, Chem 6 (2020) 41–60, https://doi.org/10.1016/j.chempr.2019.10.013.
[75] A. Juris, V. Balzani, F. Barigelletti, S. Campagna, P. Belser, A. von Zelewsky, Ru (II) polypyridine complexes: photophysics, photochemistry, electrochemistry, and chemiluminescence, Coord. Chem. Rev. 84 (1988) 85–277, https://doi.org/10.1016/0010-8545(88)80032-8.
[76] F.N. Castellano, H. Malak, I. Gryczynski, J.R. Lakowicz, Creation of metal-to-ligand charge transfer excited states with two-photon excitation, Inorg. Chem. 36 (1997) 5548–5551, https://doi.org/10.1021/ic970334y.
[77] J. Kawamata, Y. Ogata, A. Yamagishi, Two-photon fluorescence property of tris (4,7-diphenyl-1,10-phenanthroline)ruthenium(II)perchlorate, Mol. Cryst. Liq. Cryst. 379 (2002) 389–394, https://doi.org/10.1080/713738615.
[78] R.R. Birge, Two-photon spectroscopy of protein-bound chromophores, Acc. Chem. Res. 19 (1986) 138–146, https://doi.org/10.1021/ar00125a003.
[79] C.W. Stark, M. Rammo, J. Pahapill, A. Mikhaylov, A. Rebane, Probing metal-to-ligand charge transfer transitions in ruthenium complexes by quantitative two-photon absorption spectroscopy, Int. Soc. Opt. Photonics (2018) 105291D, https://doi.org/10.1117/12.2290363.
[80] R.D. Hancock, The pyridyl group in ligand design for selective metal ion complexation and sensing, Chem. Soc. Rev. 42 (2013) 1500–1524, https://doi.org/10.1039/C2CS35224A.
[81] B.J. Coe, M. Samoc, A. Samoc, L. Zhu, Y. Yi, Z. Shuai, Two-photon absorption properties of iron(II) and ruthenium(II) trischelate complexes of 2,2':4,4":4',4‴-quaterpyridinium ligands, Chem. Eur. J. 111 (2007) 472–478, https://doi.org/10.1021/jp0656072.
[82] P. Shi, B.J. Coe, S. Sánchez, D. Wang, Y. Tian, M. Nyk, M. Samoc, Uniting ruthenium(II) and platinum(II) polypyridine centers in heteropolymetallic complexes giving strong two-photon absorption, Inorg. Chem. 54 (2015) 11450–11456, https://doi.org/10.1021/acs.inorgchem.5b02089.
[83] M.G. Kuzyk, Fundamental limits on two-photon absorption cross sections, J. Chem. Phys. 119 (2003) 8327–8334, https://doi.org/10.1063/1.1611474.
[84] B.J. Coe, J. Fielden, S.P. Foxon, B.S. Brunschwig, I. Asselberghs, K. Clays, A. Samoc, M. Samoc, Combining very large quadratic and cubic nonlinear optical responses in extended, tris-chelate metallochromophores with six π-conjugated pyridinium substituents, J. Am. Chem. Soc. 132 (2010) 3496–3513, https://doi.org/10.1021/ja910538s.
[85] C. Girardot, B. Cao, J.-C. Mulatier, P.L. Baldeck, J. Chauvin, D. Riehl, J.A. Delaire, C. Andraud, G. Lemercier, Ruthenium(II) complexes for two-photon absorption-based optical power limiting, ChemPhysChem 9 (2008) 1531–1535, https://doi.org/10.1002/cphc.200800186.
[86] O. Maury, H. Le Bozec, Metal-based quadratic nonlinear optical materials, in: D. W. Bruce, D. O'Hare, R.I. Walton (Eds.), Mol. Mater, John Wiley & Sons Ltd, Chichester, UK, 2010, pp. 1–59, https://doi.org/10.1002/9780470686058.ch1.
[87] A. Reynal, E. Palomares, Ruthenium polypyridyl sensitisers in dye solar cells based on mesoporous TiO_2, Eur. J. Inorg. Chem. 2011 (2011) 4509–4526, https://doi.org/10.1002/ejic.201100516.
[88] L. Xiao, H. Wang, Q. Zhang, Y. Zhu, J. Luo, Y. Liang, S. Zhang, H. Zhou, Y. Tian, J. Wu, Novel ruthenium (II) polypyridyl complexes containing carbazole with flexible substituents: Crystal structure, nonlinear optical properties and DNA-binding interaction, Dyes Pigm. 113 (2015) 165–173, https://doi.org/10.1016/j.dyepig.2014.08.002.
[89] L. Labat, J.-F. Lamère, I. Sasaki, P.G. Lacroix, L. Vendier, I. Asselberghs, J. Pérez-Moreno, K. Clays, Synthesis, crystal structure, and second-order nonlinear optical properties of ruthenium(II) complexes with substituted bipyridine and phenylpyridine ligands, Eur. J. Inorg. Chem. 2006 (2006) 3105–3113, https://doi.org/10.1002/ejic.200600258.
[90] R.D. Costa, J. Aragó, E. Ortí, T.M. Pappenfus, K.R. Mann, K. Matczyszyn, M. Samoc, J.L. Zafra, J.T. López Navarrete, J. Casado, Impact of the synergistic collaboration of oligothiophene bridges and ruthenium complexes on the optical properties of dumbbell-shaped compounds, Chem. Eur. J. 19 (2013) 1476–1488, https://doi.org/10.1002/chem.201202456.
[91] N. Durand, A. Amar, R. Mhanna, H. Akdas-Kiliç, O. Soppera, J.-P. Malval, A. Boucekkine, J.-L. Fillaut, Two-photon absorption cooperative effects within multi-dipolar ruthenium complexes: the decisive influence of charge transfers, Molecules 27 (2022) 1493, https://doi.org/10.3390/molecules27051493.
[92] N. Durand, R. Mhanna, P. Savel, H. Akdas-Kiliç, J.-P. Malval, O. Soppera, J.-L. Fillaut, Unexpected disruption of the dimensionality-driven two-photon absorption enhancement within a multipolar polypyridyl ruthenium complex series, Chem. Commun. 56 (2020) 12801–12804, https://doi.org/10.1039/D0CC05025C.
[93] D.W. Thompson, A. Ito, T.J. Meyer, $[Ru(bpy)_3])^{2+*}$ and other remarkable metal-to-ligand charge transfer (MLCT) excited states, Pure Appl. Chem. 85 (2013) 1257–1305, https://doi.org/10.1351/PAC-CON-13-03-04.
[94] J. Kim, D. Kang, S.K. Kim, T. Joo, Role of coherent nuclear motion in the ultrafast intersystem crossing of ruthenium complexes, Phys. Chem. Chem. Phys. 22 (2020) 25811–25818, https://doi.org/10.1039/D0CP05368F.
[95] K. Kalyanasundaram, Applications of functionalized transition metal complexes in photonic and optoelectronic devices, Coord. Chem. Rev. 177 (1998) 347–414, https://doi.org/10.1016/S0010-8545(98)00189-1.
[96] J.-F. Yin, M. Velayudham, D. Bhattacharya, H.-C. Lin, K.-L. Lu, Structure optimization of ruthenium photosensitizers for efficient dye-sensitized solar cells – A goal toward a "bright" future, Coord. Chem. Rev. 256 (2012) 3008–3035, https://doi.org/10.1016/j.ccr.2012.06.022.
[97] S. Campagna, F. Nastasi, G. La Ganga, S. Serroni, A. Santoro, A. Arrigo, F. Puntoriero, Self-assembled systems for artificial photosynthesis, Phys. Chem. Chem. Phys. 25 (2023) 1504–1512, https://doi.org/10.1039/d2cp03655j.
[98] T. Mede, M. Jäger, U.S. Schubert, "Chemistry-on-the-complex": functional RuII polypyridyl-type sensitizers as divergent building blocks, Chem. Soc. Rev. 47 (2018) 7577–7627, https://doi.org/10.1039/C8CS00096D.
[99] G.E. Giacomazzo, M. Schlich, L. Casula, L. Galantini, A. Del Giudice, G. Pietraperzia, C. Sinico, F. Cencetti, S. Pecchioli, B. Valtancoli, L. Conti, S. Murgia, C. Giorgi, Ruthenium(ii) polypyridyl complexes with π-expansive ligands: synthesis and cubosome encapsulation for photodynamic therapy of non-melanoma skin cancer, Inorg. Chem. Front. 10 (2023) 3025–3036, https://doi.org/10.1039/D2QI02678C.
[100] M. Carlotti, V. Mattoli, Functional materials for two-photon polymerization in microfabrication, Small 15 (2019) 1902687, https://doi.org/10.1002/smll.201902687.
[101] Z. Huang, G. Shao, L. Li, Micro/nano functional devices fabricated by additive manufacturing, Prog. Mater Sci. 131 (2023) 101020, https://doi.org/10.1016/j.pmatsci.2022.101020.
[102] J.K. Hohmann, M. Renner, E.H. Waller, G. Von Freymann, Three-dimensional μ-printing: an enabling technology, Adv. Opt. Mater. 3 (2015) 1488–1507, https://doi.org/10.1002/adom.201500328.
[103] H.M. Kim, B.R. Cho, Small-molecule two-photon probes for bioimaging applications, Chem. Rev. 115 (2015) 5014–5055, https://doi.org/10.1021/cr5004425.
[104] Y. Chen, R. Guan, C. Zhang, J. Huang, L. Ji, H. Chao, Two-photon luminescent metal complexes for bioimaging and cancer phototherapy, Coord. Chem. Rev. 310 (2016) 16–40, https://doi.org/10.1016/j.ccr.2015.09.010.
[105] S. Wu, J. Serbin, M. Gu, Two-photon polymerisation for three-dimensional micro-fabrication, J. Photochem. Photobiol. Chem. 181 (2006) 1–11, https://doi.org/10.1016/j.jphotochem.2006.03.004.
[106] B.S. Calin, I.A. Paun, A review on stimuli-actuated 3D micro/nanostructures for tissue engineering and the potential of laser-direct writing via two-photon polymerization for structure fabrication, Int. J. Mol. Sci. 23 (2022) 14270, https://doi.org/10.3390/ijms232214270.
[107] J.-P. Fouassier, F. Morlet-Savary, J. Lalevée, X. Allonas, C. Ley, Dyes as photoinitiators or photosensitizers of polymerization reactions, Materials 3 (2010) 5130–5142, https://doi.org/10.3390/ma3125130.
[108] Y. Bao, Recent trends in advanced photoinitiators for vat photopolymerization 3D printing, Macromol. Rapid Commun. 43 (2022) 2200202, https://doi.org/10.1002/marc.202200202.
[109] V. Ferraro, C.R. Adam, A. Vranic, S. Bräse, Recent advances of transition metal complexes for photopolymerization and 3D printing under visible light, Adv. Funct. Mater. (2023) 2302157, https://doi.org/10.1002/adfm.202302157.
[110] A. Spangenberg, J.-P. Malval, H. Akdas-Kilig, J.-L. Fillaut, F. Stehlin, N. Hobeika, F. Morlet-Savary, O. Soppera, Enhancement of two-photon initiating efficiency of a 4,4′-diaminostyryl-2,2′-bipyridine derivative promoted by complexation with silver Ions, Macromolecules 45 (2012) 1262–1269, https://doi.org/10.1021/ma202224c.
[111] K. Iwai, M. Uesugi, F. Takemura, Tris(2,2′-bipyridine)ruthenium(II)-sensitized photopolymerization of acrylamide, Polym. J. 17 (1985) 1005–1011, https://doi.org/10.1295/polymj.17.1005.
[112] T.S. Bergstedt, B.T. Hauser, K.S. Schanze, Microstructured photopolymer films of a ruthenium(II) polypyridine complex. Fabrication of an electrochemically switchable phase grating, J. Am. Chem. Soc. 116 (1994) 8380–8381, https://doi.org/10.1021/ja00097a061.
[113] S. Uemura, M. Yoshie, N. Kobayashi, T. Nakahira, Photopolymerization of aniline dimer by photocatalytic reaction of ruthenium trisbipyridyl in the interlayer of hectorite clay, Polym. J. 32 (2000) 987–990, https://doi.org/10.1295/polymj.32.987.
[114] C.R. Rivarola, S.G. Bertolotti, C.M. Previtali, Polymerization of acrylamide photoinitiated by tris(2,2′-bipyridine)ruthenium(II)-amine in aqueous solution:

Effect of the amine structure, J. Polym. Sci. Part Polym. Chem. 39 (2001) 4265–4273, https://doi.org/10.1002/pola.10084.
[115] J. Lalevée, N. Blanchard, M.-A. Tehfe, F. Morlet-Savary, J.P. Fouassier, Green bulb light source induced epoxy cationic polymerization under air using tris(2,2′-bipyridine)ruthenium(II) and silyl radicals, Macromolecules 43 (2010) 10191–10195, https://doi.org/10.1021/ma1023318.
[116] T. Chen, Y. Xu, Z. Peng, A. Li, J. Liu, Simultaneous utilization of a bifunctional ruthenium complex as an efficient catalyst for RAFT controlled photopolymerization and a sensing probe for the facile fabrication of an ECL platform, Polym. Chem. 7 (2016) 5880–5887, https://doi.org/10.1039/C6PY01016D.
[117] D.A. Fancy, C. Denison, K. Kim, Y. Xie, T. Holdeman, F. Amini, T. Kodadek, Scope, limitations and mechanistic aspects of the photo-induced cross-linking of proteins by water-soluble metal complexes, Chem. Biol. 7 (2000) 697–708, https://doi.org/10.1016/S1074-5521(00)00020-X.
[118] K.S. Lim, B.J. Klotz, G.C.J. Lindberg, F.P.W. Melchels, G.J. Hooper, J. Malda, D. Gawlitta, T.B.F. Woodfield, Visible light cross-linking of gelatin hydrogels offers an enhanced cell microenvironment with improved light penetration depth, Macromol. Biosci. 19 (2019) 1900098, https://doi.org/10.1002/mabi.201900098.
[119] S. Bertlein, G. Brown, K.S. Lim, T. Jungst, T. Boeck, T. Blunk, J. Tessmar, G. J. Hooper, T.B.F. Woodfield, J. Groll, Thiol-ene clickable gelatin: a platform bioink for multiple 3D biofabrication technologies, Adv. Mater. 29 (2017) 1703404, https://doi.org/10.1002/adma.201703404.
[120] W. Li, M. Wang, H. Ma, F.A. Chapa-Villarreal, A.O. Lobo, Y.S. Zhang, Stereolithography apparatus and digital light processing-based 3D bioprinting for tissue fabrication, iScience 26 (2023) 106039. https://doi.org/10.1016/j.isci.2023.106039.
[121] K. Yamada, J. Sone, J. Chen, Three-dimensional photochemical microfabrication of conductive polymers in transparent polymer sheet, Opt. Rev. 16 (2009) 208–212, https://doi.org/10.1007/s10043-009-0038-z.
[122] K. Yamada, A. Kyoya, J. Sone, J. Chen, Evaluations of vertical resolution of conductive polymer three-dimensional microstructures photofabricated in transparent polymer sheet, Opt. Rev. 18 (2011) 162–165, https://doi.org/10.1007/s10043-011-0016-0.
[123] J. Sone, K. Yamada, A. Asami, J. Chen, Sub-micrometer size structure fabrication using a conductive polymer, Micromachines 6 (2014) 96–109, https://doi.org/10.3390/mi6010096.
[124] K. Yamada, M. Watanabe, J. Sone, Three-dimensional printing of conducting polymer microstructures into transparent polymer sheet: Relationship between process resolution and illumination conditions, Opt. Rev. 21 (2014) 679–682, https://doi.org/10.1007/s10043-014-0109-7.
[125] A.T. Cullen, A.D. Price, Method and system for 3d printing of electrically conductive polymer structures, US20200055233A1, 2020. https://patents.google.com/patent/US20200055233A1/en.
[126] K. Yamada, Y. Kimura, S. Suzuki, J. Sone, J. Chen, S. Urabe, Multiphoton-sensitized polymerization of pyrrole, Chem. Lett. 35 (2006) 908–909, https://doi.org/10.1246/cl.2006.908.
[127] V. Balzani, G. Bergamini, P. Ceroni, From the photochemistry of coordination compounds to light-powered nanoscale devices and machines, Coord. Chem. Rev. 252 (2008) 2456–2469, https://doi.org/10.1016/j.ccr.2007.11.009.
[128] K. Yamada, Y. Yamada, J. Sone, Three-dimensional photochemical microfabrication of poly(3,4-ethylene- dioxythiophene) in transparent polymer sheet, Thin Solid Films 554 (2014) 102–105, https://doi.org/10.1016/j.tsf.2013.08.023.
[129] L. Vurth, P. Baldeck, O. Stéphan, G. Vitrant, Two-photon induced fabrication of gold microstructures in polystyrene sulfonate thin films using a ruthenium(II) dye as photoinitiator, Appl. Phys. Lett. 92 (2008) 171103, https://doi.org/10.1063/1.2917810.
[130] B. Van Der Sanden, L. Gredy, D. Wion, O. Stephan, 3D two-photon polymerization of smart cell gelatin – collagen matrixes with incorporated ruthenium complexes for the monitoring of local oxygen tensions, Acta Biomater. 130 (2021) 172–182, https://doi.org/10.1016/j.actbio.2021.06.021.
[131] T. Yoshihara, Y. Hirakawa, M. Hosaka, M. Nangaku, S. Tobita, Oxygen imaging of living cells and tissues using luminescent molecular probes, J. Photochem. Photobiol. C: Photochem. Rev. 30 (2017) 71–95, https://doi.org/10.1016/j.jphotochemrev.2017.01.001.
[132] R. Mhanna, N. Durand, P. Savel, H. Akdas-Kiliç, S. Abdallah, D.-L. Versace, O. Soppera, J.-L. Fillaut, N. Sojic, J.-P. Malval, Micropatterning of electrochemiluminescent polymers based on multipolar Ru-complex two-photon initiators, Chem. Commun. 58 (2022) 9678–9681, https://doi.org/10.1039/D2CC04159F.
[133] Y.-L. Li, A.-J. Li, S.-L. Huang, J.J. Vittal, G.-Y. Yang, Polypyridyl Ru(ii) or cyclometalated Ir(iii) functionalized architectures for photocatalysis, Chem. Soc. Rev. 52 (2023) 4725–4754, https://doi.org/10.1039/D3CS00053B.
[134] C. Han, B.K. Kundu, Y. Liang, Y. Sun, Near-infrared light-driven photocatalysis with an emphasis on two-photon excitation: concepts, materials, and applications, Adv. Mater. 36 (2024) 2307759, https://doi.org/10.1002/adma.202307759.
[135] G. Han, G. Li, J. Huang, C. Han, C. Turro, Y. Sun, Two-photon-absorbing ruthenium complexes enable near infrared light-driven photocatalysis, Nat. Commun. 13 (2022) 2288, https://doi.org/10.1038/s41467-022-29981-3.
[136] J.-H. Tang, G. Han, G. Li, K. Yan, Y. Sun, Near-infrared light photocatalysis enabled by a ruthenium complex-integrated metal–organic framework via two-photon absorption, iScience 25 (2022) 104064, https://doi.org/10.1016/j.isci.2022.104064.
[137] C. Xie, W. Sun, H. Lu, A. Kretzschmann, J. Liu, M. Wagner, H.-J. Butt, X. Deng, S. Wu, Reconfiguring surface functions using visible-light-controlled metal-ligand coordination, Nat. Commun. 9 (2018) 3842, https://doi.org/10.1038/s41467-018-06180-7.
[138] Y. Salinas, O. Brüggemann, U. Monkowius, I. Teasdale, Visible light photocleavable ruthenium-based molecular gates to reversibly control release from mesoporous silica nanoparticles, Nanomaterials 10 (2020) 1030, https://doi.org/10.3390/nano10061030.
[139] V. Balzani, P. Ceroni, A. Credi, M. Venturi, Ruthenium tris(bipyridine) complexes: Interchange between photons and electrons in molecular-scale devices and machines, Coord. Chem. Rev. 433 (2021) 213758, https://doi.org/10.1016/j.ccr.2020.213758.
[140] T.L. Rapp, Y. Wang, M.A. Delessio, M.R. Gau, I.J. Dmochowski, Designing photolabile ruthenium polypyridyl crosslinkers for hydrogel formation and multiplexed, visible-light degradation, RSC Adv. 9 (2019) 4942–4947, https://doi.org/10.1039/C8RA09764J.
[141] J. Liu, Y. Chen, G. Li, P. Zhang, C. Jin, L. Zeng, L. Ji, H. Chao, Ruthenium(II) polypyridyl complexes as mitochondria-targeted two-photon photodynamic anticancer agents, Biomaterials 56 (2015) 140–153, https://doi.org/10.1016/j.biomaterials.2015.04.002.
[142] M.R. Gill, J.A. Thomas, Ruthenium(II) polypyridyl complexes and DNA-from structural probes to cellular imaging and therapeutics, Chem. Soc. Rev. 41 (2012) 3179–3192, https://doi.org/10.1039/C2CS15299A.
[143] A. Li, C. Turro, J.J. Kodanko, Ru(II) polypyridyl complexes as photocages for bioactive compounds containing nitriles and aromatic heterocycles, Chem. Commun. 54 (2018) 1280–1290, https://doi.org/10.1039/C7CC09000E.
[144] A. Soupart, F. Alary, J.-L. Heully, P.I.P. Elliott, I.M. Dixon, Recent progress in ligand photorelease reaction mechanisms: Theoretical insights focusing on Ru(II) ^{3}MC states, Coord. Chem. Rev. 408 (2020) 213184, https://doi.org/10.1016/j.ccr.2020.213184.
[145] R.N. Garner, L.E. Joyce, C. Turro, Effect of electronic structure on the photoinduced ligand exchange of Ru(II) polypyridine complexes, Inorg. Chem. 50 (2011) 4384–4391, https://doi.org/10.1021/ic102482c.
[146] L. Salassa, C. Garino, G. Salassa, R. Gobetto, C. Nervi, Mechanism of ligand photodissociation in photoactivable $[Ru(bpy)_2L_2]^{2+}$ complexes: a density functional theory study, J. Am. Chem. Soc. 130 (2008) 9590–9597, https://doi.org/10.1021/ja8025906.
[147] S.E. Greenough, M.D. Horbury, N.A. Smith, P.J. Sadler, M.J. Paterson, V. G. Stavros, Excited-state dynamics of a two-photon-activatable ruthenium prodrug, ChemPhysChem 17 (2016) 221–224, https://doi.org/10.1002/cphc.201501075.
[148] L. Zayat, M. Salierno, R. Etchenique, Ruthenium(II) bipyridyl complexes as photolabile caging groups for amines, Inorg. Chem. 45 (2006) 1728–1731, https://doi.org/10.1021/ic0512983.
[149] L. Zayat, O. Filevich, L.M. Baraldo, R. Etchenique, Ruthenium polypyridyl phototriggers: from beginnings to perspectives, Philos. Trans. R. Soc. A 371 (2013) 20120330, https://doi.org/10.1098/rsta.2012.0330.
[150] Y. Liu, D.B. Turner, T.N. Singh, A.M. Angeles-Boza, A. Chouai, K.R. Dunbar, C. Turro, Ultrafast ligand exchange: detection of a pentacoordinate Ru(II) intermediate and product formation, J. Am. Chem. Soc. 131 (2009) 26–27, https://doi.org/10.1021/ja806860w.
[151] M.R. Camilo, C.R. Cardoso, R.M. Carlos, A.B.P. Lever, Photosolvolysis of cis-$[Ru(\alpha\text{-diimine})_2(4\text{-aminopyridine})_2]^{2+}$ complexes: photophysical, spectroscopic, and density functional theory analysis, Inorg. Chem. 53 (2014) 3694–3708, https://doi.org/10.1021/ic5000205.
[152] L. Salassa, E. Borfecchia, T. Ruiu, C. Garino, D. Gianolio, R. Gobetto, P.J. Sadler, M. Cammarata, M. Wulff, C. Lamberti, Photo-induced pyridine substitution in *cis*-$[Ru(bpy)_2(py)_2]Cl_2$: a snapshot by time-resolved X-ray solution scattering, Inorg. Chem. 49 (2010) 11240–11248, https://doi.org/10.1021/ic102021k.
[153] E. Borfecchia, C. Garino, D. Gianolio, L. Salassa, R. Gobetto, C. Lamberti, Monitoring excited state dynamics in *cis*-$[Ru(bpy)_2(py)_2]^{2+}$ by ultrafast synchrotron techniques, Catal. Today 229 (2014) 34–45, https://doi.org/10.1016/j.cattod.2013.11.057.
[154] E. Wachter, E.C. Glazer, Mechanistic study on the photochemical "light switch" behavior of $[Ru(bpy)_2dmdppz]^{2+}$, Chem. Eur. J. 118 (2014) 10474–10486, https://doi.org/10.1021/jp504249a.
[155] R. Cabrera, M. Gabriel, L.C. Estrada, R. Etchenique, Direct measurement of two-photon action cross section, Anal. Chem. 91 (2019) 5968–5972, https://doi.org/10.1021/acs.analchem.9b00392.
[156] R. Cabrera, O. Filevich, B. García-Acosta, J. Athilingam, K.J. Bender, K. E. Poskanzer, R. Etchenique, A visible-light-sensitive caged serotonin, ACS Chem. Neurosci. 8 (2017) 1036–1042, https://doi.org/10.1021/acschemneuro.7b00083.
[157] J. Liu, H. Butt, S. Wu, Reconfigurable surfaces based on photocontrolled dynamic bonds, Adv. Funct. Mater. (2019) 1907605, https://doi.org/10.1002/adfm.201907605.
[158] V. San Miguel, M. Álvarez, O. Filevich, R. Etchenique, A. del Campo, Multiphoton reactive surfaces using ruthenium(II) photocleavable cages, Langmuir 28 (2012) 1217–1221, https://doi.org/10.1021/la2033687.
[159] S. Theis, A. Iturmendi, C. Gorsche, M. Orthofer, M. Lunzer, S. Baudis, A. Ovsianikov, R. Liska, U. Monkowius, I. Teasdale, Metallo-supramolecular gels that are photocleavable with visible and near-infrared irradiation, Angew. Chem. Int. Ed. 56 (2017) 15857–15860, https://doi.org/10.1002/anie.201707321.
[160] M. Mital, Z. Ziora, Biological applications of Ru(II) polypyridyl complexes, Coord. Chem. Rev. 375 (2018) 434–458, https://doi.org/10.1016/j.ccr.2018.02.013.

[161] W. Li, G.-B. Jiang, J.-H. Yao, X.-Z. Wang, J. Wang, B.-J. Han, Y.-Y. Xie, G.-J. Lin, H.-L. Huang, Y.-J. Liu, Ruthenium(II) complexes: DNA-binding, cytotoxicity, apoptosis, cellular localization, cell cycle arrest, reactive oxygen species, mitochondrial membrane potential and western blot analysis, J. Photochem. Photobiol. B 140 (2014) 94–104, https://doi.org/10.1016/j.jphotobiol.2014.07.011.
[162] K. Qiu, J. Wang, C. Song, L. Wang, H. Zhu, H. Huang, J. Huang, H. Wang, L. Ji, H. Chao, Crossfire for two-photon photodynamic therapy with fluorinated ruthenium (II) photosensitizers, ACS Appl. Mater. Interfaces 9 (2017) 18482–18492, https://doi.org/10.1021/acsami.7b02977.
[163] L. Wu, J. Liu, P. Li, B. Tang, T.D. James, Two-photon small-molecule fluorescence-based agents for sensing, imaging, and therapy within biological systems, Chem. Soc. Rev. 50 (2021) 702–734, https://doi.org/10.1039/D0CS00861C.
[164] E.W. Reynolds, J.N. Demas, B.A. DeGraff, Viscosity and temperature effects on the rate of oxygen quenching of tris-(2,2′-bipyridine)ruthenium(II), J. Fluoresc. 23 (2013) 237–241, https://doi.org/10.1007/s10895-012-1139-9.
[165] C. Malins, H.G. Glever, T.E. Keyes, J.G. Vos, W.J. Dressick, B.D. MacCraith, Sol–gel immobilised ruthenium(II) polypyridyl complexes as chemical transducers for optical pH sensing, Sens. Actuators B Chem. 67 (2000) 89–95, https://doi.org/10.1016/S0925-4005(00)00411-1.
[166] K.J. Morris, M.S. Roach, W. Xu, J.N. Demas, B.A. DeGraff, Luminescence lifetime standards for the nanosecond to microsecond range and oxygen quenching of ruthenium(II) complexes, Anal. Chem. 79 (2007) 9310–9314, https://doi.org/10.1021/ac0712796.
[167] Y. Clarke, W. Xu, J.N. Demas, B.A. DeGraff, Lifetime-based pH sensor system based on a polymer-supported ruthenium(II) complex, Anal. Chem. 72 (2000) 3468–3475, https://doi.org/10.1021/ac000111g.
[168] M. Tsvirko, S. Tkaczyk, M. Kozak, B. Kalota, Luminescent temperature sensor based on $[Ru(bpy)_3]^{2+}$ incorporated into chitosan, Funct. Mater. 20 (2013) 127–132, https://doi.org/10.15407/fm20.01.127.
[169] E. Baggaley, J.A. Weinstein, J.A.G. Williams, Lighting the way to see inside the live cell with luminescent transition metal complexes, Coord. Chem. Rev. 256 (2012) 1762–1785, https://doi.org/10.1016/j.ccr.2012.03.018.
[170] C.-T. Poon, P.-S. Chan, C. Man, F.-L. Jiang, R.N.S. Wong, N.-K. Mak, D.W. J. Kwong, S.-W. Tsao, W.-K. Wong, An amphiphilic ruthenium(II)–polypyridyl appended porphyrin as potential bifunctional two-photon tumor-imaging and photodynamic therapeutic agent, J. Inorg. Biochem. 104 (2010) 62–70, https://doi.org/10.1016/j.jinorgbio.2009.10.004.
[171] F. Jiang, W. Wong, X. Zhu, G. Zhou, W. Wong, P. Wu, H. Tam, K. Cheah, C. Ye, Y. Liu, Synthesis, characterization, and photophysical properties of some heterodimetallic bisporphyrins of ytterbium and transition metals – enhancement and lifetime extension of Yb^{3+} emission by transition-metal porphyrin sensitization, Eur. J. Inorg. Chem. 2007 (2007) 3365–3374, https://doi.org/10.1002/ejic.200700153.
[172] K. Qiu, H. Zhu, T.W. Rees, L. Ji, Q. Zhang, H. Chao, Recent advances in lysosome-targeting luminescent transition metal complexes, Coord. Chem. Rev. 398 (2019) 113010, https://doi.org/10.1016/j.ccr.2019.07.007.
[173] J. Shen, T.W. Rees, L. Ji, H. Chao, Recent advances in ruthenium(II) and iridium (III) complexes containing nanosystems for cancer treatment and bioimaging, Coord. Chem. Rev. 443 (2021) 214016, https://doi.org/10.1016/j.ccr.2021.214016.
[174] C. Liu, W. Zhang, R. Zhang, X. Gao, B. Song, J. Yuan, Ruthenium(II) complex-based long-lived two-photon luminescence probe for dynamic monitoring of glutathione S-transferases in mouse models of drug-induced liver injury, Sens. Actuators B Chem. 357 (2022) 131440, https://doi.org/10.1016/j.snb.2022.131440.
[175] A.M.A. Mazari, L. Zhang, Z.-W. Ye, J. Zhang, K.D. Tew, D.M. Townsend, The multifaceted role of glutathione S-transferases in health and disease, Biomolecules 13 (2023) 688, https://doi.org/10.3390/biom13040688.
[176] R. Guan, L. Xie, T.W. Rees, L. Ji, H. Chao, Metal complexes for mitochondrial bioimaging, J. Inorg. Biochem. 204 (2020) 110985, https://doi.org/10.1016/j.jinorgbio.2019.110985.
[177] H.K. Saeed, S. Sreedharan, J.A. Thomas, Photoactive metal complexes that bind DNA and other biomolecules as cell probes, therapeutics, and theranostics, Chem. Commun. 56 (2020) 1464–1480, https://doi.org/10.1039/C9CC09312E.
[178] E. Baggaley, M.R. Gill, N.H. Green, D. Turton, I.V. Sazanovich, S.W. Botchway, C. Smythe, J.W. Haycock, J.A. Weinstein, J.A. Thomas, Dinuclear ruthenium(II) complexes as two-photon, time-resolved emission microscopy probes for cellular DNA, Angew. Chem. Int. Ed. 53 (2014) 3367–3371, https://doi.org/10.1002/anie.201309427.
[179] E. Du, X. Hu, S. Roy, P. Wang, K. Deasy, T. Mochizuki, Y. Zhang, Taurine-modified Ru(II)-complex targets cancerous brain cells for photodynamic therapy, Chem. Commun. 53 (2017) 6033–6036, https://doi.org/10.1039/C7CC03337K.
[180] H. Wang, R. Zhang, K.R. Bridle, A. Jayachandran, J.A. Thomas, W. Zhang, J. Yuan, Z.P. Xu, D.H.G. Crawford, X. Liang, X. Liu, M.S. Roberts, Two-photon dual imaging platform for in vivo monitoring cellular oxidative stress in liver injury, Sci. Rep. 7 (2017) 45374, https://doi.org/10.1038/srep45374.
[181] B. Yang, Y. Chen, J. Shi, Reactive oxygen species (ROS)-based nanomedicine, Chem. Rev. 119 (2019) 4881–4985, https://doi.org/10.1021/acs.chemrev.8b00626.
[182] P. Zhang, H. Huang, Y. Chen, J. Wang, L. Ji, H. Chao, Ruthenium(II) anthraquinone complexes as two-photon luminescent probes for cycling hypoxia imaging in vivo, Biomaterials 53 (2015) 522–531, https://doi.org/10.1016/j.biomaterials.2015.02.126.
[183] K. Tanabe, N. Hirata, H. Harada, M. Hiraoka, S. Nishimoto, Emission under hypoxia: one-electron reduction and fluorescence characteristics of an indolequinone-coumarin conjugate, ChemBioChem 9 (2008) 426–432, https://doi.org/10.1002/cbic.200700458.
[184] F.E. Poynton, S.A. Bright, S. Blasco, D.C. Williams, J.M. Kelly, T. Gunnlaugsson, The development of ruthenium(II) polypyridyl complexes and conjugates for in vitro cellular and in vivo applications, Chem. Soc. Rev. 46 (2017) 7706–7756, https://doi.org/10.1039/C7CS00680B.
[185] D.-Y. Zhang, Y. Zheng, H. Zhang, L. He, C.-P. Tan, J.-H. Sun, W. Zhang, X. Peng, Q. Zhan, L.-N. Ji, Z.-W. Mao, Ruthenium complex-modified carbon nanodots for lysosome-targeted one- and two-photon imaging and photodynamic therapy, Nanoscale 9 (2017) 18966–18976, https://doi.org/10.1039/C7NR05349E.
[186] K.O. Boakye-Yiadom, S. Kesse, Y. Opoku-Damoah, M.S. Filli, M. Aquib, M.M. B. Joelle, M.A. Farooq, R. Mavlyanova, F. Raza, R. Bavi, B. Wang, Carbon dots: Applications in bioimaging and theranostics, Int. J. Pharm. 564 (2019) 308–317, https://doi.org/10.1016/j.ijpharm.2019.04.055.
[187] H. Manisha, P.D. Priya Swetha, Y.-B. Shim, K.S. Prasad, Revisiting fluorescent carbon nanodots for environmental, biomedical applications and puzzle about fluorophore impurities, Nano-Struct. Nano-Obj. 20 (2019) 100391, https://doi.org/10.1016/j.nanoso.2019.100391.
[188] L. Nguyen, M. Li, S. Woo, Y. You, Development of prodrugs for PDT-based combination therapy using a singlet-oxygen-sensitive linker and quantitative systems pharmacology, J. Clin. Med. 8 (2019) 2198, https://doi.org/10.3390/jcm8122198.
[189] S. Kwiatkowski, B. Knap, D. Przystupski, J. Saczko, E. Kędzierska, K. Knap-Czop, J. Kotlińska, O. Michel, K. Kotowski, J. Kulbacka, Photodynamic therapy – mechanisms, photosensitizers and combinations, Biomed. Pharmacother. 106 (2018) 1098–1107, https://doi.org/10.1016/j.biopha.2018.07.049.
[190] M. Khurana, H.A. Collins, A. Karotki, H.L. Anderson, D.T. Cramb, B.C. Wilson, Quantitative in vitro demonstration of two-photon photodynamic therapy using Photofrin® and Visudyne®, Photochem. Photobiol. 83 (2007) 1441–1448, https://doi.org/10.1111/j.1751-1097.2007.00185.x.
[191] L. Conti, E. Macedi, C. Giorgi, B. Valtancoli, V. Fusi, Combination of light and Ru (II) polypyridyl complexes: Recent advances in the development of new anticancer drugs, Coord. Chem. Rev. 469 (2022) 214656, https://doi.org/10.1016/j.ccr.2022.214656.
[192] T.C. Pham, V.-N. Nguyen, Y. Choi, S. Lee, J. Yoon, Recent strategies to develop innovative photosensitizers for enhanced photodynamic therapy, Chem. Rev. 121 (2021) 13454–13619, https://doi.org/10.1021/acs.chemrev.1c00381.
[193] L.K. McKenzie, H.E. Bryant, J.A. Weinstein, Transition metal complexes as photosensitisers in one- and two-photon photodynamic therapy, Coord. Chem. Rev. 379 (2019) 2–29, https://doi.org/10.1016/j.ccr.2018.03.020.
[194] F. Heinemann, J. Karges, G. Gasser, Critical overview of the use of Ru(II) polypyridyl complexes as photosensitizers in one-photon and two-photon photodynamic therapy, Acc. Chem. Res. 50 (2017) 2727–2736, https://doi.org/10.1021/acs.accounts.7b00180.
[195] J.D. Knoll, C. Turro, Control and utilization of ruthenium and rhodium metal complex excited states for photoactivated cancer therapy, Coord. Chem. Rev. 282–283 (2015) 110–126, https://doi.org/10.1016/j.ccr.2014.05.018.
[196] X. Zhao, J. Liu, J. Fan, H. Chao, X. Peng, Recent progress in photosensitizers for overcoming the challenges of photodynamic therapy: from molecular design to application, Chem. Soc. Rev. 50 (2021) 4185–4219, https://doi.org/10.1039/D0CS00173B.
[197] Y. Arenas, S. Monro, G. Shi, A. Mandel, S. McFarland, L. Lilge, Photodynamic inactivation of Staphylococcus aureus and methicillin-resistant Staphylococcus aureus with Ru(II)-based type I/type II photosensitizers, Photodiagn. Photodyn. Ther. 10 (2013) 615–625, https://doi.org/10.1016/j.pdpdt.2013.07.001.
[198] J. Karges, Clinical development of metal complexes as photosensitizers for photodynamic therapy of cancer, Angew. Chem. Int. Ed. 61 (2022) e202112236, https://doi.org/10.1002/anie.202112236.
[199] V.-N. Nguyen, Z. Zhao, B.Z. Tang, J. Yoon, Organic photosensitizers for antimicrobial phototherapy, Chem. Soc. Rev. 51 (2022) 3324–3340, https://doi.org/10.1039/D1CS00647A.
[200] R. Youf, M. Müller, A. Balasini, F. Thétiot, M. Müller, A. Hascoët, U. Jonas, H. Schönherr, G. Lemercier, T. Montier, T. Le Gall, Antimicrobial photodynamic therapy: latest developments with a focus on combinatory strategies, Pharmaceutics 13 (2021) 1995, https://doi.org/10.3390/pharmaceutics13121995.
[201] N. Soliman, V. Sol, T.-S. Ouk, C.M. Thomas, G. Gasser, Encapsulation of a Ru(II) polypyridyl complex into polylactide nanoparticles for antimicrobial photodynamic therapy, Pharmaceutics 12 (2020) 961, https://doi.org/10.3390/pharmaceutics12100961.
[202] A. Jain, N.T. Garrett, Z.P. Malone, Ruthenium-based photoactive metalloantibiotics †, Photochem. Photobiol. 98 (2022) 6–16, https://doi.org/10.1111/php.13435.
[203] X.Y. Ng, K.W. Fong, L.V. Kiew, P.Y. Chung, Y.K. Liew, N. Delsuc, M. Zulkefeli, M. L. Low, Ruthenium(II) polypyridyl complexes as emerging photosensitisers for antibacterial photodynamic therapy, J. Inorg. Biochem. 250 (2024) 112425, https://doi.org/10.1016/j.jinorgbio.2023.112425.
[204] A. Gul, M. Ahmad, R. Ullah, R. Ullah, Y. Kang, W. Liao, Systematic review on antibacterial photodynamic therapeutic effects of transition metals ruthenium and iridium complexes, J. Inorg. Biochem. 255 (2024) 112523, https://doi.org/10.1016/j.jinorgbio.2024.112523.
[205] X. Wei, W. Cui, G. Qin, X. Zhang, F. Sun, H. Li, J. Guo, A. Ren, Theoretical investigation of Ru(II) complexes with long lifetime and a large two-photon absorption cross-section in photodynamic therapy, J. Med. Chem. 66 (2023) 4167–4178, https://doi.org/10.1021/acs.jmedchem.3c00047.

[206] S.-J. Tang, M.-F. Wang, R. Yang, M. Liu, Q.-F. Li, F. Gao, More-is-better strategy for constructing homoligand polypyridyl ruthenium complexes as photosensitizers for infrared two-photon photodynamic therapy, Inorg. Chem. 62 (2023) 8210–8218, https://doi.org/10.1021/acs.inorgchem.3c00585.
[207] G.-L. Ma, X.-D. Bi, F. Gao, Z. Feng, D.-C. Zhao, F.-J. Lin, R. Yan, D. Liu, P. Liu, J. Chen, H. Zhang, Novel polypyridyl ruthenium complexes acting as high affinity DNA intercalators, potent transcription inhibitors and antitumor reagents, J. Inorg. Biochem. 185 (2018) 1–9, https://doi.org/10.1016/j.jinorgbio.2018.04.019.
[208] M. Wang, R. Yang, S. Tang, Y. Deng, G. Li, D. Zhang, D. Chen, X. Ren, F. Gao, In vivo realization of dual photodynamic and photothermal therapy for melanoma by mitochondria targeting dinuclear ruthenium complexes under civil infrared low-power laser, Angew. Chem. Int. Ed. 61 (2022) e202208721, https://doi.org/10.1002/anie.202208721.
[209] J. Mo, N.P. Mai Le, R. Priefer, Evaluating the mechanisms of action and subcellular localization of ruthenium(II)-based photosensitizers, Eur. J. Med. Chem. 225 (2021) 113770, https://doi.org/10.1016/j.ejmech.2021.113770.
[210] L. Zeng, P. Gupta, Y. Chen, E. Wang, L. Ji, H. Chao, Z.-S. Chen, The development of anticancer ruthenium(II) complexes: from single molecule compounds to nanomaterials, Chem. Soc. Rev. 46 (2017) 5771–5804, https://doi.org/10.1039/C7CS00195A.
[211] S.C. Boca, M. Four, A. Bonne, B. van der Sanden, S. Astilean, P.L. Baldeck, G. Lemercier, An ethylene-glycol decorated ruthenium(II) complex for two-photon photodynamic therapy, Chem. Commun. (2009) 4590, https://doi.org/10.1039/b907143a.
[212] H. Ke, H. Wang, W.-K. Wong, N.-K. Mak, D.W.J. Kwong, K.-L. Wong, H.-L. Tam, Responsive and mitochondria-specific ruthenium(II) complex for dual in vitro applications: two-photon (near-infrared) induced imaging and regioselective cell killing, Chem. Commun. 46 (2010) 6678, https://doi.org/10.1039/c0cc01848a.
[213] J. Zhang, K.-L. Wong, W.-K. Wong, N.-K. Mak, D.W.J. Kwong, H.-L. Tam, Two-photon induced luminescence, singlet oxygen generation, cellular uptake and photocytotoxic properties of amphiphilic Ru(II) polypyridyl–porphyrin conjugates as potential bifunctional photodynamic therapeutic agents, Org. Biomol. Chem. 9 (2011) 6004, https://doi.org/10.1039/c1ob05415e.
[214] Y. Yang, S. Karakhanova, W. Hartwig, J.G. D'Haese, P.P. Philippov, J. Werner, A. V. Bazhin, Mitochondria and mitochondrial ROS in cancer: novel targets for anticancer therapy: antioxidants for anticancer therapy, J. Cell. Physiol. 231 (2016) 2570–2581, https://doi.org/10.1002/jcp.25349.
[215] A.P. Trotta, J.E. Chipuk, Mitochondrial dynamics as regulators of cancer biology, Cell. Mol. Life Sci. 74 (2017) 1999–2017, https://doi.org/10.1007/s00018-016-2451-3.
[216] T.L.C. Figueiredo, R.A.W. Johnstone, A.M.P.S. Sørensen, D. Burget, P. Jacques, Determination of fluorescence yields, singlet lifetimes and singlet oxygen yields of water-insoluble porphyrins and metalloporphyrins in organic solvents and in aqueous media, Photochem. Photobiol. 69 (1999) 517–528, https://doi.org/10.1111/j.1751-1097.1999.tb03322.x.
[217] Z. Zhou, J. Liu, T.W. Rees, H. Wang, X. Li, H. Chao, P.J. Stang, Heterometallic Ru–Pt metallacycle for two-photon photodynamic therapy, Proc. Natl. Acad. Sci. 115 (2018) 5664–5669, https://doi.org/10.1073/pnas.1802012115.
[218] J. Karges, S. Kuang, Y.C. Ong, H. Chao, G. Gasser, One- and two-photon phototherapeutic effects of Ru^{II} polypyridine complexes in the hypoxic centre of large multicellular tumor spheroids and tumor-bearing mice**, Chem. Eur. J. 27 (2021) 362–370, https://doi.org/10.1002/chem.202003486.
[219] P.R. Ogilby, Singlet oxygen: there is indeed something new under the sun, Chem. Soc. Rev. 39 (2010) 3181, https://doi.org/10.1039/b926014p.
[220] T. Mishchenko, I. Balalaeva, A. Gorokhova, M. Vedunova, D.V. Krysko, Which cell death modality wins the contest for photodynamic therapy of cancer? Cell Death Dis. 13 (2022) 455 https://doi.org/10.1038/s41419-022-04851-4.
[221] C.A. Puckett, J.K. Barton, Methods to explore cellular uptake of ruthenium complexes, J. Am. Chem. Soc. 129 (2007) 46–47, https://doi.org/10.1021/ja0677564.
[222] C.A. Puckett, J.K. Barton, Mechanism of cellular uptake of a ruthenium polypyridyl complex, Biochemistry 47 (2008) 11711–11716, https://doi.org/10.1021/bi800856t.
[223] J. Hess, H. Huang, A. Kaiser, V. Pierroz, O. Blacque, H. Chao, G. Gasser, Evaluation of the medicinal potential of two ruthenium (II) polypyridine complexes as one-and two-photon photodynamic therapy photosensitizers, Chem. Eur. J. 23 (2017) 9888–9896, https://doi.org/10.1002/chem.201701392.
[224] H. Vakifahmetoglu-Norberg, A.T. Ouchida, E. Norberg, The role of mitochondria in metabolism and cell death, Biochem. Biophys. Res. Commun. 482 (2017) 426–431, https://doi.org/10.1016/j.bbrc.2016.11.088.
[225] J. Zielonka, J. Joseph, A. Sikora, M. Hardy, O. Ouari, J. Vasquez-Vivar, G. Cheng, M. Lopez, B. Kalyanaraman, Mitochondria-targeted triphenylphosphonium-based compounds: syntheses, mechanisms of action, and therapeutic and diagnostic applications, Chem. Rev. 117 (2017) 10043–10120, https://doi.org/10.1021/acs.chemrev.7b00042.
[226] S. Chakrabortty, B.K. Agrawalla, A. Stumper, N.M. Vegi, S. Fischer, C. Reichardt, M. Kögler, B. Dietzek, M. Feuring-Buske, C. Buske, S. Rau, T. Weil, Mitochondria targeted protein-ruthenium photosensitizer for efficient photodynamic applications, J. Am. Chem. Soc. 139 (2017) 2512–2519, https://doi.org/10.1021/jacs.6b13399.
[227] IUPAC-IUB Joint Commission on Biochemical Nomenclature (JCBN), Nomenclature and symbolism for amino acids and peptides (Recommendations 1983), Pure Appl. Chem. 56 (1984) 595–624, https://doi.org/10.1351/pac198456050595.
[228] L.K.K. Holland, I.Ø. Nielsen, K. Maeda, M. Jäättelä, SnapShot: lysosomal functions, Cell 181 (2020) 748–748.e1, https://doi.org/10.1016/j.cell.2020.03.043.
[229] H. Huang, B. Yu, P. Zhang, J. Huang, Y. Chen, G. Gasser, L. Ji, H. Chao, Highly charged ruthenium(II) polypyridyl complexes as lysosome-localized photosensitizers for two-photon photodynamic therapy, Angew. Chem. 127 (2015) 14255–14258, https://doi.org/10.1002/ange.201507800.
[230] H. Kitao, M. Iimori, Y. Kataoka, T. Wakasa, E. Tokunaga, H. Saeki, E. Oki, Y. Maehara, DNA replication stress and cancer chemotherapy, Cancer Sci. 109 (2018) 264–271, https://doi.org/10.1111/cas.13455.
[231] A. Raza, S.A. Archer, S.D. Fairbanks, K.L. Smitten, S.W. Botchway, J.A. Thomas, S. MacNeil, J.W. Haycock, A dinuclear ruthenium(II) complex excited by near-infrared light through two-photon absorption induces phototoxicity deep within hypoxic regions of melanoma cancer spheroids, J. Am. Chem. Soc. 142 (2020) 4639–4647, https://doi.org/10.1021/jacs.9b11313.
[232] L. Zeng, S. Kuang, G. Li, C. Jin, L. Ji, H. Chao, A GSH-activatable ruthenium(II)-azo photosensitizer for two-photon photodynamic therapy, Chem. Commun. 53 (2017) 1977–1980, https://doi.org/10.1039/C6CC10330H.
[233] N. Traverso, R. Ricciarelli, M. Nitti, B. Marengo, A.L. Furfaro, M.A. Pronzato, U. M. Marinari, C. Domenicotti, Role of glutathione in cancer progression and chemoresistance, Oxid. Med. Cell. Longev. 2013 (2013) 1–10, https://doi.org/10.1155/2013/972913.
[234] X. Zhao, M. Li, W. Sun, J. Fan, J. Du, X. Peng, An estrogen receptor targeted ruthenium complex as a two-photon photodynamic therapy agent for breast cancer cells, Chem. Commun. 54 (2018) 7038–7041, https://doi.org/10.1039/C8CC03786H.
[235] J. Li, L. Zeng, K. Xiong, T.W. Rees, C. Jin, W. Wu, Y. Chen, L. Ji, H. Chao, A biotinylated ruthenium(II) photosensitizer for tumor-targeted two-photon photodynamic therapy, Chem. Commun. 55 (2019) 10972–10975, https://doi.org/10.1039/C9CC05826E.
[236] C.S. Kue, A. Kamkaew, K. Burgess, L.V. Kiew, L.Y. Chung, H.B. Lee, Small molecules for active targeting in cancer, Med. Res. Rev. 36 (2016) 494–575, https://doi.org/10.1002/med.21387.
[237] M. Slim, H.F. Sleiman, Ruthenium(II)–phenanthroline–biotin complexes: synthesis and luminescence enhancement upon binding to avidin, Bioconjug. Chem. 15 (2004) 949–953, https://doi.org/10.1021/bc049919o.
[238] J. Liu, X. Liao, K. Xiong, S. Kuang, C. Jin, L. Ji, H. Chao, Boosting two-photon photodynamic therapy with mitochondria-targeting ruthenium–glucose conjugates, Chem. Commun. 56 (2020) 5839–5842, https://doi.org/10.1039/D0CC01148G.
[239] Z. Zhao, K. Qiu, J. Liu, X. Hao, J. Wang, Two-photon photodynamic ablation of tumour cells using an RGD peptide-conjugated ruthenium(II) photosensitiser, Chem. Commun. 56 (2020) 12542–12545, https://doi.org/10.1039/D0CC04943C.
[240] M. Lin, S. Zou, X. Liao, Y. Chen, D. Luo, L. Ji, H. Chao, Ruthenium(II) complexes as bioorthogonal two-photon photosensitizers for tumour-specific photodynamic therapy against triple-negative breast cancer cells, Chem. Commun. 57 (2021) 4408–4411, https://doi.org/10.1039/D1CC00661D.
[241] J.H. Kaplan, B. Forbush, J.F. Hoffman, Rapid photolytic release of adenosine 5′-triphosphate from a protected analog: utilization by the sodium:potassium pump of human red blood cell ghosts, Biochemistry 17 (1978) 1929–1935, https://doi.org/10.1021/bi00603a020.
[242] H.-M. Lee, D.R. Larson, D.S. Lawrence, Illuminating the chemistry of life: design, synthesis, and applications of "caged" and related photoresponsive compounds, ACS Chem. Biol. 4 (2009) 409–427, https://doi.org/10.1021/cb900036s.
[243] S. Sortino, Photoactivated nanomaterials for biomedical release applications, J. Mater. Chem. 22 (2012) 301–318, https://doi.org/10.1039/C1JM13288A.
[244] J. Kim, B.C. Yung, W.J. Kim, X. Chen, Combination of nitric oxide and drug delivery systems: tools for overcoming drug resistance in chemotherapy, J. Control. Release 263 (2017) 223–230, https://doi.org/10.1016/j.jconrel.2016.12.026.
[245] W. Li, J. Lin, T. Wang, P. Huang, Photo-triggered drug delivery systems for neuron-related applications, Curr. Med. Chem. 26 (2019) 1406–1422, https://doi.org/10.2174/0929867325666180622121801.
[246] J.M. Silva, E. Silva, R.L. Reis, Light-triggered release of photocaged therapeutics - Where are we now? J. Control. Release 298 (2019) 154–176, https://doi.org/10.1016/j.jconrel.2019.02.006.
[247] N.J. Farrer, L. Salassa, P.J. Sadler, Photoactivated chemotherapy (PACT): the potential of excited-state d-block metals in medicine, Dalton Trans. (2009) 10690–10701.
[248] N.A. Smith, P.J. Sadler, Photoactivatable metal complexes: from theory to applications in biotechnology and medicine, Philos. Trans. R. Soc. Math. Phys. Eng. Sci. 371 (2013) 20120519, https://doi.org/10.1098/rsta.2012.0519.
[249] S. Bonnet, Why develop photoactivated chemotherapy? Dalton Trans. 47 (2018) 10330–10343, https://doi.org/10.1039/C8DT01585F.
[250] J.-A. Cuello-Garibo, M.S. Meijer, S. Bonnet, To cage or to be caged? The cytotoxic species in ruthenium-based photoactivated chemotherapy is not always the metal, Chem. Commun. 53 (2017) 6768–6771, https://doi.org/10.1039/C7CC03469E.
[251] D. Havrylyuk, K. Stevens, S. Parkin, E.C. Glazer, Toward optimal ru(II) photocages: balancing photochemistry, stability, and biocompatibility through fine tuning of steric, electronic, and physiochemical features, Inorg. Chem. 59 (2020) 1006–1013, https://doi.org/10.1021/acs.inorgchem.9b02065.
[252] A.C. Benniston, L. Zeng, Recent advances in photorelease complexes for therapeutic applications, Dalton Trans. 51 (2022) 4202–4212, https://doi.org/10.1039/D2DT00254J.

[253] S. Bonnet, Ruthenium-based photoactivated chemotherapy, J. Am. Chem. Soc. 145 (2023) 23397–23415, https://doi.org/10.1021/jacs.3c01135.
[254] M.S. Meijer, M.M. Natile, S. Bonnet, 796 nm activation of a photocleavable ruthenium(II) complex conjugated to an upconverting nanoparticle through two phosphonate groups, Inorg. Chem. 59 (2020) 14807–14818, https://doi.org/10.1021/acs.inorgchem.0c00043.
[255] Y. Chen, L. Bai, P. Zhang, H. Zhao, Q. Zhou, The development of Ru(II)-based photoactivated chemotherapy agents, Molecules 26 (2021) 5679, https://doi.org/10.3390/molecules26185679.
[256] M. Romero Ávila, A.F. León-Rojas, P.G. Lacroix, I. Malfant, N. Farfán, R. Mhanna, R. Santillan, G. Ramos-Ortiz, J.-P. Malval, Two-photon-triggered NO release via a ruthenium-nitrosyl complex with a star-shaped architecture, J. Phys. Chem. Lett. 11 (2020) 6487–6491, https://doi.org/10.1021/acs.jpclett.0c01953.
[257] V. Nikolenko, R. Yuste, L. Zayat, L.M. Baraldo, R. Etchenique, Two-photon uncaging of neurochemicals using inorganic metal complexes, Chem. Commun. 13 (2005) 1752–1754, https://doi.org/10.1039/B418572B.
[258] E. Fino, RuBi-glutamate: two-photon and visible-light photoactivation of neurons and dendritic spines, Front. Neural Circuits 3 (2009) 556, https://doi.org/10.3389/neuro.04.002.2009.
[259] M. Salierno, E. Marceca, D.S. Peterka, R. Yuste, R. Etchenique, A fast ruthenium polypyridine cage complex photoreleases glutamate with visible or IR light in one and two photon regimes, J. Inorg. Biochem. 104 (2010) 418–422, https://doi.org/10.1016/j.jinorgbio.2009.12.004.
[260] E. Pchitskaya, I. Bezprozvanny, Dendritic spines shape analysis—classification or clusterization? Perspective, Front. Synaptic Neurosci. 12 (2020) 31, https://doi.org/10.3389/fnsyn.2020.00031.
[261] R. Araya, V. Andino-Pavlovsky, R. Yuste, R. Etchenique, Two-photon optical interrogation of individual dendritic spines with caged dopamine, ACS Chem. Neurosci. 4 (2013) 1163–1167, https://doi.org/10.1021/cn4000692.
[262] Z. Jin, S. Qi, X. Guo, Y. Jian, Y. Hou, C. Li, X. Wang, Q. Zhou, The modification of a pyrene group makes a Ru(II) complex versatile, Chem. Commun. 57 (2021) 3259–3262, https://doi.org/10.1039/D0CC08400J.
[263] Y. Wang, N. Tian, W. Sun, B. Rena, X. Guo, Y. Feng, C. Li, X. Wang, Q. Zhou, A Ru (II)-based nanoassembly exhibiting theranostic PACT activity in NIR region, Part. Part. Syst. Charact. (2020) 2000045, https://doi.org/10.1002/ppsc.202000045.
[264] N. Tian, Y. Feng, W. Sun, J. Lu, S. Lu, Y. Yao, C. Li, X. Wang, Q. Zhou, A nuclear permeable Ru(II)-based photoactivated chemotherapeutic agent towards a series of cancer cells: in vitro and in vivo studies, Dalton Trans. 48 (2019) 6492–6500, https://doi.org/10.1039/C9DT00441F.
[265] N. Soliman, G. Gasser, C.M. Thomas, Incorporation of Ru(II) polypyridyl complexes into nanomaterials for cancer therapy and diagnosis, Adv. Mater. 32 (2020) 2003294, https://doi.org/10.1002/adma.202003294.
[266] B.L. Banik, P. Fattahi, J.L. Brown, Polymeric nanoparticles: the future of nanomedicine, Wiley Interdiscip. Rev. Nanomed. Nanobiotechnol. 8 (2016) 271–299, https://doi.org/10.1002/wnan.1364.
[267] A. Zielińska, F. Carreiró, A.M. Oliveira, A. Neves, B. Pires, D.N. Venkatesh, A. Durazzo, M. Lucarini, P. Eder, A.M. Silva, A. Santini, E.B. Souto, Polymeric nanoparticles: production, characterization, toxicology and ecotoxicology, Molecules 25 (2020) 3731, https://doi.org/10.3390/molecules25163731.
[268] J. Karges, Encapsulation of Ru(II) polypyridine complexes for tumor-targeted anticancer therapy, BME Front. 4 (2023) 0024, https://doi.org/10.34133/bmef.0024.
[269] S. Thota, D.A. Rodrigues, D.C. Crans, E.J. Barreiro, Ru(II) compounds: next-generation anticancer metallotherapeutics? J. Med. Chem. 61 (2018) 5805–5821, https://doi.org/10.1021/acs.jmedchem.7b01689.
[270] J. Liu, H. Lai, Z. Xiong, B. Chen, T. Chen, Functionalization and cancer-targeting design of ruthenium complexes for precise cancer therapy, Chem. Commun. 55 (2019) 9904–9914, https://doi.org/10.1039/C9CC04098F.
[271] E. Villemin, Y.C. Ong, C.M. Thomas, G. Gasser, Polymer encapsulation of ruthenium complexes for biological and medicinal applications, Nat. Rev. Chem. 3 (2019) 261–282, https://doi.org/10.1038/s41570-019-0088-0.
[272] F. Wei, Z. Chen, X.-C. Shen, L. Ji, H. Chao, Recent progress in metal complexes functionalized nanomaterials for photodynamic therapy, Chem. Commun. 59 (2023) 6956–6968, https://doi.org/10.1039/D3CC01355C.
[273] J. Karges, J. Li, L. Zeng, H. Chao, G. Gasser, Polymeric encapsulation of a ruthenium polypyridine complex for tumor targeted one- and two-photon photodynamic therapy, ACS Appl. Mater. Interfaces 12 (2020) 54433–54444, https://doi.org/10.1021/acsami.0c16119.
[274] A.P. Blum, J.K. Kammeyer, A.M. Rush, C.E. Callmann, M.E. Hahn, N. C. Gianneschi, Stimuli-responsive nanomaterials for biomedical applications, J. Am. Chem. Soc. 137 (2015) 2140–2154, https://doi.org/10.1021/ja510147n.
[275] N. Ni, X. Zhang, Y. Ma, J. Yuan, D. Wang, G. Ma, J. Dong, X. Sun, Biodegradable two-dimensional nanomaterials for cancer theranostics, Coord. Chem. Rev. 458 (2022) 214415, https://doi.org/10.1016/j.ccr.2022.214415.
[276] P. Malaviya, D. Shukal, A.R. Vasavada, Nanotechnology-based drug delivery, metabolism and toxicity, Curr. Drug Metab. 20 (2020) 1167–1190, https://doi.org/10.2174/1389200221666200103091753.
[277] M. Awashra, P. Młynarz, The toxicity of nanoparticles and their interaction with cells: an *in vitro* metabolomic perspective, Nanoscale Adv. 5 (2023) 2674–2723, https://doi.org/10.1039/D2NA00534D.
[278] N.Ž. Knežević, V. Stojanovic, A. Chaix, E. Bouffard, K.E. Cheikh, A. Morère, M. Maynadier, G. Lemercier, M. Garcia, M. Gary-Bobo, J.-O. Durand, F. Cunin, Ruthenium(II) complex-photosensitized multifunctionalized porous silicon nanoparticles for two-photon near-infrared light responsive imaging and photodynamic cancer therapy, J. Mater. Chem. B 4 (2016) 1337–1342, https://doi.org/10.1039/C5TB02726H.
[279] P. Zhang, H. Huang, J. Huang, H. Chen, J. Wang, K. Qiu, D. Zhao, L. Ji, H. Chao, Noncovalent ruthenium(II) complexes–single-walled carbon nanotube composites for bimodal photothermal and photodynamic therapy with near-infrared irradiation, ACS Appl. Mater. Interfaces 7 (2015) 23278–23290, https://doi.org/10.1021/acsami.5b07510.
[280] G. Kandasamy, K. Kumar, Synergy between nanoparticles and breast cancer theranostics, in: Nanomedicines Breast Cancer Theranostics, Elsevier, 2020, pp. 71–106, https://doi.org/10.1016/B978-0-12-820016-2.00005-7.
[281] E.S. Shibu, M. Hamada, N. Murase, V. Biju, Nanomaterials formulations for photothermal and photodynamic therapy of cancer, J. Photochem. Photobiol. C: Photochem. Rev. 15 (2013) 53–72, https://doi.org/10.1016/j.jphotochemrev.2012.09.004.
[282] D. Jain, A. Saha, A.A. Martí, Non-covalent ruthenium polypyridyl complexes–carbon nanotubes composites: an alternative for functional dissolution of carbon nanotubes in solution, Chem. Commun. 47 (2011) 2246, https://doi.org/10.1039/c0cc05295g.
[283] F. Wei, J. Karges, S. Gao, L. Wang, X. Zhang, X.-C. Shen, L. Ji, H. Chao, Two-photon phototriggering of ROS storm in ruthenium(II) coordinated carbon nitride for robust cancer immunotherapy, Nano Today 54 (2024) 102066, https://doi.org/10.1016/j.nantod.2023.102066.
[284] F. Wei, S. Kuang, T.W. Rees, X. Liao, J. Liu, D. Luo, J. Wang, X. Zhang, L. Ji, H. Chao, Ruthenium(II) complexes coordinated to graphitic carbon nitride: Oxygen self-sufficient photosensitizers which produce multiple ROS for photodynamic therapy in hypoxia, Biomaterials 276 (2021) 121064, https://doi.org/10.1016/j.biomaterials.2021.121064.